

**UCSF**

**UC San Francisco Electronic Theses and Dissertations**

**Title**

Receptor-Mediated Uptake and Intracellular Sorting of Multivalent Lipid Nanoparticles against the Epidermal Growth Factor Receptor (EGFR) and the Human EGFR 2 (HER2)

**Permalink**

<https://escholarship.org/uc/item/29k490vp>

**Author**

Tran, David T.

**Publication Date**

2013

Peer reviewed|Thesis/dissertation

Receptor-Mediated Uptake and Intracellular Sorting of Multivalent Lipid Nanoparticles  
Against the Epidermal Growth Factor Receptor (EGFR) and the Human EGFR 2 (HER2)

by

David Tu Tran

DISSERTATION

Submitted in partial satisfaction of the requirements for the degree of

DOCTOR OF PHILOSOPHY

in

Bioengineering

in the

GRADUATE DIVISION

of the

UNIVERSITY OF CALIFORNIA, SAN FRANCISCO

Copyright 2013

by

David Tu Tran

## Acknowledgements

First and foremost, I would like to acknowledge the support and guidance of my advisor Dr. John W. Park. With his front row seat in cancer clinical therapies and detection, he introduced me to the captivating world of targeted liposomal drug delivery. His broad expertise and perspectives in science, medicine, and business were invaluable for the completion of this dissertation.

I would like to sincerely thank Dr. Francis C. Szoka, Jr. for his support, in addition to being the chair of my dissertation committee, for serving as a supportive co-advisor, mentor, and teacher. He welcomed me with opened arms to his office, laboratory, and lab meetings. His guidance and continued faith in me were also essential for the completion of this dissertation.

I would like to express my appreciation for the faculty members who have served on my dissertation committee: Dr. Seung-Wuk Lee, Dr. John W. Park, Dr. Francis C. Szoka, Jr., Dr. Tejal Desai, and Dr. James Marks. I would also like to express my appreciation for the faculty members who have served on my qualifying oral examination committee: Dr. Francis C. Szoka, Jr., Dr. Tejal Desai, Dr. James Marks, Dr. Christopher Cullander, and Dr. Kevin Healy.

Additionally, I would like to express my gratitude to all those who have made contributions to the research in this dissertation: Dr. Robert Raphael, my undergraduate advisor who paved the backbone for my liposomal knowledge; Dr. Charles Noble and Dr. Erika Kullberg who both mentored and broadened my liposomal understanding to the targeted and therapeutic fields; Dr. Daryl Drummond and Merrimack Pharmaceuticals for their drug delivery advisory roles as well as providing novel liposomal drugs; Dr. Byron Hann and the UCSF Preclinical Therapeutics Core for performing and helping me design the animal studies; Jane Gordon, Sarah Elmes, William Hyun, and the UCSF Laboratory for Cell Analysis Core for educating me on microscopy; Remi Chua and the UCSF Outpatients Clinics Pharmacy for supplying monoclonal antibodies; and Remi Hendrix for running many of the dual-targeting liposomal experiments during her short internship in our laboratory.

I would like to thank my laboratory members through the years for conversations, suggestions, and support about my research: Dr. Charles Noble, Dr. Erika Kullberg, Dr. Janet Scott, Dr. Emanuela Zacco, Dr. Christoph Mamot, Dr. Kevin Weng, Dr. Mark Magbanua, Louai Hauranieh, Eddy Sosa, Luise Sternberg, and Remi Hendrix. I would also like to thank Dr. Michael Campbell for his constructive suggestions during our joint lab meetings and the many scholars at the UCSF Helen Diller Family Comprehensive Cancer Center who have shared both scientific advice and lab equipment.

Finally, I would like to express my profound gratitude to my family and friends who have always believed in my potential and encouraged my education. They were always available to listen, support, and challenge me through my long journey here. I would like to especially thank my friend Dr. Robert Podesva for being a great yet strict writing partner and my parents for their unconditional love.

My dissertation is dedicated to my grandfather Hoc V. Tran. Although his name translated as “learn or educate” in Vietnamese, he lacked the time and opportunity to pursue a higher education in between fighting a civil war, starting a new life as a refugee in America, and supporting a family of 10. He has and remains a large part of my life.

**Receptor-Mediated Uptake and Intracellular Sorting  
of Multivalent Lipid Nanoparticles against the  
Epidermal Growth Factor Receptor (EGFR) and the Human EGFR 2 (HER2)**

by

David Tu Tran

**Abstract**

In the area of receptor-targeted lipid nanoparticles for drug delivery, efficiency has been mainly focused on cell-specificity, endocytosis, and subsequently effects on bioactivity such as cell growth inhibition. Aspects of targeted liposomal uptake and intracellular sorting are not well defined. This dissertation assessed a series of ligands as targeted functional groups against HER2 and EGFR for liposomal drug delivery. Receptor-mediated uptake, both mono-targeted and dual-targeted to multiple receptors of different ligand valence, and the intracellular sorting of lipid nanoparticles were investigated to improve the delivery of drugs to cancer cells.

Lipid nanoparticles were functionalized through a new sequential micelle transfer - conjugation method, while the micelle transfer method was extended to growth factors. Through a combination of both techniques, anti-HER2 and anti-EGFR dual-targeted immunoliposomes with different combinations of ligand valence were developed for comparative studies. With the array of lipid nanoparticles, the uptake and cytotoxicity of lipid nanoparticles in relationship to ligand valence, both mono-targeting and dual-targeting, were evaluated on a small panel of breast cancer cell lines that express HER2 and EGFR of varying levels. Comparable uptake ratios of ligand to expressed receptor

and apparent cooperativity were observed. For cell lines that express both receptors, additive dose-uptake effects were also observed with dual-targeted immunoliposomes, which translated to marginal improvements in cell growth inhibition with doxorubicin delivery. Colocalization analysis revealed that ligand-conjugated lipid nanoparticles settle to endosomal compartments similar to their attached ligands. Pathway transregulation and pathway saturation were also observed to affect trafficking. In the end, liposomes routed to the recycling endosomes were never observed to traffic beyond the endosomes nor to be exocytose like recycled ligands.

Based on the experimental data, models were developed to help interpret and predict the binding and trafficking of lipid nanoparticles. The crosslink multivalent binding model of lipid nanoparticles to monovalent receptors was able to predict ligand valence for optimum binding, cell association concentrations, offer explanations to the antagonistic effects observed from high ligand valence, and predict the binding limitations of both ligand valence and ligand affinity. Hopefully, the models will serve as valuable tools for future optimizations in targeted liposomal drug delivery.

## Table of Contents

Abstract.....	iv
List of Tables .....	xi
List of Figures.....	xi
Abbreviations.....	xiv
Chapter 1: A Review of Lipid Nanoparticles for Targeted Drug Delivery .....	1
1.1 Abstract.....	1
1.2 Design and Engineering Challenges of Drug Delivery Systems .....	2
1.3 Liposomal Drug Delivery Systems.....	3
1.4 Passive Targeting.....	6
1.5 Active Targeting .....	7
1.6 Receptor-Mediated Endocytosis .....	12
1.7 Intracellular Pathways.....	16
1.8 Uptake Efficiency and Effect.....	22
1.9 Conclusion .....	24
Chapter 2: The Engineering of HER2-Targeted and EGFR-Targeted Lipid Nanoparticles .....	26
2.1 Abstract.....	26
2.2 Introduction to the ErbB Family of Receptor Tyrosine Kinases .....	27
2.2.1 EGFR and its Ligands.....	28
2.2.2 HER2 and its Ligands .....	29
2.3 Receptor-Targeted Lipid Nanoparticles.....	30
2.4 Engineering Receptor-Targeted Lipid Nanoparticles .....	32

2.5 Results and Discussion .....	34
2.5.1 Conjugates of Antibody Fragments and Growth Factors .....	34
2.5.2 Ligand Conjugation onto Liposomes by the Micelle Transfer Method and Sequential Micelle Transfer - Conjugation Method .....	36
2.5.3 Anti-HER2 and Anti-EGFR Dual-Targeted Immunoliposomes.....	39
2.5.4 EGF-Conjugated and TGF $\alpha$ -Conjugated Liposomes .....	41
2.5.5 Anti-Tumor Efficacy Mouse Study with EGFR-Targeted Paclitaxel Immunoliposomes.....	46
2.6 Conclusion .....	48
2.6 Materials and Methods.....	50
2.6.1 Materials .....	50
2.6.2 Cell Lines.....	51
2.6.3 Liposome Preparation .....	51
2.6.4 Conjugates of Trastuzumab and Cetuximab Fab' .....	52
2.6.5 Conjugates of EGF and TGF $\alpha$ .....	53
2.6.6 Ligand Conjugation onto Liposomes by the Micelle Transfer Method and Sequential Micelle Transfer - Conjugation Method .....	54
2.6.7 Anti-HER2 and Anti-EGFR Dual-Targeted Immunoliposomes.....	54
2.6.8 Fluorescent Ligands.....	55
2.6.9 Cell Association Studies .....	56
2.6.10 Uptake Studies .....	56
2.6.11 Animal Study with EGFR-Targeted Paclitaxel Immunoliposomes.....	57
2.6.12 Statistical Analysis.....	57



Chapter 3: Uptake Efficiency and Effect.....	58
3.1 Abstract.....	58
3.2 Introduction.....	59
3.3 Results and Discussion .....	61
3.3.1 Cell Association of HER2-Targeted, EGFR-Targeted, and Dual-Targeted Immunoliposomes in HER2-Expressing and EGFR-Expressing Cell Lines.....	61
3.3.2 Uptake of HER2-Targeted Immunoliposomes and Trastuzumab in Relationship to Receptor Expression Level.....	64
3.3.3 Dose-Uptake of HER2-Targeted and EGFR-Targeted Immunoliposomes of Varying Ligand Densities .....	66
3.3.4 Additive Dose-Uptake Effect of Anti-HER2 and Anti-EGFR Dual-Targeted Immunoliposomes.....	71
3.3.5 Cytotoxicity Studies of Doxorubicin-Encapsulated HER2-Targeted, EGFR- Targeted, and Dual-targeted Immunoliposomes.....	77
3.4 Conclusion .....	81
3.5 Materials and Methods.....	82
3.5.1 Materials .....	82
3.5.2 Cell Lines.....	83
3.5.3 Cell Association Studies .....	83
3.5.4 Uptake and Dose-Uptake Studies .....	84
3.5.5 Cytotoxicity Studies.....	85
3.5.6 Statistical Analysis.....	85

Chapter 4: Analysis of Intracellular Sorting .....	86
4.1 Abstract .....	86
4.2 Introduction .....	87
4.3 Results and Discussion .....	90
4.3.1 Endosomal Colocalization Analysis of HER2-Targeted and EGFR-Targeted Liposomes and Ligands .....	90
4.3.2 Trafficking of Trastuzumab and Trastuzumab-Conjugated Immunoliposomes .....	93
4.3.3 Delivery of Trastuzumab-Conjugated Immunoliposomes Compared to Trastuzumab Conjugates .....	99
4.3.4 Trafficking of F5 scFv and F5 scFv-Conjugated Immunoliposomes .....	100
4.3.5 Trafficking of EGF, TGF $\alpha$ , EGF-Conjugated and TGF $\alpha$ -Conjugated Liposomes .....	102
4.3.6 Trafficking of Cetuximab and Cetuximab-Conjugated Immunoliposomes...	107
4.3.7 Cytotoxicity Studies of Pathway-Targeted Doxorubicin-Encapsulated HER2- Targeted and EGFR-Targeted Liposomes .....	108
4.4 Conclusion .....	112
4.5 Materials and Methods .....	114
4.5.1 Materials .....	114
4.5.2 Trafficking through the Endosomal Compartments .....	114
4.5.3 Immunocytochemistry .....	115
4.5.4 Confocal Microscopy .....	116
4.5.5 Colocalization Analysis .....	116

4.5.6 Ligand and Liposomal Recycling Assessments by Flow Cytometry .....	117
4.5.7 Cytotoxicity Studies.....	117
4.5.8 Uptake Studies .....	118
Chapter 5: Mathematical Insights on the Binding and Trafficking of Multivalent Lipid	
Nanoparticles .....	119
5.1 Abstract.....	119
5.2 Introduction.....	120
5.3 Crosslink Multivalent Binding Model of Multivalent Lipid Nanoparticles to Monovalent Receptors .....	123
5.3.1 High Receptor Expression Model.....	126
5.3.2 Intermediate and Low Receptor Expression Models.....	132
5.3.3 Data Fitting, Limitations, and Optimization .....	133
5.4 Compartmental Model of the Intracellular Trafficking of Multivalent Lipid Nanoparticles .....	137
5.5 Conclusion .....	139
5.6 Methods.....	140
Chapter 6: Concluding Remarks.....	141
References.....	144

## List of Tables

Table 2.1 Formulations of HER2-targeted, EGFR-targeted, and dual-targeted immunoliposomes (ILS) .....	41
Table 3.1 Uptake studies of trastuzumab, trastuzumab-conjugated and F5 scFv-conjugated immunoliposomes (ILS) in BT-474 and MCF-7/HER2 cells. ....	65
Table 3.2 Accumulation of liposomes (LS) and ligands (Lg) from HER2-targeted, EGFR-targeted, and dual-targeted immunoliposomes (ILS).....	73
Table 4.1 Colocalization percentage of HER2-targeted immunoliposomes (ILS) and ligands in the recycling endosomes (RE) and the late endosomes (LE) of BT-474 and MCF-7/HER2 cells. ....	96
Table 4.2 Colocalization percentage of EGFR-targeted liposomes (LS) and ligands in the recycling endosomes (RE) and the late endosomes (LE) of MKN-7 and MDA-468 cells. ....	107

## List of Figures

Figure 1.1 Receptor-targeted lipid nanoparticles.....	4
Figure 1.2 Passive and active targeted delivery.....	7
Figure 1.3 Schematic of the rapid screening and identifying of high-affinity internalizing ligands from a phage display library(42).....	10
Figure 1.4 Schematic of receptor-mediated endocytosis and intracellular sorting .....	15
Figure 1.5 Recycling behaviors of EGF, TGF $\alpha$ , and trastuzumab discussed in the literature.....	17

Figure 1.6 Dose-dependent trafficking and transduction of adeno-associated virus type-2 (AAV2) discussed in the literature(89).....	20
Figure 2.1 The ErbB family of receptor tyrosine kinases.....	27
Figure 2.2 Synthesis of trastuzumab-Fab'-PEG-DSPE and cetuximab-Fab'-PEG-DSPE. .....	35
Figure 2.3 Synthesis of EGF-PEG-DSPE and TGF $\alpha$ -PEG-DSPE.....	36
Figure 2.4 Schematic of the micelle transfer method and the sequential micelle transfer - conjugation method.....	38
Figure 2.5 Schematic of constructing anti-HER2 and anti-EGFR dual-targeted immunoliposomes.....	40
Figure 2.6 Cell association of EGF-conjugated and TGF $\alpha$ -conjugated liposomes (LS) in MDA-468 cells.....	44
Figure 2.7 Anti-tumor efficacy of anti-EGFR cetuximab-conjugated paclitaxel immunoliposomes (ILS) and liposomal paclitaxel in mice.....	48
Figure 3.1 Cell association of HER2-targeted, EGFR-targeted, and dual-targeted immunoliposomes (ILS) of varying ligand densities.....	63
Figure 3.2 Dose-uptake studies of HER2-targeted, EGFR-targeted, and dual-targeted immunoliposomes (ILS) of varying ligand densities.....	70
Figure 3.3 Scatchard plots for dose-uptake studies of HER2-targeted, EGFR-targeted, and dual-targeted immunoliposomes (ILS) of varying ligand densities.....	75
Figure 3.4 Cytotoxicity studies of doxorubicin-encapsulated HER2-targeted, EGFR- targeted, and dual-targeted immunoliposomes (ILS).....	79

Figure 4.1 Colocalization analysis of pixel shifted TetraSpeck fluorescent microspheres. .....	92
Figure 4.2 Cellular uptake of anti-HER2 trastuzumab and F5 scFv-PEG-DSPE in BT-474, MCF-7/HER2, and SK-BR-3 cells visualized by microscopy.....	93
Figure 4.3 Endosomal colocalization analysis of trastuzumab-conjugated immunoliposomes (ILS) and trastuzumab in HER2-expressing cells. ....	95
Figure 4.4 Ligand and liposomal recycling assessments by flow cytometry. ....	98
Figure 4.5 Endosomal colocalization analysis of F5 scFv-conjugated immunoliposomes (ILS) and F5 scFv-PEG-DSPE in HER2-expressing MCF-7/HER2 cells. ....	100
Figure 4.6 Cellular uptake of anti-EGFR EGF, TGF $\alpha$ , cetuximab, and ligand-conjugated liposomes (LS) in MDA-468 cells visualized by microscopy. ....	102
Figure 4.7 Endosomal colocalization analysis of EGFR-targeted liposomes (LS) and ligands in EGFR-expressing cells. ....	104
Figure 4.8 Cytotoxicity studies of doxorubicin-encapsulated anti-HER2 trastuzumab-conjugated immunoliposomes (ILS) and geldanamycin (GA) in BT-474 and MCF-7/HER2 cells. ....	109
Figure 4.9 Cytotoxicity and uptake studies of doxorubicin-encapsulated anti-EGFR cetuximab-conjugated immunoliposomes (ILS) and phorbol myristate acetate (PMA) in MDA-468 cells.....	111
Figure 5.1 Schematic of monovalent binding. ....	120
Figure 5.2 Schematic of the crosslink multivalent binding model of multivalent lipid nanoparticles to monovalent receptors.....	123

Figure 5.3 Cell association of F5 scFv-conjugated immunoliposomes (ILS) with increasing valence in MCF-7/HER2 cells.....	127
Figure 5.4 Crosslink multivalent binding model predictions in high receptor expressing cells. ....	129
Figure 5.5 Crosslink multivalent binding model predictions for all plausible valence and effective valence ( $f \leq v$ ) in high receptor expressing cells. ....	131
Figure 5.6 Crosslink multivalent binding model predictions in intermediate and low receptor expressing cells. ....	133
Figure 5.7 Crosslink multivalent binding model prediction for increased affinity.....	135
Figure 5.8 Compartmental model of the intracellular trafficking of multivalent lipid nanoparticles. ....	137
Figure 5.9 Mathcad data calculations for the crosslink multivalent binding model.....	140

## Abbreviations

AAV2	Adeno-associated virus type-2
Ab	Antibody
AF488	Alexa Fluor 488
AF546	Alexa Fluor 546
$C_{Beq}$	Cell associated liposomes concentration at equilibrium
$C_i$	Concentration of a lipid nanoparticle bound to the cell surface via $i$ of its available surface-attached ligands
$C_{Lg}$	Ligand/receptor complex
Cy3	Cyanine 3
DAPI	4',6-Diamidino-2-phenylindole
DiD	1,1'-Dioctadecyl-3,3',3',3'-tetramethylindodicarbocyanine perchlorate
DiO	3,3'-Dioctadecyloxycarbocyanine perchlorate
Dox	Doxorubicin
DSPC	1,2-Distearoyl-sn-glycero-3-phosphocholine
DSPE	1,2-Distearoyl-sn-glycero-3-phosphoethanolamine
EDTA	Ethylenediaminetetraacetic acid

EE	Early endosome
EGF	Epidermal growth factor
EGFR	Epidermal growth factor receptor
EPR	Enhanced permeability and retention effect
Eq	Equilibrium
Equiv.	Equivalent
ExHy	Immunoliposomes with $x$ anti-EGFR ligands and $y$ anti-HER2 ligands per liposome
$f$	Effective valence
$f_{\text{deg}}$	Fraction degraded
$f_{\text{rec}}$	Fraction recycled
F5 scFv	F5 single-chain variable fragment that binds HER2
Fab'	Antigen-binding fragment
Fab <sub>2</sub>	Two antigen-binding fragments connected by disulfide bonds
Fc	Crystallizable fragment
FITC	Fluorescein isothiocyanate
GA	Geldanamycin
Geld	Geldanamycin
GF	Growth factor
HBS	HEPES-buffered saline
HEPES	4-(2-Hydroxyethyl)-1-piperazineethanesulfonic acid
HER1	Human epidermal growth factor receptor 1
HER2	Human epidermal growth factor receptor 2
HER3	Human epidermal growth factor receptor 3
HER4	Human epidermal growth factor receptor 4
$i$	Number of bounds
IC50	Half maximal inhibitory concentration
IgG	Immunoglobulin G
ILS	Immunoliposome
$K_D$	Equilibrium dissociation constant
$k_d$	Dissociation rate constant
$k_{\text{endo}}$	Endocytosis rate constant
$k_{\text{exo}}$	Exocytosis rate constant
$k_f$	Associating rate constant
$K_x$	Crosslinking equilibrium constant
$k_x$	Receptor crosslinking rate constant
$k_{-x}$	Receptor decrosslinking rate constant
$L$	Lipid nanoparticle concentration (free)
$L_o$	Lipid nanoparticle concentration (free), initial
LE	Late endosome
Lg	Ligand
LS	Liposome
mAb	Monoclonal antibody
Mal	Maleimide
Mal-PEG-DSPE	1,2-Distearoyl-sn-glycero-3-phosphoethanolamine-N-[maleimide(polyethylene glycol)-2000]



MES	2-(N-Morpholino)ethanesulfonic acid
MFI	Mean fluorescent intensity
MOI	Multiplicities of infection
MOPS	3-(N-Morpholino)propanesulfonic acid
MP	Megapixel
MTT	(3-(4,5-Dimethylthiazol-2-yl)-2,5-diphenyltetrazolium bromide
NaCl	Sodium chloride
NE	Not evaluable
NT	Non-targeted (liposome)
Nu	Nucleus
PBS	Phosphate-buffered saline
PEG	Polyethylene glycol
PEG-DSPE	1,2-Distearoyl-sn-glycero-3-phosphoethanolamine-N-[methoxy(polyethylene glycol)-2000]
PL	Phospholipid
PMA	Phorbol myristate acetate
Q	Pertaining to receptor or lipid nanoparticle
R	Receptor concentration
RE	Recycling endosome
$R_{eq}$	Free receptors concentration at equilibrium
RES	Reticuloendothelial system
RhuMAb	Recombinant humanized monoclonal antibody
RT	Room temperature
$R_T$	Total receptors
scFv	Single-chain variable fragment
SCID	Severe combined immunodeficiency
SDS-PAGE	Sodium dodecyl sulfate polyacrylamide gel electrophoresis
SE	Standard error
SH	Sulfhydryl group
TEA	Triethanolamine
TGF $\alpha$	Transforming growth factor receptor alpha
Tras	Trastuzumab
UCSF	University of California San Francisco
UV	Ultraviolet
v	Valence (ligands per lipid nanoparticle)
$V^R$	Receptor synthesis

# **Chapter 1: A Review of Lipid Nanoparticles for Targeted Drug Delivery**

## **1.1 Abstract**

Recent advancements in the systemically administration of chemotherapeutic agents for the treatment of cancer have benefited from the repackaging of the highly toxic yet nonspecific small molecule drugs into more favorable distributing drug delivery systems. Drugs tethered as conjugates or encapsulated into nanoparticles composed from lipids, polymers, and peptides have significantly altered its delivery profile by taking on the pharmacokinetics and drug delivery capabilities of the carrier and resulting often with more efficient therapeutic effects. Lipid nanoparticles such as liposomes haven proven to be a biocompatible delivery system with increased bioavailability due to prolonged circulation times of drugs and high drug accumulation in pathological sites attributed to the enhanced permeability and retention effect. In addition, lipid nanoparticles can further target and be endocytosed into targeted tissues with the surface attachment of ligands specific to overexpressed receptors displayed on the tissues. This chapter describes the design and engineering challenges of drug delivery systems, the benefits of liposomes as a drug delivery system, both passive and active targeting strategies, and finally essential components of active targeting including uptake and intracellular sorting.

## 1.2 Design and Engineering Challenges of Drug Delivery Systems

The objective of drug delivery systems is to increase drug flux to cells of interest for therapeutic effects while minimizing interaction with the rest of the body. To better design such systems for the treatment of cancer, one must better understand the shortcomings of current chemotherapy. The treatment of cancer still heavily relies on the administration of chemotherapeutic agents with the intent of killing rapidly dividing cells. The outcome may be curative, to prolong life, or to palliate symptoms. Most cytotoxic drugs are nonspecific, distributed within the body rather evenly and proportionally to the regional blood flow, resulting in substantial indiscriminant toxicity to other tissue in the body. In addition to the high level of toxicity in healthy tissues, small molecule chemotherapeutic agents have a large volume of distribution on intravenous administration and a narrow therapeutic index(1-3). With the large volume of distribution, rapid clearance rate from circulation, and nonspecific targeting to tumors, high doses are often required for therapeutic effects.

The drug delivery system must minimize interaction with the rest of the body. In terms of distribution, the system should reduce the volume of distribution, increase accumulation in tissues of interest, decrease accumulation in nonspecific tissues, and hence decrease nonspecific toxicities. The system should be biocompatible and non-immunogenic, reducing clearance rates by macrophages of the reticuloendothelial system (RES) as well as degrade to nontoxic components. Long circulating times can be beneficial, allowing the drug delivery system time to accumulate in the target tissue, increasing the bioavailability, and hence increasing drug flux to cells of interest. High drug loading can also increase availability.

To keep the drug active, the system formulation should be stable and protect the drug from metabolism and inactivation in the plasma, yet leaks drug at sufficient rate to become bioavailable at the tumor. The attachment of ligands targeting receptor overexpressed on the tumors can also increase the delivery of drugs to the cells of interest. These ligands need to be stable, target-specific, non-immunogenic, capable of receptor-mediated endocytosis, and readily accessible to target receptors(4). The choice of the targeted receptor offers cell-specificity and receptor-mediated uptake, but much is still unknown about uptake efficiency and subsequently the intracellular routing.

### **1.3 Liposomal Drug Delivery Systems**

Liposomes, first described by Dr. Alec D. Bangham in 1961, are artificially-prepared vesicles composed of a lipid bilayer. Having an aqueous interior space protected from a lipid bilayer, they are popular as delivery vehicles for pharmaceutical drugs, nutrients, and markers. The aqueous interior is favorable to entrap water-soluble chemotherapeutic agents while lipid-soluble hydrophobic agents can be partitioned into the lipid bilayer (Figure 1.1). Polyethylene glycol (PEG) is often incorporated to provide a protective layer. The surface of liposomes can also be functionalized with ligands such as antibodies to target receptors expressed on cells of interest. Liposomes are considered nontoxic and biocompatible unless administered at very high doses with little antigenic, pyrogenic, allergic, and toxic reactions(1, 5, 6). They are easily biodegraded and protect the host from undesirable effects of the encapsulated drug and well as protect the drug from metabolism and inactivation of the physiological medium. PEG is also considered nontoxic at 1.9-5 kDa and excreted unmetabolized in the urine(7).

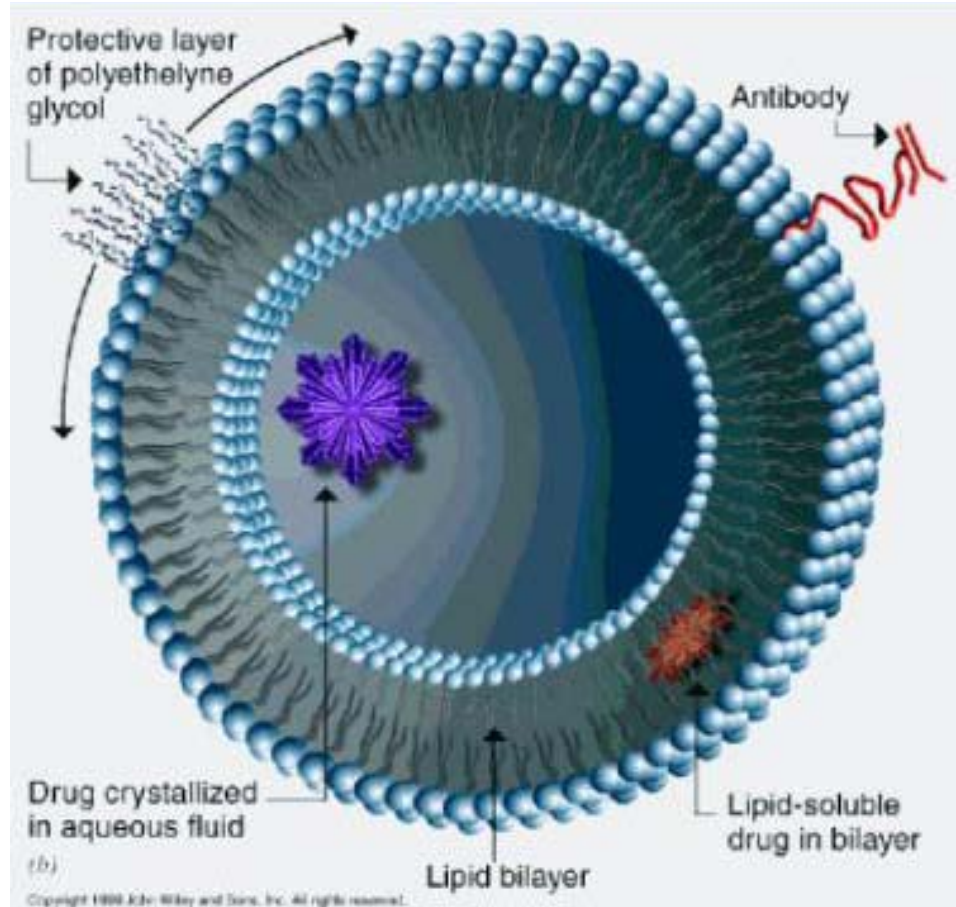


**Figure 1.1 Receptor-targeted lipid nanoparticles.** Liposomes contain a lipid membrane with an aqueous interior favorable to entrap water-soluble chemotherapeutic agents; lipid-soluble hydrophobic agents can be partitioned into the lipid bilayer. Polyethylene glycol is incorporated to provide a protective layer. The surface of liposomes can also be functionalized with ligands such as antibodies to target receptors expressed on cells of interest. Image acquired from Nanopharmaceuticals.org.

As a drug delivery system for chemotherapeutic agents in the treatment of cancer, the ideal liposome is 70-120 nm, charge-neutral, composed of high-phase transition phospholipids and cholesterol, and shielded with PEG(4). The inclusion of a polymer coating PEG in the liposome composition results in clearance rates that are relatively insensitive to size in the range of 80-250 nm (8-10), membrane fluidity, and surface charge(1, 11). PEG in the stealth liposomes provides sterical stabilization to the liposome, limit binding of serum opsonins as well as interaction with cells like

macrophages in RES, and hence increase circulation time and tumor localization(1, 2, 12, 13). The presence of negatively charged lipids in liposomes may result in rapid uptake by RES and interference with stability(14, 15), but it is not always true. Anionic lipids such as ganglioside GM<sub>1</sub> or phosphatidylinositol(16) or charged liposomes coated with PEG may increase circulation(1, 17, 18).

Liposomes as a drug delivery system alter the pharmacokinetic profile of the drug encapsulated to the profile of liposomal carrier. Some chemotherapeutic drugs encapsulated in the aqueous core or incorporated in the lipid bilayer layer include daunomycin, doxorubicin, cisplatin, vinorelbine, topotecan, AraC, vinblastine, vincristine, PALA, methotrexate, paclitaxel, and irinotecan(1). Doxil (Janssen Products, Johnson & Johnson) is a sterically stabilized liposome-encapsulated form of doxorubicin used for the treatment of ovarian cancer, multiple myeloma, and Kaposi's sarcoma. The surface of the Doxil is pegylated, ensuring long circulation times and high drug accumulation in solid tumors, antitumor activity improved toxicity profile, reduced cardiotoxicity and haematological toxicities(1, 19). Stealth liposomes have non-saturable, log-linear kinetics(11). The terminal half-life in humans for pegylated liposomal doxorubicin is 79 hr(20), with an area under the curve (AUC) for concentration versus time in plasma 200-1000 times greater than that for most unencapsulated drugs(1). Peak doxorubicin levels are 3-15 fold greater in tumors when delivered via liposomes compared with free drug(1).

## 1.4 Passive Targeting

Solid tumors are supported by a discontinuous microvasculature with pore sizes varying between 100-780 nm, allowing the passage of large molecules and nanoparticles(21, 22). The accumulation of large molecules and liposomes in tumors, the result of a leaky microvasculature and an impaired lymphatics supporting the tumor area, is a phenomenon known as the enhanced permeability and retention effect (EPR) (Figure 1.2)(23, 24). EPR is limited to pathological sites with affected and leaky vasculature such as solid tumors, sites of inflammations, and infarcted areas. Large molecules or particles 10-500 nm like liposomes can extravasate through the endothelium and localize in the tumor interstitium(25, 26). Because free cytotoxic agents are small, they are localized in the tumor rapidly, but are also cleared rapidly, resulting in considerable lower tumor AUC for free drug than liposomal drugs(27, 28). Despite the increased in tumor accumulation, distribution of liposomes within the tumor interstitium is still limited, resulting from high interstitial pressure and a large interstitial space.

Liposomes in the interstitium space are not usually found within tumor cells but are found inside tumor macrophages. Ideally once in the interstitium space, drug leaks at sufficient rate to become bioavailable at the tumor. Drug may leak due to instabilities from conditions in the interstitium, plasma protein, enzymes, or liposomal degradation by macrophages. Released drug can act on neighboring cells via a bystander effect. Passive targeting is limited to pathological sites susceptible to the EPR. In addition, it relies on the diffusion of drugs from the liposomes into the cells of interest. As a result, the delivery of drugs and nucleotides that are prone to degradation from the plasma

environment is not ideal in this technique. Active targeting with intracellular delivery can be a more promising route.

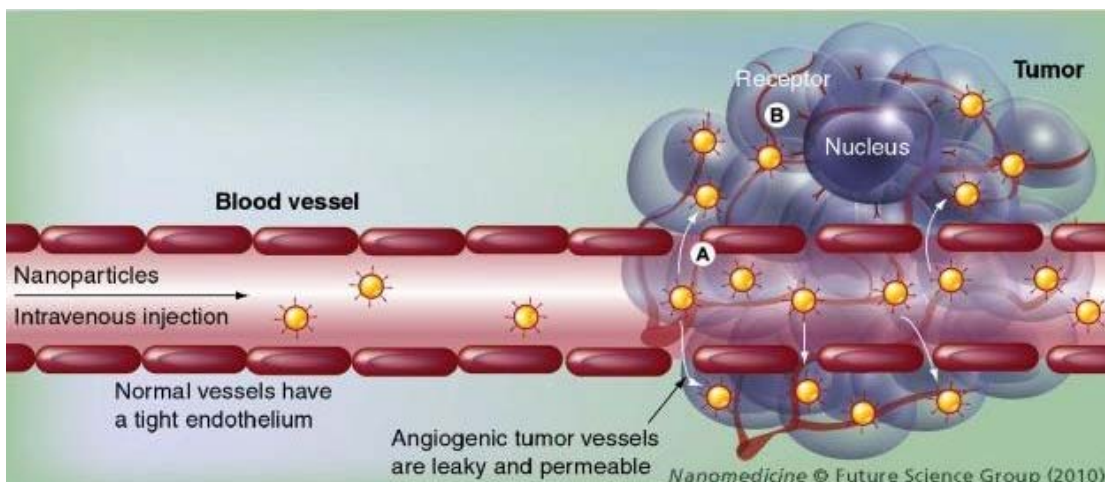


**Figure 1.2 Passive and active targeted delivery.** *A.* Passive targeting - nanoparticles accumulate in tumors through the leaky and permeable tumor vasculature and impaired lymphatic system known as the enhanced permeability and retention effect. *B.* Active targeting - ligand-conjugated nanoparticles bind to receptors expressed on tumor cells of interest resulting in cell-specific recognition and improved drug delivery to solid tumors. Image acquired from the Nanomedicine Future Science Group.

## 1.5 Active Targeting

Ligands that induce receptor-mediated endocytosis upon binding can be engineered onto liposomes for the delivery of drugs intracellularly to tumors (Figure 1.2). Liposomes delivered for solid tumors first benefit from passive targeting, accumulating in the tumor interstitium due to the EPR. Once trapped, targeting increases the opportunity for intracellular uptake. Once internalized, drugs are believed to be released by degradative enzymes in the late endosomes and lysosomes, increasing drug bioavailability and reducing diffusion from the tumor(29). Ligand targeting increases the delivery of drugs beyond solid tumors that require extravasation to readily accessible cells via the intravascular route including blood-borne malignancies and angiogenic



blood vessels. Targeting angiogenic microvasculature focuses on triggering apoptosis in the endothelial cells instead of the tumor, diminish blood supply to the tumor, and damage the vasculature.

Although ligand-targeting liposomes for the treatment of cancer are still in clinical trials, many therapeutic antibodies have been approved by the FDA such as anti-HER2 Herceptin (Roche), anti-EGFR Erbitux (ImClone LLC), anti-CD52 Campath (Genzyme), anti-vascular endothelial growth factor-A Avastin (Roche), anti-CD30 Adcetris (Seattle Genetics), anti-EGFR Vectibix (Amgen Inc.), and anti-CD20 Rituxan (Roche)(4, 30). Antibody-directed therapies also have been approved such as anti-CD33 calicheamicin conjugate gemtuzumab Mylotarg (Wyeth, withdrawn from market in 2010), and anti-CD20 yttrium-90 conjugate ibritumomab Zevalin (Spectrum Pharmaceuticals)(4, 30). These antibodies can alter normal receptor function, inhibit binding of receptor ligands, regulate downstream receptor functions, induce apoptosis, and direct therapeutics to the site of disease.

Receptor expression in human cancer is heterogeneous. Targeted receptor should be selectively expressed or overexpressed on target cells and lowly expressed level on non-targeted cells to decrease toxicity. For example, HER2 is a good target for drug delivery because it is overexpressed on a variety of cancers, has a homogenous expression pattern, lack significant shedding, and capable of inducing internalization(4, 31, 32). Other popular targets for solid tumor antigens include EGFR, CD44, GD2, folate receptor, transferrin receptor, and integrins. Many ligands have been utilized for ligand-targeted liposomes including antibodies or antibody fragments, proteins such as

transferrin, small molecules such as folic acid or folate, peptides, sugars, and RNA aptamers.

There are advantages of delivering drugs via liposomes instead of directly conjugating them to ligands. As discussed earlier, liposomes have favorable circulations times mainly attributed to EPR, which can be reduced with smaller conjugates. The liposomes protect the drug while conjugates are exposed. While liposomes with a size of 100 nm can encapsulate  $15-40 \times 10^3$  drug molecules per liposome and require 15-40 antibody fragments or 300-1000 peptides per liposome for optimum delivery, drug conjugated directly to an antibody usually has a maximum density of 8-12 drugs per antibody(4, 33-37). Hence another benefit for ligand-targeting liposomes as a drug delivery system is the high payload. The amount of drug that can be delivered to target per one ligand molecule is high.

There has been much development with the rapid screening and identifying of tumor-specific high affinity internalizing human antibodies and antibody fragments from phage and yeast display of non-immune phage antibody libraries (Figure 1.3)(38-42). Selection of ligands should be based on internalization, not just binding. The antitumor activity of HER2-targeted liposomal doxorubicin has been shown to be more significant when delivered from by more efficient internalizing ligands than by less efficient ones(43, 44). Antibodies attached to liposomes can increase clearance due to either an immune response to foreign protein or to recognizable fragment crystallizable region (Fc) receptor on macrophages. To reduced immunogenicity, antibodies should be human or humanized. Antibody fragments such as antigen-binding fragment (Fab') or single-chain

variable fragment (scFv) are preferable to full IgG because they are recognized by the Fc receptor present on macrophages of RES resulting in increased clearance(45, 46).

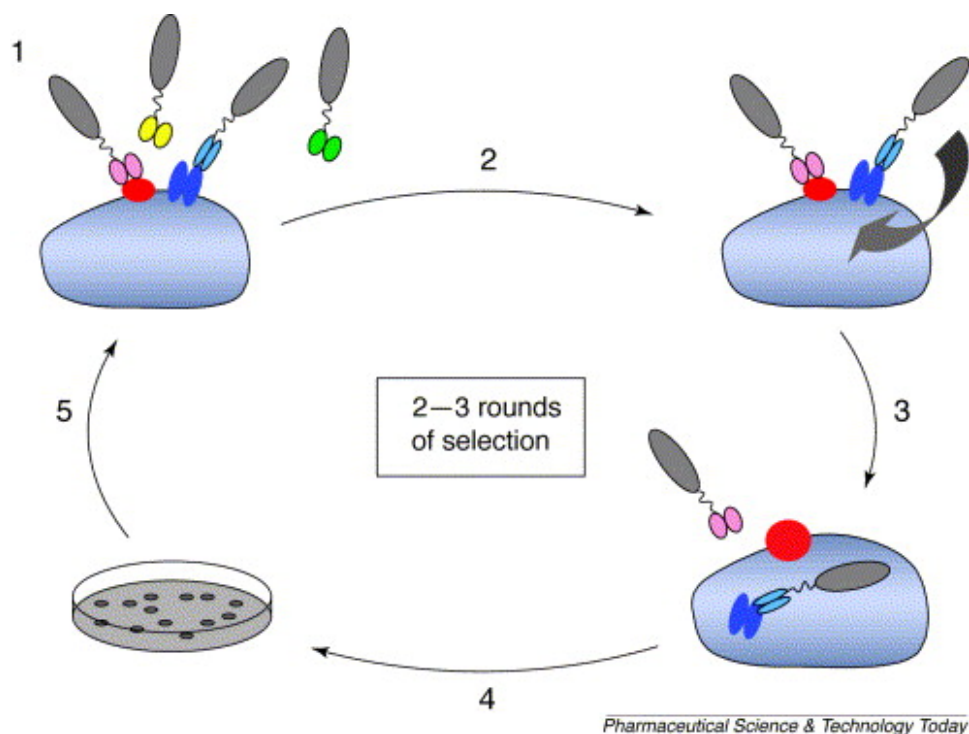


**Figure 1.3 Schematic of the rapid screening and identifying of high-affinity internalizing ligands from a phage display library(42).** 1. Phage antibody library is incubated with the target cells at 4° C to reduce internalization. 2. Unbound phage is washed away and cells are returned to 37° C for < 15 minutes to enable the internalization of phage bound to internalizing receptors. 3. Cell-surface-bound phage are stripped with a low pH acid buffer. 4. Cells are lysed and phage recovered by re-infection into Escherichia coli. 5. Phage are re-amplified for additional rounds of selection. Image acquired from Pharmaceutical Science & Technology Today.

Amphiphilic conjugates of targeting ligands consisting of a hydrophilic polymer spacer between a lipid anchor and a ligand group can be attached to the surface of liposomes to offer receptor-specific targeting. The conjugate can be synthesized with three main conjugation methods: reaction between activated carboxyl groups and amino groups yielding an amide bond, reaction between pyridyldithiols and thiols yielding disulfide bonds, and reaction between maleimide derivatives and thiols yielding thioether

bonds(26). With the later, conjugation of ligands such as antibody fragments with maleimide chemistry using naturally occurring cysteine residue, engineered C-terminal cysteine, or thiolated with Traut's reagent provide strong stable bonds. Reactions with the cysteine on antibody fragments can offer ideal orientation, distant from antibody binding site, minimizing interference with binding. A polymer linker like PEG also helps with the orientation, extending the ligand far enough from the PEG shielding so the ligand are accessible to receptors on cells.

Through the micelle transfer method, micellar conjugates of the ligand and an amphiphilic lipid co-incubated with preformed liposomes spontaneously insert themselves into liposome bilayers without the loss of the liposome integrity(47), providing a rapid and simple method for transforming non-targeted liposomes into antibody-targeted liposomes(48, 49). Insertion is performed at 55-60° C, so the denaturation of protein ligands is a concern, but longer overnight incubation at 37° C is also possible(34, 48). Liposomes remain mostly unaltered through conjugations, and the techniques have shown to be simple and reproducible.

HER2-targeted and EGFR-targeted liposomes encapsulating drugs such as doxorubicin have been shown to undergo specific receptor-mediated endocytosis, resulting in significant cytotoxic activity in receptor-overexpressing cells *in vitro* and *in vivo*(34-36, 44, 50, 51). The pharmacokinetics of HER2-targeted liposomes are not affected by the conjugation of antibody fragments, having similar pharmacokinetics to non-targeted liposomes(52). In addition, the cytotoxicity effects are not directly dependent on the antibody effects on the tumor; free Herceptin (trastuzumab) and liposomal doxorubicin or empty HER2-targeted immunoliposomes have inferior activity.

The highly specific antitumor activity of anti-HER2 immunoliposomal doxorubicin in HER2-overexpressing models resulted from efficient *in vivo* delivery of liposomal therapeutic intracellularly. Biodistribution studies for tumor localization are nearly identical comparing non-targeted and HER2-targeted liposomes, suggesting that extravasation and the EPR effect are primarily responsible for tumor accumulation of liposomes in solid tumors(50); other studies are in agreement with these results(53). HER2-targeted immunoliposomes that reside intracellularly in tumor cells had a more diffuse distribution within the tumor; non-targeted localized in tumor interstitium and inside tumor-associated macrophages(50).

The intracellular delivery of molecules into cells as opposed to simple diffusion increases the bioavailability. Hydrophobic, easily denatured, and metabolized drugs benefit from the protection of the lipid bilayer from the plasma. Because of the low efficiency of internalizing on their own, they also benefit from the intracellular delivery of ligand-targeting liposomes. Finally, intracellular drug delivery with immunoliposomes have also been shown to overcome multidrug resistance mechanisms, with immunoliposomes exhibiting better accumulation and cytotoxic effects than free drug for multi-drug resistant cell lines *in vitro* and *in vivo*(54-56). Targeted, intracellular delivery has been demonstrated to enhance the liposomal drug delivery system.

## **1.6 Receptor-Mediated Endocytosis**

All eukaryotic cells exhibit some form of endocytosis to maintain homeostasis, at the cellular level by recovering protein and lipid components and at the organismal level by controlling activities including transmission of neuronal, metabolic, and proliferative

signals, nutrient uptake, and defense preparation(57). Multiple types of endocytosis exist including phagocytosis, clathrin-independent endocytosis, and clathrin-dependent endocytosis. The endocytosis of many signaling receptors is stimulated by ligand-induced activation, with virtually every signaling receptor family undergoing clathrin-dependent endocytosis(58). To ensure the internalization of lipid nanoparticles into targeted cells, attached high affinity ligands must be internalizing to induce receptor-mediated clathrin-dependent endocytosis upon binding. In essence, the lipid nanoparticles are piggybacking on the ligands during endocytosis.

Endocytosis is typically initiated by the binding of transmembrane receptors and their extracellular ligands into cytoplasmic vesicles that are pinched off from the plasma membrane (Figure 1.4). Receptor-ligand complexes are recruited to clathrin-coated pits and invaginate inwards to form clathrin-coated vesicles(59). Endocytosed vesicles fuse with early endosomes, and subsequently receptor-ligand complexes can dissociate and traffic to the recycling compartment containing Rab11 or to the late endosomal compartment containing Rab7(57, 58). Many receptor-ligand complexes dissociate in the early endosomes due to the slightly acidic pH (pH ~6.0-6.8)(57, 58, 60-63). While receptors and ligands in recycling endosomes are returned to the plasma membrane, fusion of late endosomes with lysosomes (pH ~4.0-5.5) carrying proteolytic enzymes results in cargo degradation(57, 63).

Endosomal trafficking is controlled by several Rab proteins, small guanosine triphosphate-binding proteins(57, 58). The Rab family is the largest branch of the Ras superfamily with more than 60 members found in mammalian cells. Rab proteins reside in particular types of endosomes and function by recruiting specific effector proteins.

Rab proteins distinguish certain intracellular compartments and are involved in vesicle budding, vesicular movement, membrane tethering, membrane docking, and membrane fusion(64, 65). Rab7 is primarily localized on the late endosomes and has been shown to be essential for lysosomes biogenesis(66). Rab11 is primarily localized on the recycling endosomes(67), and has been extensively studied for its involvement in transferrin receptor recycling(68, 69). Tagged Rab proteins as markers are useful for the isolation and localization of nanoparticles within the late endosomes and the recycling endosomes.

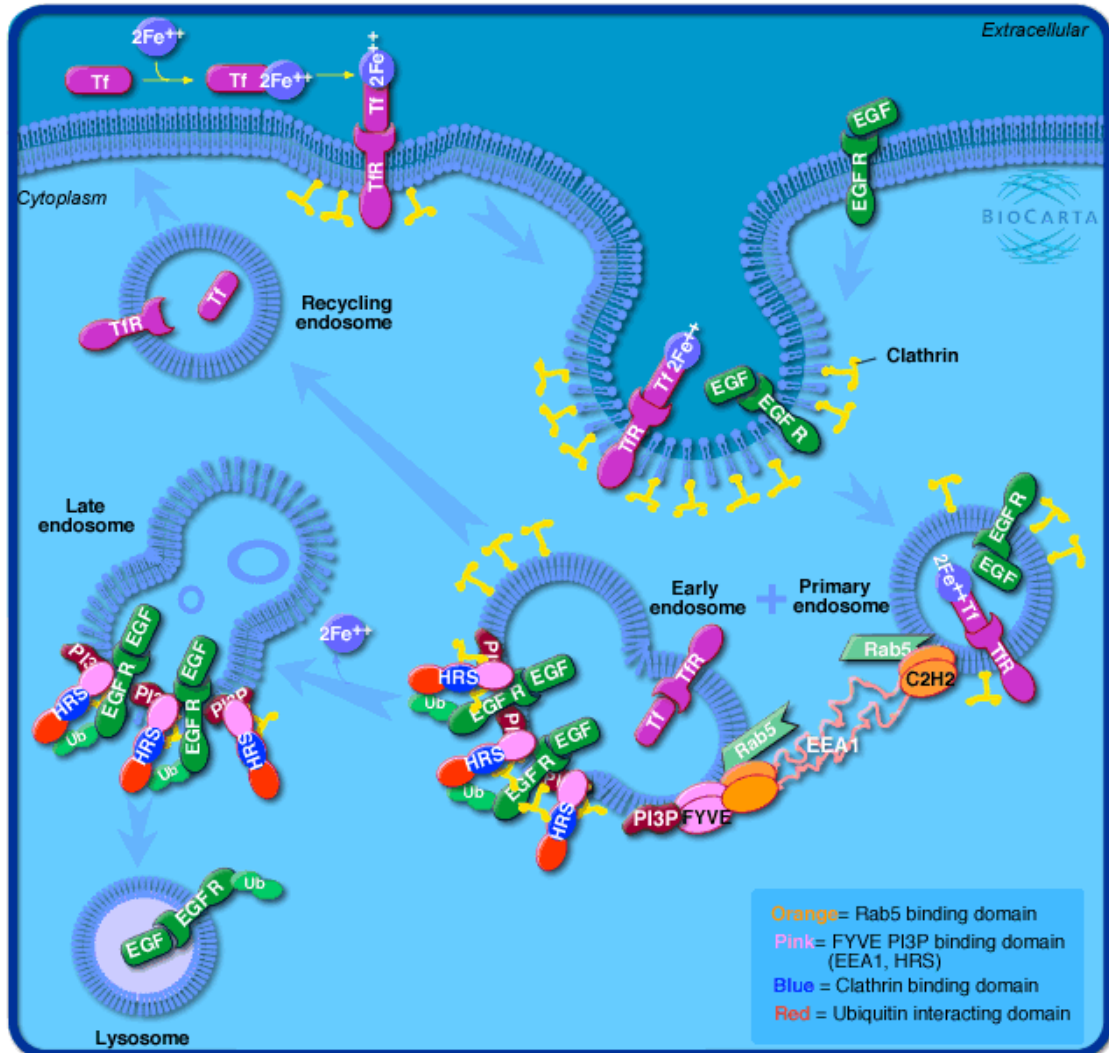


**Figure 1.4 Schematic of receptor-mediated endocytosis and intracellular sorting.** The transferrin receptor (TfR) mediates uptake of iron by binding diferric-transferrin (Tf-2Fe<sup>++</sup>) from the plasma. Endocytosis of the receptor is initiated by the formation of a clathrin-coated pit in the cell membrane, which subsequently forms the primary endosome and then fuses with the early endosome. Iron is released in the early endosome due to the slightly acidic pH and moves to the cytosol. The receptor-apotransferrin (Tf) complex is sorted in recycling endosomes back to the cell membrane. At the cell surface the apotransferrin is replaced with diferric-transferrin and the cycle repeats. Internalized membrane proteins can either be sorted for recycling from the early endosome like the transferrin receptor or be retained in the late endosome and directed to the lysosome for degradation like the epidermal growth factor receptor (EGFR) bound to the epidermal growth factor (EGF). Vesicular trafficking and proper sorting of internalized proteins require the recruitment of cytosolic proteins to a specific endosomal membrane in a reversible and regulated manner including the phosphatidylinositol 3-phosphate (PI3P) with binds proteins with a FYVE-finger motif such as the early endosomal autoantigen (EEA1) and HRS. Image acquired from Biocarta.com.



## 1.7 Intracellular Pathways

Upon receptor-mediated endocytosis, receptor-bound ligands are sorted in the early endosomes to the recycling or the degradative endosomal pathways. While receptors in the recycling endosomes are returned to the cell surface, receptors in the degradative pathway are routed to the late endosomes and lysosomes for degradation. For example, transferrin, the major iron-carrying protein, has been long studied to internalize with the transferrin receptor and then both ligand and receptor are continuously recycled back to the cell surface largely undegraded (Figure 1.4)(70-75). The fates of EGFR and HER2 are less certain. Both receptors and their associated ligands may play pivotal roles in intracellular sorting. Not only do the relationship of the targeted receptors and ligands determine the sorted pathway, but other mechanisms may dictate routing such as transregulation and pathway saturation.

The pathways of a few EGFR-binding and HER2-binding ligands have been documented. The epidermal growth factor (EGF) and transforming growth factor alpha (TGF $\alpha$ ) are the key EGFR binding ligands. Although both growth factors are structurally related in size and structure and have comparable affinity constants and function, EGFR-EGF complexes are largely degraded while EGFR-TGF $\alpha$  complexes are regularly recycled(76-78). Similar to transferrin, TGF $\alpha$  dissociates from the receptor-ligand complex at a much higher pH than EGF, and is more rapidly recycled with a substantial portion undegraded compared to EGF(77). Subsequently, TGF $\alpha$  do not induce a complete downregulation of cell surface receptors and hence have a faster ligand-binding recovery(77). French and colleagues found that that fraction of internalized EGFR-EGF complexes sorted to the degradative pathway was a function of concentration (Figure

1.5)(76). As the number of intracellular occupied receptors increased, the fraction of internalized EGF that was degraded dropped from 70 to 20% while the fraction of internalized TGF $\alpha$  remained uniform at ~50% at all ligand concentrations.

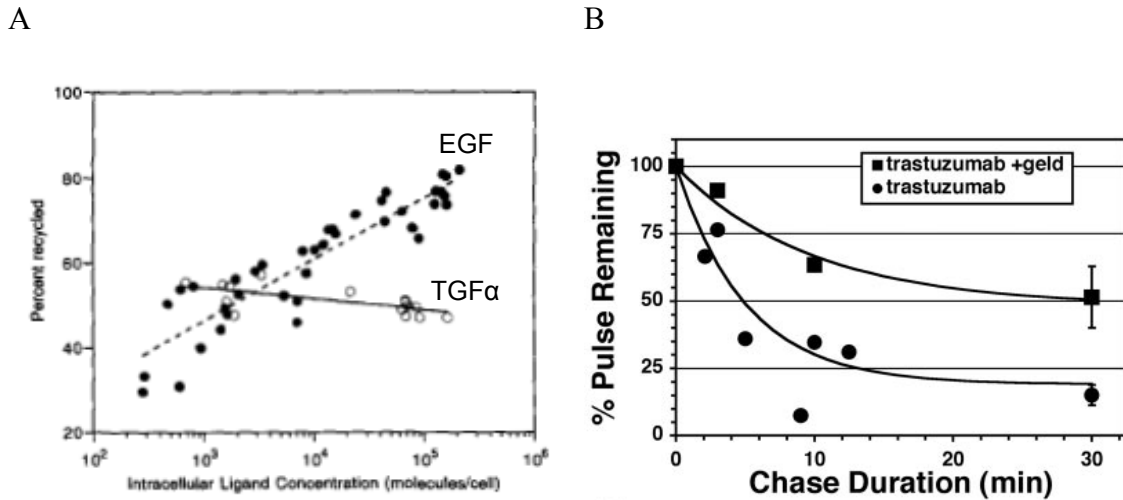


**Figure 1.5 Recycling behaviors of EGF, TGF $\alpha$ , and trastuzumab discussed in the literature. A.** EGFR-transfected B82 cells were incubated at 37° C for 2 hr in 0.008 to 17 nM of <sup>125</sup>I-EGF (enclosed circle) or <sup>125</sup>I-TGF $\alpha$  (empty circle) and chased with excess unlabeled ligand. Recycled concentration was determined by radioactivity. While a relatively constant percentage of TGF $\alpha$  was recycled at all ligand concentrations, EGF preferentially was degraded until high concentrations where it reversed(76). **B.** Geldanamycin-pretreated (enclosed square) or untreated (enclosed circle) HER2-expressing SK-BR-3 cells incubated with surface-bound trastuzumab labeled with Alexa Fluor 488 were pulsed for 10 min at 37° C and then chased for the indicated intervals and examined by fluorometry. Internalized trastuzumab efficiently recycles in the absence but not the presence of geldanamycin(79). Images acquired from referenced journals.

The intracellular trafficking of recently discovered monoclonal antibodies such as anti-EGFR cetuximab and matuzumab are still uncertain, with research showing contradictory evidence of EGFR downregulation and lack thereof(78, 80, 81). Austin and associates demonstrated that anti-HER2 trastuzumab are receptor-mediated endocytosed, but the monoclonal antibody subsequently recycles passively with no downregulation of surface HER2 (Figure 1.5)(79). F5 single-chain variable fragments (scFv), selected from an antibody phage library by panning HER2-overexpressing cells, efficiently bind HER2, triggering receptor-mediated endocytosis and inducing

downstream signaling through HER2(38). The intracellular trafficking like F5 scFv is still unknown.

Mutations of the receptor may alter its trafficking. Receptor tyrosine kinases like EGFR are thought to be recruited into clathrin-coated pits by direct interaction of tyrosine- and di-leucine-based motifs in their cytoplasmic domains with the clathrin adaptor protein complex(58). Hence, mutations of these domains as often evident in cancer cells may vary the sorting. With EGFR, lysine 721 is necessary for degradative sorting, and can be diverted to recycling compartments if mutated to alanine/methionine; essentially kinase-negative EGFR routes to recycling(76, 82, 83). Di-leucine 679 is crucial for degradative targeting, and mutations to di-alanine 679 lead to recycling targeting(84, 85). Truncated EGFR 1022-1123 also hinders degradative targeting, and hence modifications of the phosphorylation sites can also shifted sorting away from the degradative pathway(76, 83). There are also transregulation sites such as threonine 654 and when phosphorylated, EGFR is recycled but when mutated to alanine 654, the pathway favors degradation(86-88). Therefore, when choosing receptors for targeting, one must be aware that these receptors may be mutated and hence one's expectations for the uptake and the intracellular fate may change significantly too.

In addition, the intracellular pathway of receptors can be modulated by receptor transregulation and pathway saturation. With EGFR, protein kinase C stimulation of threonine 654 with phorbol myristate acetate shifts the pathway from degradative to recycling for EGF(86-88). With HER2, chaperone heat shock protein 90 inhibition by geldanamycin shifts the default recycling to degradative sorting for trastuzumab (Figure 1.5)(79). Hence, one can regulate the intracellular pathway by inducing the receptors

prior to incubation with ligands. The degradative endosomal pathway is saturable not only for ligands but also large carriers such as viruses(76, 87-89). In essence, for complexes with preferential degradative pathway sorting, eventually the cargo delivered to late endosomes gets saturated, diverting the remaining receptor and cargo to recycling endosomes.

Ding and colleagues investigated the intracellular trafficking and transduction of the adeno-associated virus type-2 (AAV2) in HeLa cells using imaging and immunoisolation strategies, and found that the virus traffics through both the late endosomes and the recycling endosomes in a dose-dependent fashion (Figure 1.6)(89). At a low effective multiplicities of infection (<100 genomes/cell), AAV2 preferentially trafficked from the early endosomes to the late endosomes ~100-fold more effectively than the recycling endosomes. In contrast, at a higher effective multiplicities of infection (>100 genomes/cell), AAV2 preferentially trafficked to the recycling endosomes ~17-fold more effectively than to the late endosomes. Viral trafficking through the late endosomes saturated starting at 100 genomes/cell giving rise to preferential trafficking to the recycling endosomes. Viral movement through the recycling endosomal compartments was more competent for transgene expression (~100-fold) than viral movement through the late endosomal compartments. The authors suggested that strategies to shunt viral movement from the late endosomes to the recycling endosomes may be effective at increasing viral transduction for gene therapy.

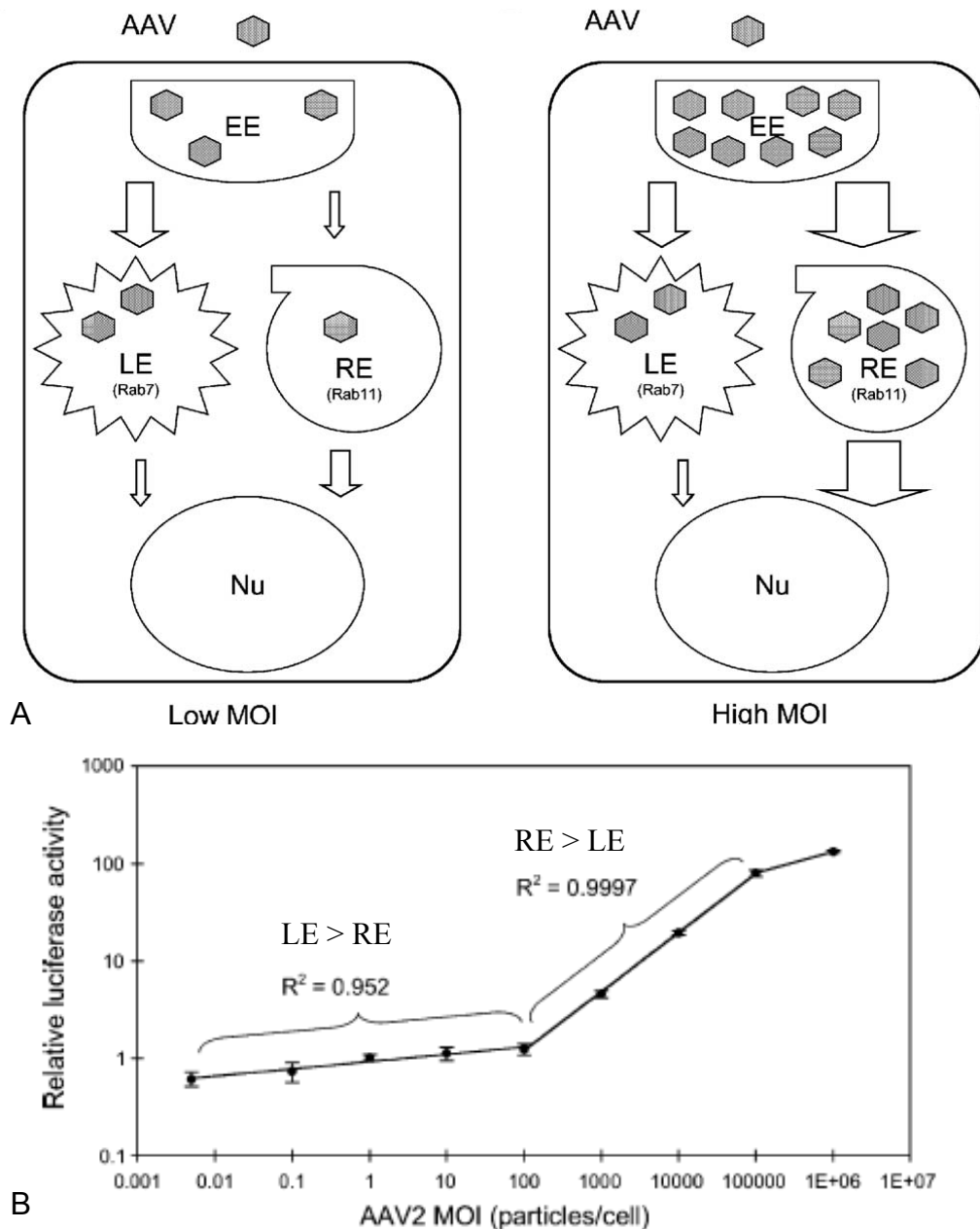


**Figure 1.6 Dose-dependent trafficking and transduction of adeno-associated virus type-2 (AAV2) discussed in the literature(89).** **A.** Schematic of AAV2 trafficking - at a low effective multiplicities of infection (MOI) (<100 genomes/cell), AAV2 preferentially trafficked from the early endosomes (EE) to the Rab7 late endosomes (LE) more effectively than the Rab11 recycling endosomes (RE). In contrast, at a higher MOI (>100 genomes/cell), AAV2 preferentially trafficked to the recycling endosomes more effectively than to the late endosomes. **B.** HeLa cells were transfected at the indicated MOI of AAV2 with luciferase transgene. Virus was pre-bound at 4° C for 1 hr, followed by a 37° C infection for 24 hr, and harvested for luciferase assay. Two linear phases of transduction existed. Viral movement through the recycling endosomal compartments was more competent for nucleus (Nu) targeting and transgene expression than viral movement through the late endosomal compartments. Images acquired from referenced journal.

Which is the preferred pathway? For viruses like the AAV2, higher bioactivity was evident when the virus sorted to recycling endosomes and away from the degradative endosomes prone of nucleotide digestion(89). The resulted pathway and the consequential biological activity in the delivery of drugs may differ from viruses and potentially nucleotides. First, the intracellular sorting of receptor-mediated lipid nanoparticles to the degradative and the recycling endosomal pathways may be governed by the sorting of the targeted receptor. Second, lipid nanoparticles diverted from the degradative to the recycling endosomal pathway may enhance biological activity for membrane impermeable, pH-sensitive molecules such as nucleotides and large hydrophobic drugs. Essentially, molecules that are easily denatured and have difficulty escaping the late endosomes may benefit from recycling endosomal targeting, where the pH is more neutral and the lack of digestive enzymes. Stable, resilient molecules and drugs may not gain any advantages from diverting away from the late endosomes since endosomal escape may be more rate limiting.

Pathway sorting of ligands and possibly ligand-conjugated lipid nanoparticles also can determine the sorting of the receptors. When ligands like transferrin and TGF $\alpha$  recycle, their corresponding receptors also recycle instead of being downregulated and degraded. Hence one potential advantage of recycling receptors, with the quick turnaround, is that more free recycled receptors are made available to bind and internalize more extracellular ligands or ligand-conjugated lipid nanoparticles. This can potentially increase the accumulation of liposomal drug delivery since there is always a high accessible supply of surface receptors.

## 1.8 Uptake Efficiency and Effect

To optimize the uptake of ligand-conjugated liposomes to cells, ligands should have high affinity binding to the targeted receptors. The rapid screening and identifying of tumor-specific high affinity internalizing human antibodies and antibody fragments from phage and yeast display of non-immune phage antibody libraries has provided a powerful tool for ligand selection(38-41). Internalization is crucial for drug delivery as the antitumor activity of HER2-targeted liposomal doxorubicin has been shown to be more significant when delivered by more efficient internalizing ligands than by less efficient ones(43, 44). Access of the ligand to the receptor is also important. A polymer linker such as PEG was shown to be vital to distance low molecular weight ligands such as folate from the liposomal surface and to allow receptor binding(90). Coupling of ligands to polymer linkers of various lengths to the distal terminals of antibody fragments and other ligands have been documented to improve binding, internalizing, and overall bioactivity in the delivery of drugs(35, 37, 91, 92).

Interestingly, Zhou and colleagues demonstrated that even when engineering ultrahigh affinity scFv against EGFR, they may be unnecessary for optimal nanoparticles targeting; high scFv per liposome densities of ultrahigh affinity scFv compared to high affinity scFv against EGFR resulted in no significant effect on binding, uptake, or cytotoxicity(93). The affinity of soluble ligands and ligands conjugated to liposomes are not drastically different. The conjugation of anti-HER2 F5 scFv to liposomes does not significantly affect the ligand interaction with HER2 in HER2-overexpressing cell lines since the  $K_D$  for the binding of monovalent F5 scFv conjugated liposomes ( $K_D = 111$  nM) and of soluble F5 scFv ( $K_D = 160$  nM) are comparable(34). In fact, the binding of F5

scFv conjugated to liposomes is directly proportional to density of ligands per liposomes until saturation.

Similarly to F5 scFv, the high affinity binding of Fab'-conjugated immunoliposomes derived from antibody fragments of trastuzumab is comparable to that of free Fab' and intact antibody(94). Increasing the surface density of ligands per liposomes correlates to increased targeted uptake in cells until a plateau, after which additional ligands may decrease binding and internalization(34-37). In HER2-overexpressing human breast cancer cells, it has been documented that the cell binding and internalization of anti-HER2 immunoliposomes increased at higher surface density of conjugated ligands, reaching a plateau at ~40 trastuzumab-Fab'/liposome(35) and a plateau at ~30 F5 scFv/liposome(34). Similarly in EGFR-overexpressing human breast cancer cells, a plateau was reached at ~30-40 cetuximab-Fab'/liposome(36). Apparently, the limit on the binding and uptake of ligand-conjugated liposomes is more dependent on ligand density per liposome and receptor expression level on the cells than to ligand affinity.

If increasing ligand valence has limits, possibly adding a second ligand type can improve uptake. Anti-HER2 and anti-EGFR dual-targeted immunoliposomes may increase uptake for dual-targeting receptors both expressed on the cells. Combination therapy with anti-HER2 mAb 4D5 and anti-EGFR mAb cetuximab has been shown to augment the inhibition of cell proliferation in ovarian carcinoma cells(95). In addition, dual-targeted liposomes against CD19 and CD20 have also been demonstrated to increase uptake and improved cytotoxicity in B lymphoma cells(96). Dual-targeted immunoliposomes will also allow us to examine the antagonistic effects of a non-specific



ligand possibly from sterical hindrance on cells expressing only one of the receptors. Dual-targeting liposomes against HER2 and EGFR may improve the delivery of immunoliposomes to cell lines expressing both receptors by increasing the receptor density, but can also serve to simplify the formulation of ligand-targeted lipid nanoparticles that can target a larger array of cells, similar to a cocktail-targeting approach.

## **1.9 Conclusion**

Liposomes as a drug carrier for cancer therapy have been promising in the clinic and in clinical trials due to their high preferential accumulation in the tumor interstitium from passive targeting and their adaptability and ease of modifications for new functionalities including improved stability and biocompatibility, prolonged circulation, high drug loading efficiency, controlled release kinetics, and highly specific targeting. For resilient and membrane permeable drugs such as doxorubicin, passive targeting may be sufficient for the treatment of solid tumors. Even though the conjugation of surface ligands to liposomes that target overexpressed receptors on tumors may not increase accumulation of drug-load liposomes in the tumor interstitium, ligand-targeting do increase intracellular delivery of drugs to targeted tissues. Uptake of ligand-conjugated lipid nanoparticles with such a large payload of drugs such as doxorubicin, irinotecan, and topotecan have demonstrated to significantly thwart tumor growth compared to non-targeted liposomes in HER2 and EGFR overexpressing tumors.

Little is known about the uptake and trafficking of liposomes beyond the final measurement of bioactivity such as cell viability with cytotoxic drugs. A better

understanding of the anti-HER2 and anti-EGFR receptor-mediated uptake and intracellular sorting of lipid nanoparticles may allow engineers to improve the delivery of drugs and nucleotides to tumor cells with low intracellular bioavailability. There have been no rational explanations offered that can reasonably rationalize the ideal valence observed for optimum cell association. As a result, cellular uptake has been difficult to improve. Is the optimum ligand density for cell association at saturation a limitation of ligand density on the liposomes or receptor expression level? In terms of uptake, can liposomal delivery be further optimized?

In this thesis, I investigated the uptake and intracellular sorting of anti-HER2, anti-EGFR, and dual-targeted lipid nanoparticles with a series of antibody fragments and growth factors in breast cancer cell lines of various HER2 and EGFR expression levels. Ligand valence and receptor expression levels will be investigated in relationship to mono-targeting and dual-targeting lipid nanoparticles. Intracellular sorting will also be examined for basic liposomal trafficking knowledge as well as any subsequent side-effects with improved drug delivery. Finally, models fitted to experimental data will be proposed to rationalize the binding and trafficking of ligand-targeted lipid nanoparticles, identify their current limitations, and offer a means to predict their behavior for optimization.

## **Chapter 2: The Engineering of HER2-Targeted and EGFR-Targeted Lipid Nanoparticles**

### **2.1 Abstract**

An array of anti-HER2, anti-EGFR, and dual-targeted lipid nanoparticles at varying ligand densities were formulated with receptor-specific targeting against cells lines expressing HER2 and/or EGFR. For HER2-targeting, liposomes were functionalized with antigen-binding fragment (Fab') reduced from trastuzumab or F5 single-chain variable fragment (scFv). For EGFR-targeting, liposomes were functionalized with Fab' reduced from cetuximab, the epidermal growth factor (EGF), or the transforming growth factor alpha (TGF $\alpha$ ). The surface attachment of ligand conjugates onto liposomes was achieved by the micelle transfer method or a novel sequential micelle transfer - conjugation method. Through a combination of both the sequential micelle transfer - conjugation and the micelle transfer methods, dual-targeted immunoliposomes of various ligand ratios of anti-HER2 F5 scFv and anti-EGFR cetuximab-Fab' were constructed. EGF and TGF $\alpha$  were investigated as potential targeting groups for liposomal delivery to EGFR-expressing cell lines. Liposomes conjugated with EGF and TGF $\alpha$  proved effective in cell association with MDA-468 cells, and may provide a useful means to study the intracellular sorting of receptor-mediated lipid nanoparticles. Finally, liposomal paclitaxel functionalized with cetuximab-Fab' was investigated for EGFR-targeted drug delivery in MDA-MB-231 orthotopic tumor xenograft model / SCID-beige mice. EGFR-targeted paclitaxel immunoliposomes

resulted in increased anti-tumor efficacy compared to non-targeted paclitaxel liposomes and free paclitaxel.

## 2.2 Introduction to the ErbB Family of Receptor Tyrosine Kinases

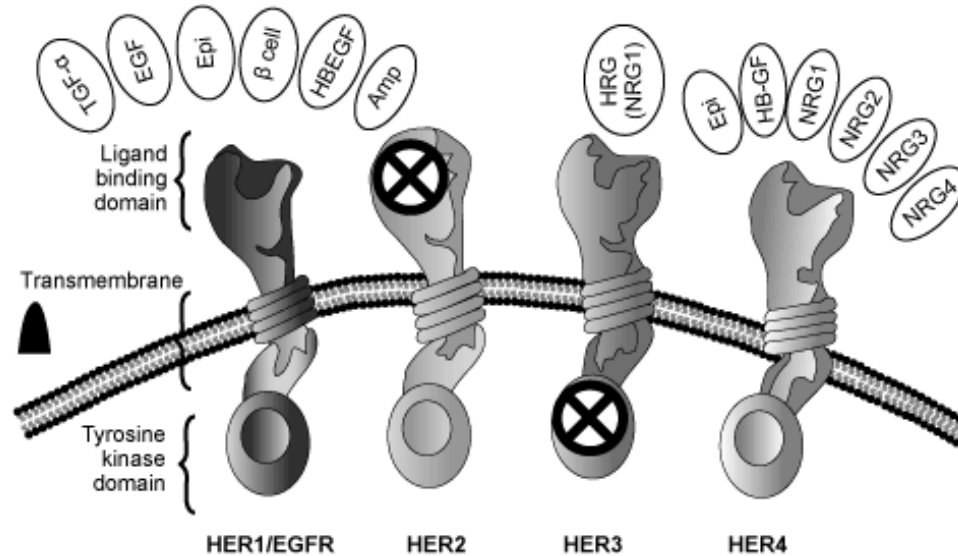


**Figure 2.1 The ErbB family of receptor tyrosine kinases.** The family consists of four structurally related transmembrane receptors EGFR/HER1 (epidermal growth factor receptor/human EGFR 1), HER2 (human EGFR 2), HER3 (human EGFR 3), and HER4 (human EGFR 4). The receptor is composed of an extracellular ligand binding domain, a transmembrane domain, and a cytoplasmic tyrosine kinase domain. Naturally, HER2 is ligand-independent and HER3 has an inactive tyrosine kinase domain (labeled by the crossed-circles). There are 13 recognized ligands that bind the ErbB family (left to right): transforming growth factor  $\alpha$ , epidermal growth factor, epiregulin, betacellulin, heparin-binding EGF, amphiregulin, heregulin (neuregulin 1), epigen, heparin-binding growth factor, and neuregulin 1-4. Other antibodies and antibody fragments have been discovered to bind the receptors: cetuximab (EGFR), trastuzumab (HER2), F5 single-chain variable fragment (HER2), etc. Image acquired from Clinicaloptions.com.

The ErbB family consists of four structurally related transmembrane receptor tyrosine kinases EGFR/HER1 (epidermal growth factor receptor/human EGFR 1), HER2 (human EGFR 2), HER3 (human EGFR 3), and HER4 (human EGFR 4) with key roles in development, tissue renewal, and cancer (Figure 2.1). In response to the binding of ligands on the extracellular domain, the activation of the cytoplasmic tyrosine kinase

domain promotes the formation of homodimers and heterodimers of the four receptors, followed by internalization, phosphorylated events, and downstream signaling. There are 13 recognized ligands that bind the ErbB family, but none of which binds HER2(97, 98). In addition, the tyrosine kinase domain of HER3 is inactive(97, 98). Both receptors rely heavily on the association with their family members for signaling. While insufficient ErbB signaling is associated with defects in organ development and neurodegenerative diseases(99), excessive ErbB signaling is associated with the development of many cancers. EGFR and HER2 overexpression occurs in many solid tumors, and being accessible transmembrane receptors capable of mediating endocytosis, both receptors are good candidates for targeted liposomal drug delivery.

### **2.2.1 EGFR and its Ligands**

EGFR is the prototypic member of the ErbB family vital for cell proliferation. EGFR overexpression occurs in many human cancers including breast, lung, colorectal and brain cancers and can result in poor prognosis(98, 100, 101). Epidermal growth factor (EGF), transforming growth factor alpha (TGF $\alpha$ ), epiregulin, betacellulin, heparin-binding EGF, and amphiregulin are known EGFR binding ligands that induce receptor dimerization and tyrosine autophosphorylation. Of the six, EGF and TGF $\alpha$  are the key EGFR binding ligands. Although both growth factors are structurally related in size (5-6 kDa), structure, and have comparable affinity constants and function, EGFR-EGF complexes are largely degraded while EGFR-TGF $\alpha$  complexes are regularly recycled(76-78). Many monoclonal antibody-based cancer therapies against EGFR-expressing tumors have also been developed such as cetuximab, panitumumab, zalutumumab,

nimotuzumab, and matuzumab. In addition, a selection of high affinity cell binding and internalizing anti-EGFR antibodies have been discovered from a phage display library(102). For EGFR-targeting, our studies functionalized lipid nanoparticles with either antigen-binding fragments (Fab') of cetuximab, growth factor EGF or TGF $\alpha$ .

### **2.2.2 HER2 and its Ligands**

HER2 is a member of the ErbB family vital for cell proliferation. Although ligand-independent, HER2 can heterodimerize with any of the ErbB family receptors, resulting in autophosphorylation of tyrosine residues within the cytoplasmic domain and initiation a variety of signaling pathways. 20-30% of human breast cancers overexpress HER2, most commonly due to amplification of the ErbB2 proto-oncogene(103-106). Overexpression is associated with increased disease recurrence and poor prognosis(103-106). HER2 overexpression is also known to occur in ovarian, stomach, prostate, lung, uterine, pancreas, and thyroid carcinomas(106, 107).

Although no known ligand directly binds HER2, a variety of antibodies and antibody fragments have been discovered and engineered to target and bind HER2. Trastuzumab and pertuzumab are two monoclonal antibody-based breast cancer therapies that bind HER2 with antiproliferative activity in HER2-expressing tumors on their own, but they are most efficacious when combined with chemotherapy(108-110). Although trastuzumab induces receptor-mediated endocytosis, the antibody subsequently recycles passively with no downregulation of surface HER2(79). F5 single-chain variable fragments (scFv), selected from an antibody phage library by panning HER2-overexpressing cells, efficiently bind HER2, triggering receptor-mediated endocytosis and

inducing downstream signaling through HER2(38). For HER2-targeting, our studies functionalized lipid nanoparticles with either trastuzumab Fab' or F5 scFv.

### **2.3 Receptor-Targeted Lipid Nanoparticles**

Receptor-targeted lipid nanoparticles with the surface conjugation of ligands combine the cell-specificity and receptor-mediated uptake of ligands with the pharmacokinetics and drug delivery capabilities of sterically stabilized liposomes. HER2 and EGFR of the ErbB family of receptor tyrosine kinases are attractive targets for ligand-targeting liposomal drug delivery because they are overexpressed on a variety of cancers, have a homogenous expression pattern, lack significant shedding, and capable of inducing internalization(4, 31, 32). In the last two decades, there has been much advancement with the delivery of drug-encapsulated immunoliposomes targeting tumors overexpressing HER2 and EGFR with comparable results in tumor accumulation and overall superior antitumor efficacy. HER2-targeted and EGFR-targeted liposomes encapsulating cytotoxic drugs such as doxorubicin, vinorelbine, methotrexate, and epirubicin have been shown to undergo specific receptor-mediated endocytosis receptor-overexpressing cells, resulting in significant cytotoxic activity *in vitro* and *in vivo*(34-36, 44, 50, 51). In these tumor xenograft models, the targeted delivery of the immunoliposomes resulted in growth inhibition, regression, and even cures at 50-60%. Currently, a few anti-HER2 and anti-EGFR liposomal drugs developed from our laboratory and collaborators are in clinical trials.

The improved antitumor efficacy of targeted liposomal drug delivery was a result of the new engineered targeted delivery system as a whole, and not merely additive

effects of the individual components which may be cytotoxic on their own. For example, the functionalizing of doxorubicin-encapsulated liposomes with a recombinant humanized monoclonal antibody (RhuMAb) of trastuzumab had significantly superior antitumor efficacy compared to free doxorubicin, liposomal doxorubicin, trastuzumab, and combinations of trastuzumab with free doxorubicin or liposomal doxorubicin(44). Although high concentrations of trastuzumab conjugated drug-empty liposomes were shown to have improved cytotoxic effects *in vitro*, it was not observed *in vivo* probably due to the low concentration of antibody fragments that are eventually taken up by tumors(44, 94). Unlike trastuzumab which inhibits growth on its own, the screened anti-HER2 scFv such as F5 and C6.5 lack growth inhibition activity(111). Similar higher antitumor efficacies from immunoliposomes targeting EGFR were also seen in tumor xenograft models(51).

For both HER2-targeting and EGFR-targeting, the biodistribution and total accumulations of targeted immunoliposomes and non-targeted liposomes in receptor-overexpressing tumors were comparable, but only immunoliposomes internalized extensively within tumor cells (>90% of analyzed cells for immunoliposomes compared to <5% for non-targeted liposomes)(35, 50, 51). The prolonged circulation times and size of the targeted and non-targeted liposomes allow preferential extravasation in solid tumors because of vascular abnormalities associated with tumor angiogenesis(21-24). Because sterically stabilized liposomes do not interact directly with tumor cells but release drug for eventual diffusion into tumor cells(112), the observed improved antitumor efficacy is believed to be due to intracellular delivery.



Ligands selected for HER2 and EGFR targeting derived from recent advancements in monoclonal antibody antitumor therapies as well as new screening techniques for isolating high affinity antibodies from phage display. These ligands were attractive due to their binding and internalizing properties. For HER2-targeting, ligands conjugated to the surface of liposomes included recombinant humanized Fab' derived from monoclonal antibody trastuzumab (rhuMAb HER2-Fab')(44, 94, 113), C6.5 scFv, and F5 scFv generated by phage display screening of antibody library(34, 42, 114). For EGFR-targeting, liposomal surface conjugated ligands included Fab' reduced from cetuximab, C10 scFv, and other anti-EGFR scFv generated by phage display screening of antibody library(36, 51, 93).

The surface attachment of these ligands preserves the high affinity binding association with the antigens. For example, the high affinity binding of ligand-conjugated immunoliposomes derived from antibody fragments such as trastuzumab-Fab' and F5 scFv is comparable to that of free ligand and intact antibody(34, 94). In addition, the attachment of different ligands such as anti-HER2 trastuzumab-Fab' or C6.5 scFv resulted in comparable therapeutic efficacy(44). Our studies focused on the anti-HER2 ligands trastuzumab-Fab' and F5 scFv and anti-EGFR cetuximab-Fab', EGF, and TGF $\alpha$  for targeting liposomal drug delivery.

## **2.4 Engineering Receptor-Targeted Lipid Nanoparticles**

To study the receptor-specific targeted drug delivery of liposomes against cells lines expressing HER2 and/or EGFR, an array of anti-HER2, anti-EGFR, and dual-targeted lipid nanoparticles at varying ligand densities (trastuzumab, F5 scFv, cetuximab,

EGF and TGF $\alpha$ ) were formulated. The various engineered liposomal formulations served as probes to help understand the uptake efficiency of immunoliposomes relative to ligand surface density and receptor expression level, mono-targeting as well as dual-targeting to multiple receptors, intracellular trafficking, and ultimately the consequential biological activity in the delivery of drugs. For receptor-specific targeting, sterically stabilized liposomes were functionalized with the attachment of anti-HER2 and/or anti-EGFR ligands. Liposomes were approximately 100-120 nm in diameter, composed of 1,2-distearoyl-sn-glycero-3-phosphocholine (DSPC), cholesterol, 1,2-distearoyl-sn-glycero-3-phosphoethanolamine-N-[methoxy(polyethylene glycol)-2000] (PEG-DSPE), and a fluorescent lipophilic tracer 1,1'-dioctadecyl-3,3',3',3'-tetramethylindodicarbocyanine perchlorate (DiD), or 3,3'-dioctadecyloxacarbocyanine perchlorate (DiO). For cell viability and tumor growth inhibition experiments, doxorubicin or paclitaxel were also encapsulated.

Although the intracellular pathways of many ligand-receptor complexes have been documented in the literature, the pathways of receptor-targeted lipid nanoparticles after endocytosis are still a mystery. Ligand-receptor complexes favoring distinct sorting to either the degradative or recycling endosomal pathways are of interest. Hence, ligand targets were selected because of the following characteristics: 1.) functional for marker modification and lipid conjugation, 2.) comparable affinity constants, and 3.) controlled sorting to the degradative and the recycling endosomal pathways. For HER2-targeting, liposomes were functionalized with Fab' reduced from trastuzumab or F5 scFv. Both antibody fragments have been well studied in our lab for targeted liposomal drug delivery. As a ligand, trastuzumab recycles passively with HER2, but the pathway can be

diverted with transregulation(79). For EGFR-targeting, liposomes were functionalized with Fab' reduced from cetuximab, EGF, or TGF $\alpha$ . Although EGFR-targeting with cetuximab has been studied in our lab, little is known about EGF and TGF $\alpha$  as targeted ligands for liposomal drug delivery. Even though both growth factors bind EGFR with comparable affinity constants, they are of interest due to their vastly distinct intracellular trafficking. Like receptor-targeted lipid nanoparticles, the intracellular pathways for F5 scFv and cetuximab not well documented.

Amphiphilic targeting ligand conjugates synthesized by maleimide chemistry consisting of a hydrophilic polymer spacer PEG between a lipid anchor DSPE and a ligand group were attached to the surface of liposomes to offer receptor-specific targeting. The conjugation of ligands such as antibody fragments by reactions between maleimide derivatives and thiols using naturally occurring cysteine residue, engineered C-terminal cysteine, or thiolated with Traut's reagent provide strong stable thioether bonds. Reactions with the cysteine on antibody fragments can offer ideal orientation, distant from antibody binding site, minimizing interference with binding. A polymer linker like PEG also helps with the orientation, extending the ligand far enough from the PEG shielding so the ligand are accessible to receptors on cells.

## **2.5 Results and Discussion**

### **2.5.1 Conjugates of Antibody Fragments and Growth Factors**

Fab' conjugates of cetuximab and now trastuzumab with 1,2-distearoyl-sn-glycero-3-phosphoethanolamine-N-[maleimide(polyethylene glycol)-2000] (Mal-PEG-DSPE) were synthesized as previously described(35, 36), taking advantage of the

naturally occurring cysteine residue of Fab'. Briefly, cetuximab and trastuzumab IgG were cleaved with pepsin to two antigen-binding fragments connected by disulfide bonds (Fab<sub>2</sub>), reduced with cysteamine to Fab', and conjugated to Mal-PEG-DSPE (Figure 2.2). The yielded efficiency of Fab'-PEG-DSPE confirmed by size-exclusion chromatography and SDS-PAGE was a reasonable 25-50%. Unfortunately, Fab' conjugates derived from Mal-PEG-DSPE manufactured by Avanti Polar Lipids poorly incorporated to the surface of liposomes by the micelle transfer method (discussed in the next section).

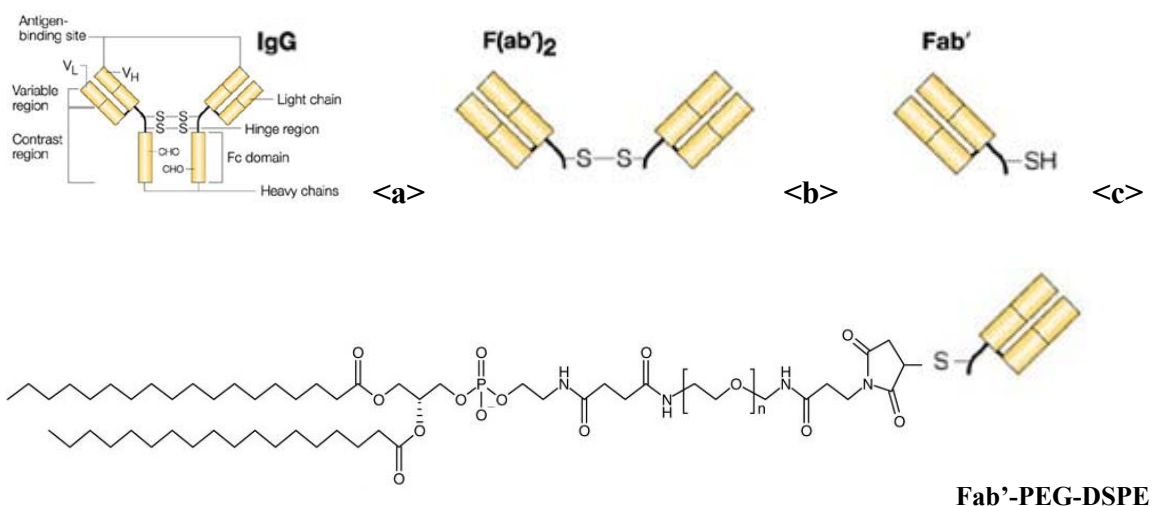


**Figure 2.2** Synthesis of trastuzumab-Fab'-PEG-DSPE and cetuximab-Fab'-PEG-DSPE. *Reagents and conditions:* a) pepsin (0.2 equiv.), CH<sub>3</sub>COONa, 37° C, 2 hr; b) cysteamine (1700 equiv.), 37° C, 1 hr; c) Mal-PEG-DSPE (5 equiv.), rt, 2 hr

Due to the lack of free cysteine residues, EGF and TGF $\alpha$  were thiolated with Traut's reagent before conjugation to Mal-PEG-DSPE (Figure 2.3). Similar to the conjugation with Fab', the yielded growth factor-PEG-DSPE was 25-50% efficient as confirmed by size-exclusion chromatography and SDS-PAGE. 100% conjugation efficiency was achievable when the growth factors were reacted with higher

concentrations of Traut's reagent (>500 fold), but the ligand conjugates were prone to crosslink resulting in poor receptor binding. F5 scFv conjugated to Mal-PEG-DSPE was manufactured by the National Cancer Institute as previously described(38, 42). The surface attachment of ligand conjugates onto liposomes was achieved by the micelle transfer method or the sequential micelle transfer - conjugation method.

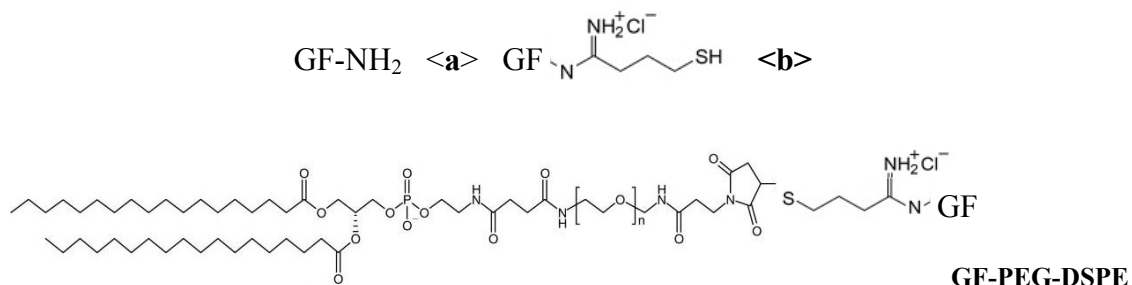


**Figure 2.3 Synthesis of EGF-PEG-DSPE and TGF $\alpha$ -PEG-DSPE.** *Reagents and conditions:* a) 2-iminothiolane (7 equiv.), TEA, EDTA, rt, 1 hr; b) Mal-PEG-DSPE (5 equiv.), rt, 2 hr; growth factor (GF), either EGF or TGF $\alpha$ ; amino group (NH<sub>2</sub>)

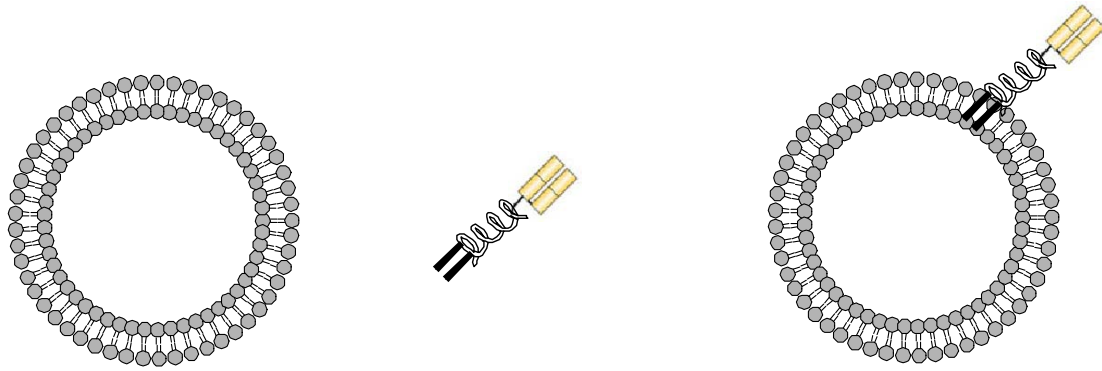
## 2.5.2 Ligand Conjugation onto Liposomes by the Micelle Transfer Method and Sequential Micelle Transfer - Conjugation Method

Through the micelle transfer method(35, 44), micellar conjugates of the ligand and an amphiphilic lipid co-incubated with preformed liposomes spontaneously insert themselves into liposome bilayers without the loss of the liposome integrity(47), providing a rapid and simple method for transforming non-targeted liposomes into antibody-targeted liposomes(48, 49) (Figure 2.4). Insertion is performed at 50-60° C, so the denaturation of protein ligands is a concern, but longer overnight incubation at 37° C is also possible(34, 48). Liposomes remain mostly unaltered through conjugations, and the techniques have shown to be simple and reproducible.

In our experiments, insertion efficiency for ligand conjugates of F5 scFv-PEG-DSPE, EGF-PEG-DSPE and TGF $\alpha$ -PEG-DSPE onto liposomes via the micelle transfer method(35, 44) was highly efficient (90-100%). Unfortunately, the insertion efficiency of Fab'-PEG-DSPE from trastuzumab and cetuximab onto liposomes was low (5-10%). No more than 10 Fab' per liposome was possible despite an excessive concentration of Fab'-PEG-DSPE incubation, and receptor-specific cell association was low. Previously attempts of the micelle transfer of Fab'-PEG-DSPE were more successful using Mal-PEG-DSPE manufactured by Shearwaters Polymers(35, 36) instead of the current available stock from Avanti Polar Lipids, but they are no longer in production. This was also confirmed by our prior laboratory member Dr. Christoph Mamot who pioneered the conjugation technique.

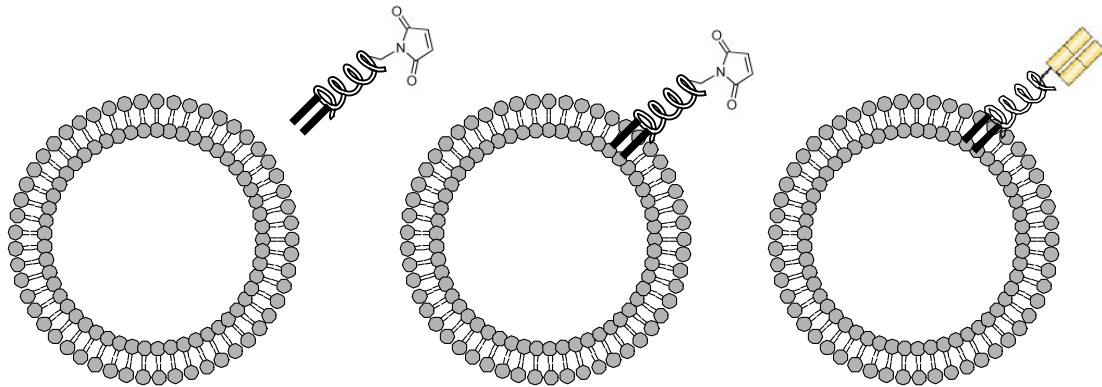
Due to the low transfer of Fab'-PEG-DSPE synthesized from Mal-PEG-DSPE by Avanti Polar Lipids onto liposomes by the micelle transfer method, a novel sequential micelle transfer - conjugation method was developed. IgG (cetuximab & trastuzumab) were cleaved with pepsin, reduced with cysteamine, and conjugated to liposomes micelle transferred with Mal-PEG-DSPE (Figure 2.4). Through this method, a range of 0-200 Fab' per liposome at approximately 25-50% efficiency was achieved. Approximately 50 Fab' per liposome was conjugated for every 0.25% Mal-PEG-DSPE transferred. Attempts of higher densities (ie, >1% Mal-PEG-DSPE transferred) often resulted in liposomal precipitation.

**Micelle transfer method:**



Liposome + Ligand-PEG-DSPE <a> Ligand-Liposome

**Sequential micelle transfer - conjugation method:**



Liposome + Mal-PEG-DSPE <a> Mal-Liposome <b> Ligand-Liposome

**Figure 2.4 Schematic of the micelle transfer method and the sequential micelle transfer - conjugation method.** Reagents and conditions: a) 50° C, 40 min; b) Ligand-SH (1-400 equiv.), rt, 2 hr

Hence, Mal-PEG-DSPE available from Avanti Polar Lipids conjugated to small ligands (F5 scFv, EGF, and TGF $\alpha$ ) is effective for liposomal insertion by the micelle transfer method, but is also effective for Fab' if Mal-PEG-DSPE is sequential micelle transfer - onto liposomes prior to Fab' conjugation. Another benefit of the sequential

micelle transfer - conjugation method is the reduced exposure of the ligands to high temperature incubations required of micelle transfer. This may help with protein stability. Compared to constructing liposomes pre-consisting of Mal-PEG-DSPE, this method allows for a more controlled means to functionalized pre-existing liposomes. Finally, the method also allows for the serial addition of a second targeting group in the case of anti-HER2 and anti-EGFR dual-targeted

### **2.5.3 Anti-HER2 and Anti-EGFR Dual-Targeted Immunoliposomes**

Through a combination of both the sequential micelle transfer - conjugation and the micelle transfer methods, dual-targeted immunoliposomes of various ligand ratios of anti-HER2 F5 scFv and anti-EGFR cetuximab-Fab' were achieved. Liposomes were functionalized with cetuximab-Fab' via the sequential micelle transfer - conjugation method, followed by insertion of F5 scFv-PEG-DSPE via the micelle transfer method (Figure 2.5). Based on the optimum ligand densities for the cell association of mono-targeted immunoliposomes as previously determined by flow cytometry, liposomes of varying ligand densities of anti-HER2 F5 scFv (0-40 ligands/liposomes), anti-EGFR cetuximab-Fab' (0-60 ligands/liposomes), and combinations of both for dual-targeting were constructed (Table 2.1).



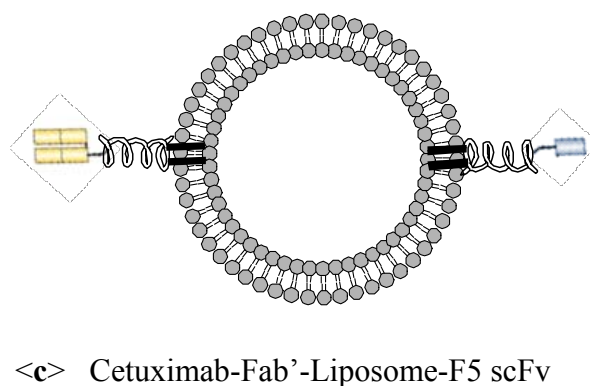
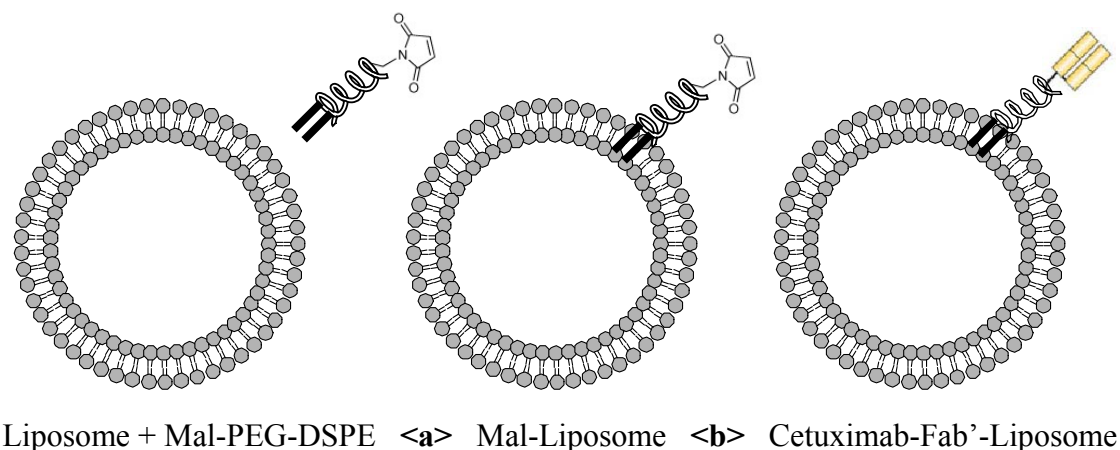


**Figure 2.5 Schematic of constructing anti-HER2 and anti-EGFR dual-targeted immunoliposomes.**  
*Reagents and conditions:* a) 50° C, 40 min; b) cetuximab-Fab' (1-400 equiv.), rt, 2 hr; c) F5 scFv-PEG-DSPE (1-100 equiv.), 50° C, 40 min

Conjugate incorporation efficiency was measured and determined by ImageJ (National Institutes of Health) from SDS-PAGE (Bio-Rad) stained with SYPRO Ruby. Because the conjugation efficiency of cetuximab-Fab' to Mal-PEG-DSPE sequential micelle transfer - conjugated liposomes was variable at 25-50%, lower than the ~100% insertion efficiency of F5 scFv-PEG-DSPE, a range of cetuximab-Fab' conjugated immunoliposomes were first constructed and quantified for ligand density. From these, cetuximab-Fab' conjugated liposomes of desired ligand densities were selected for F5

scFv-PEG-DSPE micelle transfer. Cell association studies showed ligand density dependent binding of liposomes with cells overexpressing HER2 and/or EGFR, and were further investigated in Chapter 3 for dose-uptake and cytotoxicity studies.

Liposomes	DiD, Dox	DiO	DiO, Dox
Non-Targeted	E0H0/NT	E0H0/NT	E0H0/NT
EGFR-Targeted: Cetuximab-Fab'	E5H0 E20H0 E40H0	E10H0 E20H0	E10H0 E60H0
HER2-Targeted: F5 scFv	E0H5 E0H20 E0H40	E0H5 E0H10 E0H15	E0H5 E0H10 E0H15
Dual-Targeted: Cetuximab-Fab' & F5 scFv	E5H5 E5H15 E20H5 E20H20 E40H20	E10H5 E10H10 E20H5 E20H10 E20H15	E10H5 E10H10 E10H15 E60H5 E60H10 E60H15

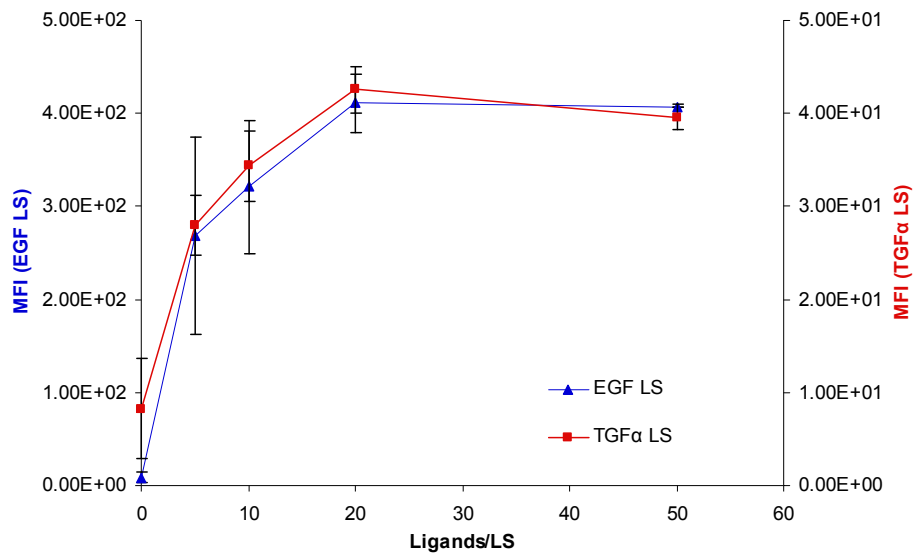
**Table 2.1 Formulations of HER2-targeted, EGFR-targeted, and dual-targeted immunoliposomes (ILS).** Liposomes are labeled with DiD or DiO, and encapsulated with doxorubicin (Dox) or empty. For ExHy ILS, *x* and *y* specify the number of ligands per liposome against EGFR (cetuximab-Fab') and HER2 (F5 scFv), respectively.

#### 2.5.4 EGF-Conjugated and TGF $\alpha$ -Conjugated Liposomes

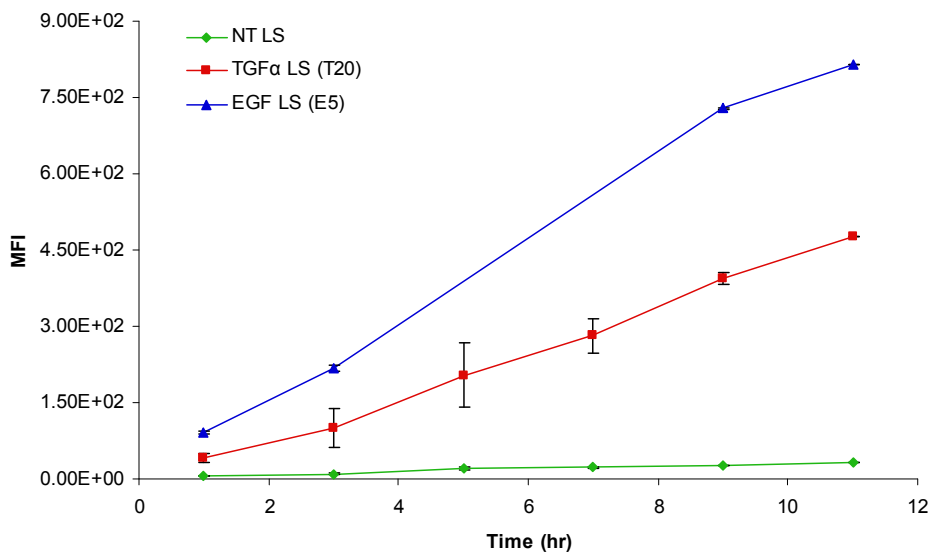
As mentioned previously, EGF and TGF $\alpha$  were thiolated with Traut's reagent, conjugated to Mal-PEG-DSPE, and micelle transferred onto liposomes. An array of liposomes with up to 50 growth factors of either EGF or TGF $\alpha$  per liposome was constructed. Although the cell association and trafficking of EGF and TGF $\alpha$  are well characterized, little has been documented for their EGFR-targeting capabilities as functional groups on liposomes in EGFR-overexpressing cells. Cell association studies of EGF-conjugated and TGF $\alpha$ -conjugated liposomes in EGFR-overexpressing MDA-468

cells were conducted to determine optimum ligand densities, incubation times, and phospholipid concentrations. MDA-468 cells were incubated with EGFR-targeted liposomes labeled with DiD of varying ligand densities of EGF (0-50 ligands/liposomes) and TGF $\alpha$  (0-50 ligands/liposomes) at 37° C for 1-24 hr, 0-750  $\mu$ M PL, and analyzed by flow cytometry and fluorometry.

Increasing the density of EGF and TGF $\alpha$  ligands per liposomes correlated to amplified targeted binding in MDA-468 cells until a plateau (Figure 2.6). Similar to the binding results of other anti-HER2 and anti-EGFR targeted immunoliposomes, maximum binding was achieved at ~20 ligand per liposome for both EGF-conjugated and TGF $\alpha$ -conjugated liposomes. Although the ligand density ratio dependent uptake was similar for 0-50 ligands per liposomes, the binding of EGF-conjugated liposomes was 10-fold higher than that of TGF $\alpha$ -conjugated liposomes. By increasing the incubation times from 1-11 hr, binding also increased but saturation was not reached (Figure 2.6). Increasing the phospholipid concentration from 0-750  $\mu$ M PL showed evidence of a possible plateau (Figure 2.6). There was a less than a magnitude difference in binding between EGF-conjugated and TGF $\alpha$ -conjugated liposomes at higher incubation times and concentration.

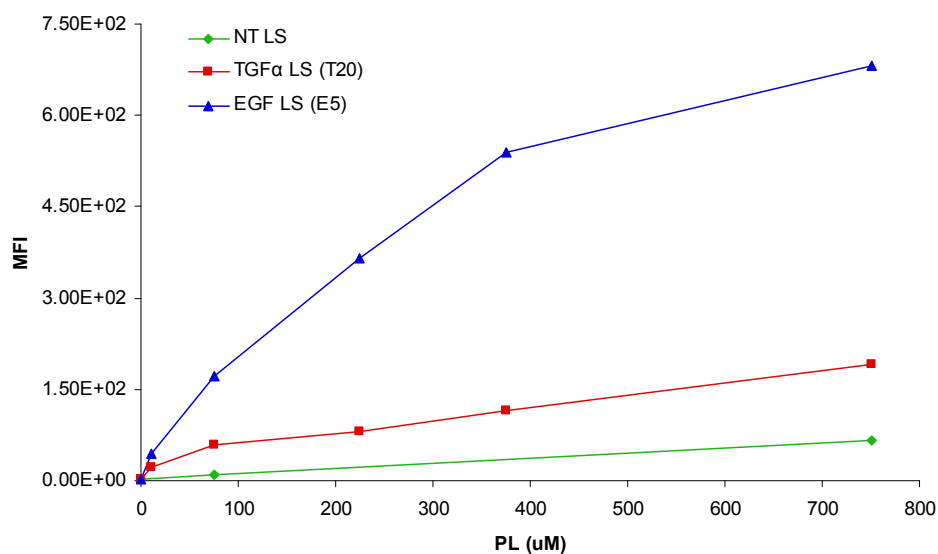


A

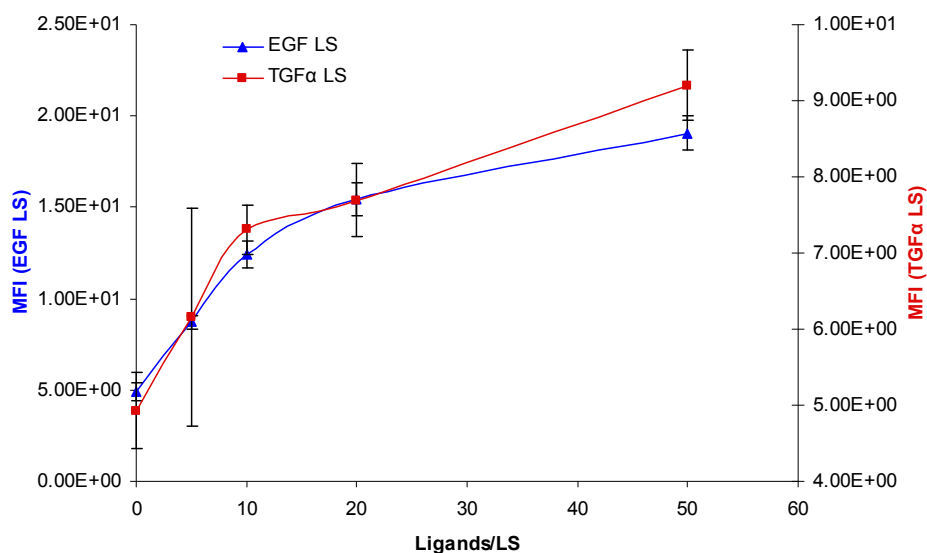


B

Continued on next page...



C



D

**Figure 2.6 Cell association of EGF-conjugated and TGF $\alpha$ -conjugated liposomes (LS) in MDA-468 cells.** Cells were incubated with liposomes labeled with DiD at 37 $^{\circ}$  C and analyzed by flow cytometry (mean fluorescent intensity [MFI] with a tight spread of  $5 \times 10^3$  cells) at **A.** increasing ligand densities and 75  $\mu\text{M}$  PL for 1 hr, **B.** varying incubation times and 75  $\mu\text{M}$  PL, and **C.** varying PL concentrations for 2 hr. **D.** Uptake study of EGF-conjugated and TGF $\alpha$ -conjugated liposomes of increasing ligand densities in MDA-468 cells: Cells were incubated with liposomes labeled with DiD and 400  $\mu\text{M}$  PL for 24 hr, lysed, and analyzed by fluorometry. Phospholipid (PL), non-targeted (NT), 5 EGF/LS (E5), 20 TGF $\alpha$ /LS (T20)

In addition to the cell association analysis by flow cytometry, the uptake of anti-EGFR liposomes encapsulated with doxorubicin in MDA-468 cells was also evaluated by fluorometry (Figure 2.6). Results correlated with the binding experiments where maximum binding was achieved at ~20 ligands per liposome in a ligand density ratio dependent uptake fashion, and that EGF-conjugated liposomes had a magnitude of higher binding than TGF $\alpha$ -conjugated liposomes. Because the equilibrium dissociation constants for both ligands are close ( $K_D$  2.2-2.6 nM)(77), one hypothesis that may explain the difference in uptake is due to the sterical hindrance resulting from binding to different epitopes on EGFR(115). Unlike F5 scFv, there binding and internalizing abilities may also be altered by surface attachment to liposomes.

EGF-conjugated and TGF $\alpha$ -conjugated liposomes also exhibited 1-2 magnitude lower cell association than cetuximab-conjugated immunoliposomes as expected since the equilibrium dissociation constant for cetuximab (0.1–0.4 nM)(116) is one magnitude lower than that of the growth factors. With the lower binding of EGF-conjugated and TGF $\alpha$ -conjugated liposomes, it may explain why the plateau is harder to reach despite higher concentrations and incubation times. EGFR is not depleted, insuring a constant stream of binding and uptake. EGF-conjugated and TGF $\alpha$ -conjugated liposomes proved effective in cell association with MDA-468 cells, and were further evaluated for intracellular trafficking in Chapter 4. In addition, the modeling of crosslink multivalent binding of lipid nanoparticles to monovalent receptors in Chapter 5 can offer some insights on the relationship of equilibrium dissociation constant and cell association.

## 2.5.5 Anti-Tumor Efficacy Mouse Study with EGFR-Targeted Paclitaxel

### Immunoliposomes

To investigate the EGFR-targeting benefits of cetuximab as a targeting ligand by the sequential micelle transfer - conjugation and a novel lipid-soluble chemotherapeutic liposomal formulation of paclitaxel *in vivo*, an anti-tumor efficacy mouse study was conducted. Paclitaxel is a mitotic inhibitor used in cancer chemotherapy for ovarian, breast, lung, head and neck cancer, and melanoma. Unfortunately, drug delivery issues arise from its poor aqueous solubility, requiring the administration of the excipient Cremophor EL (polyethoxylated castor oil) with known side effects in toxicity, hypersensitivity, inflammation, and non-linear pharmacokinetics. Abraxane (Abraxis BioScience) is an albumin-bound paclitaxel conjugate that neglects Cremophor EL and hence it's side effects. Similarly, the encapsulation of paclitaxel in liposomes do not require the administration of Cremophor EL, and may also reap the benefits of liposomal delivery with increase stability, decrease toxicity, and improve pharmacokinetics and pharmacodynamics.

For EGFR-targeting, we functionalized a new paclitaxel liposomal formulation manufactured by Merrimack Pharmaceuticals (Cambridge, MA) with cetuximab via the sequential micelle transfer - conjugation method. EGFR-targeted paclitaxel immunoliposomes resulted in significantly increased anti-tumor efficacy compared to non-targeted liposomal paclitaxel ( $P < 0.028$ ) and free paclitaxel ( $P < 0.0064$ ) in MDA-MB-231 orthotopic tumor xenograft model / SCID-beige mice (Figure 2.7). Non-targeted liposomal paclitaxel and free paclitaxel were comparable in efficacy ( $P < 0.96$ ), but significantly superior to saline ( $P < 0.016$ ). The study demonstrated that liposomal

paclitaxel is a viable alternative to free paclitaxel to inhibit tumor growth *in vivo*. The attachment of anti-EGFR cetuximab-Fab' significantly augmented the efficacy compared to liposomal paclitaxel with 10 ligands per liposome. We were limited with the supply of liposomal paclitaxel, and should dosage should be increased in future studies. With a high drug:lipid ratio (18.5%), not only are higher doses possible, but combined with a potentially lower toxicity attributed to the absence of a toxic excipient may increase efficacy similar to other liposomal chemotherapies.



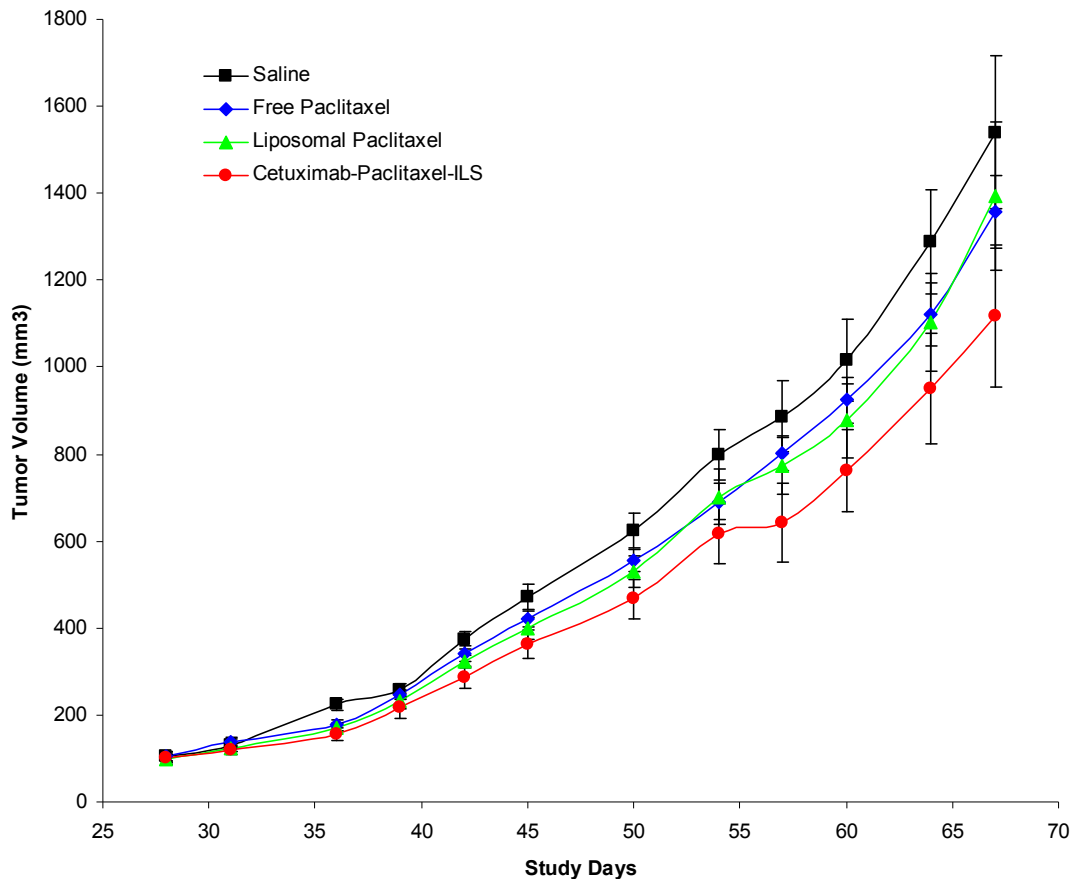


**Figure 2.7 Anti-tumor efficacy of anti-EGFR cetuximab-conjugated paclitaxel immunoliposomes (ILS) and liposomal paclitaxel in mice.** MDA-MB-231 orthotopic tumor xenograft model / SCID-beige mice (n = 10 per treatment condition) were treated by tail vein intravenous injection at a paclitaxel dose of 2.5 mg/kg every 4<sup>th</sup> day for a total of 6 times starting on day 28 post-tumor implantation. Other treatment groups included saline, free paclitaxel, free irinotecan, and liposomal irinotecan (all data not shown). EGFR-targeted paclitaxel immunoliposomes was significantly superior to all other treatment conditions displayed (P < 0.028 versus liposomal paclitaxel, P < 0.0064 versus free paclitaxel). Liposomal paclitaxel was not significant from free paclitaxel (P < 0.96), but was significantly superior to saline (P < 0.016). Data represents mean tumor volumes; bars, SE.

## 2.6 Conclusion

Anti-HER2, anti-EGFR, and dual-targeted lipid nanoparticles at varying ligand densities (trastuzumab, F5 scFv, cetuximab, EGF and TGF $\alpha$ ) were formulated with receptor-specific targeting against cells lines expressing HER2 and/or EGFR. For HER2-targeting, liposomes were functionalized with Fab' reduced from trastuzumab or F5 scFv.

For EGFR-targeting, liposomes were functionalized with Fab' reduced from cetuximab, EGF, or TGF $\alpha$ . Although the surface attachment of F5 scFv, EGF, and TGF $\alpha$  conjugates onto liposomes was effective with the micelle transfer method, Fab' of trastuzumab and cetuximab benefited from the sequential micelle transfer - conjugation method where Fab' is directly conjugated to maleimide micelle transferred onto the liposomes. Through a combination of both the sequential micelle transfer - conjugation and the micelle transfer methods, dual-targeted immunoliposomes of various ligand ratios of anti-HER2 F5 scFv and anti-EGFR cetuximab-Fab' were made possible for further studies.

EGF and TGF $\alpha$  were investigated as potential targeting groups for liposomal delivery to EGFR-expressing cell lines. Despite the 10-fold higher cell association of EGF-conjugated liposomes compared to TGF $\alpha$ -conjugated liposomes, liposomes conjugated with either growth factor displayed optimum binding at a density of 20 ligands per liposome similar to results seen with other anti-EGFR and anti-HER2 immunoliposomes. Both proved effective in cell association with EGFR-overexpressing MDA-468 cells, and may provide a useful means to study the intracellular sorting of receptor-mediated lipid nanoparticles. Finally, liposomal paclitaxel functionalized with cetuximab was investigated for EGFR-targeted drug delivery in MDA-MB-231 orthotopic tumor xenograft model / SCID-beige mice, resulting in an increased anti-tumor efficacy compared to non-targeted paclitaxel liposomes and free paclitaxel. Not only did the study demonstrate the improved efficacy of EGFR-targeted drug delivery, but also that of non-targeted paclitaxel liposomes as a viable alternative to free paclitaxel.

## 2.6 Materials and Methods

### 2.6.1 Materials

1,2-distearoyl-sn-glycero-3-phosphocholine (DSPC), 1,2-distearoyl-sn-glycero-3-phosphoethanolamine-N-[methoxy(polyethylene glycol)-2000] (PEG-DSPE), and 1,2-distearoyl-sn-glycero-3-phosphoethanolamine-N-[maleimide(polyethylene glycol)-2000] (Mal-PEG-DSPE) were purchased from Avanti Polar Lipids (Alabaster, AL). 1,1'-dioctadecyl-3,3,3',3'-tetramethylindodicarbocyanine perchlorate (DiD) and 3,3'-dioctadecyloxacarbocyanine perchlorate (DiO), and Alexa Fluor 488 carboxylic acid succinimidyl ester mixed isomers were purchased from Life Technologies (Grand Island, NY). Cholesterol was obtained from Calbiochem (San Diego, CA).

Trastuzumab/Herceptin (Roche) and cetuximab/Erbitux (ImClone LLC) were donated by the UCSF Outpatients Clinics Pharmacy (San Francisco, CA) from discarded immunotherapy treatments. F5 single-chain variable fragment (scFv) conjugated to Mal-PEG-DSPE was manufactured by the National Cancer Institute as previously described(38, 42). EGF and TGF $\alpha$  were purchased from Millipore (Billerica, MA) and Peprotech (Rocky Hill, NJ). Doxorubicin (Dox; Bedford Laboratories) was purchased from the UCSF Pharmacy (San Francisco, CA). Pepsin, cysteamine, 2-iminothiolane, and glycine were purchased from Sigma-Aldrich (St. Louis, MO). Cell culture media, fetal calf serum, penicillin-streptomycin, trypsin, and phosphate buffered saline (PBS) were purchased from the UCSF Cell Culture Facility (San Francisco, CA).

### **2.6.2 Cell Lines**

The MDA-468 human breast cancer cell line was obtained from the American Type Culture Collection (Rockville, MD). MDA-468 cells were maintained in Leibovitz's L-15 medium without NaHCO<sub>3</sub> and supplemented with 10% fetal calf serum and 1% penicillin-streptomycin. Cells were cultured as monolayer at 37° C in the absence of CO<sub>2</sub>. The MDA-MB-231 human breast cancer cell line was maintained by the UCSF Preclinical Therapeutics Core (San Francisco, CA) in Dulbecco's Modified Eagle Medium supplemented with 10% fetal calf serum and 1% penicillin-streptomycin.

### **2.6.3 Liposome Preparation**

Liposomes were prepared by the lipid film hydration-extrusion method(117). Lipid solution of DSPC, cholesterol, PEG-DSPE (3:2:0.3), and a fluorescent lipophilic tracer (DiD or DiO, 0.5%) were dissolved in chloroform with a few drops of methanol, and dried under reduced pressure at 60° C using rotary evaporation. Lipid films were hydrated in HEPES buffered saline (HBS 6.5; 5 mM HEPES, 135 mM NaCl, pH 6.5), and liposomes were prepared according to the repeated freeze-thawing method (6 cycles). Liposomes were subsequently extruded 10 times through 100 nm polycarbonate membrane filters using an extruder, resulting in liposomes of 100-120 nm diameter as determined by dynamic light scattering. Liposome concentration was measured using a standard phosphate assay(118).

For encapsulation of doxorubicin, the remote-loading method using ammonium sulfate was performed(119, 120). Lipid films were hydrated in ammonium sulfate (250 mM, pH 6), followed by the freeze-thawing method and extrusion as described. Free

ammonium sulfate was removed by size-exclusion chromatography using a Sephadex G75 column eluted with MES buffered saline (20 mM MES, 135 mM NaCl, pH 5.5). Liposomes were then incubated with doxorubicin (150  $\mu$ g Dox/ $\mu$ mol PL) at 60° C for 1 hr. Unencapsulated drugs were removed by size-exclusion chromatography using a Sephadex G75 column eluted with HBS 6.5. Loading efficiencies were typically in the range of 95-100% as determined by fluorometry (485/20:590/35 nm). Final liposomal formulations were all filtered through a 0.2  $\mu$ m Nalgene polyethersulfone membrane (Thermo Scientific) before cellular experiments.

#### **2.6.4 Conjugates of Trastuzumab and Cetuximab Fab'**

IgG (trastuzumab or cetuximab) was cleaved and reduced to Fab' (35, 36), but incorporated onto liposomes via a modified version of the micelle transfer method (35, 44). IgG was cleaved with pepsin (weight ratio 1:20) in sodium acetate (0.1 M, pH 3.7) at 37° C for 2 h under argon, followed by dialysis against MES buffered saline (5 mM MES, 135 mM NaCl, pH 6.0). The Fab<sub>2</sub> was reduced with cysteamine (16 mM) at 37° C for 1 h under argon, followed by size-exclusion chromatography on a Sephadex G25 column eluted with MOPS buffered saline (5 mM MOPS, 135mM NaCl, pH 7.0). For standards, the resulting Fab' was conjugated with a 5:1 excess of Mal-PEG-DSPE at room temperature for 2 hr under argon. The mixture was quenched with 1 mM 2-mercaptoethanol at room temperature for 15 min under argon. Unbound Fab' was removed by size-exclusion chromatography on an AcA34 column eluted with HBS (5 mM HEPES, 135 mM NaCl, pH 7.4) in 1 ml fractions. The fraction of Fab' conjugated

to micellar lipids was measured and determined by UV absorbance (280 nm) and SDS-PAGE (Bio-Rad).

### **2.6.5 Conjugates of EGF and TGF $\alpha$**

EGF and TGF $\alpha$  were thiolated with Traut's reagent(121), conjugated to Mal-PEG-DSPE, and incorporated onto liposomes via the micelle transfer method(35, 44). EGF or TGF $\alpha$  at 0.2-0.5 g/l in Traut's buffer (50 mM triethanolamine, 150 mM NaCl, 1 mM ethylenediaminetetraacetic acid, pH 8) was modified with a 7:1 excess of 2-iminothiolane at room temperature for 1 hr under argon. Excess reagent was removed by size-exclusion chromatography on a Sephadex G25 column eluted with sodium phosphate buffer (0.1 M sodium phosphate, 0.1 M NaCl, pH 7.5) in 200 ul fractions. The thiolated EGF or TGF $\alpha$  was conjugated with a 5:1 excess of Mal-PEG-DSPE at room temperature for 2 hr under argon. The mixture was quenched with 1 mM 2-mercaptoethnaol (200 mM stock in 5 mM MES, 135 mM NaCl, pH 6.0) at room temperature for 15 min under argon. Unbound growth factor was removed by size-exclusion chromatography on a Sephadex G75 column eluted with HBS (20 mM Hepes, 150 mM NaCl, pH 7.4) in 200 ul fractions. The fraction of growth factor conjugated to micellar lipids was measured and determined by BCA Protein Assay Kit (Thermo Scientific), Quant-iT Protein Assay Kit (Life Technologies), and SDS-PAGE (Bio-Rad).

### **2.6.6 Ligand Conjugation onto Liposomes by the Micelle Transfer Method and Sequential Micelle Transfer - Conjugation Method**

Ligands were incorporated onto liposomes either by the micelle transfer method(35, 44) or the sequential micelle transfer - conjugation method. For the micelle transfer method, conjugates of F5 scFv-PEG-DSPE, EGF-PEG-DSPE or TGF $\alpha$ -PEG-DSPE were incubated with liposomes at 50° C for 40 min under argon (0-100 ligands per liposome, assuming  $8 \times 10^4$  PL per liposome)(35, 122). Unincorporated conjugates were removed by size-exclusion chromatography on a Sepharose 4B column eluted with HBS 6.5. For the sequential micelle transfer - conjugation method, Mal-PEG-DSPE (0-1%) was first incubated with liposomes at 50° C for 40 min under argon, followed by incubation with freshly reduced Fab' (trastuzumab or cetuximab) at room temperature for 2 hr under argon (1:1 Fab':Mal-PEG-DSPE). Unbound Fab' was removed by size-exclusion chromatography on a Sepharose 4B eluted with HBS 6.5. Conjugate incorporation efficiency was measured and determined by ImageJ (National Institutes of Health) from SDS-PAGE (Bio-Rad) stained with SYPRO Ruby.

### **2.6.7 Anti-HER2 and Anti-EGFR Dual-Targeted Immunoliposomes**

Dual-targeted immunoliposomes of various ligand ratios were achieved by a combination of both the sequential micelle transfer - conjugation and the micelle transfer methods. For anti-HER2 and anti-EGFR dual-targeted immunoliposomes, Mal-PEG-DSPE (0-1%) was first incubated with liposomes at 50° C for 40 min under argon, followed by incubation with cetuximab-Fab' at room temperature for 2 hr under argon (1:1 Fab':Mal-PEG-DSPE). Unbound Fab' was removed by size-exclusion

chromatography on a Sepharose 4B eluted with HBS 6.5. Subsequently, F5 scFv-PEG-DSPE (0-1%) was incubated with cetuximab-ILS at 50° C for 40 min under argon. Unincorporated conjugates were again removed by size-exclusion chromatography on a Sepharose 4B column eluted with HBS 6.5. Alternatively, F5 scFv-PEG-DSPE (0-1%) and Mal-PEG-DSPE (0-1%) can simultaneously be incubated with liposomes at 50° C for 40 min under argon, followed by incubation with cetuximab-Fab' at room temperature for 2 hr under argon. Conjugate incorporation efficiency was measured and determined by ImageJ (National Institutes of Health) from SDS-PAGE (Bio-Rad) stained with SYPRO Ruby following each conjugation step. F5 scFv conjugation was assumed to be 100% as previously determined.

### **2.6.8 Fluorescent Ligands**

For ligand trafficking experiments, ligands were fluorescently labeled with Alexa Fluor 488 or 546. Trastuzumab, F5 scFv, cetuximab, EGF, and TGF $\alpha$  were conjugated with Alexa Fluor 488 carboxylic acid succinimidyl ester (Life Technologies) as described by vendor, yielding 1-2 fluorophores per ligand. Alexa Fluor 546 carboxylic acid succinimidyl ester (Life Technologies) yielded 3-4 fluorophores per ligand. The relative efficiency of labeling was determined by measurements on the NanoDrop 1000 spectrophotometer and Quant-iT Protein Assay Kit (Life Technologies).



### **2.6.9 Cell Association Studies**

For the assessment of targeted binding by flow cytometry, cells cultured overnight in 24-well plates ( $75 \times 10^3$  cells/well) were incubated with liposomes labeled with DiD (0-750  $\mu$ M PL) at 37° C for 1-11 hr, washed with PBS 3x, detached with trypsin, resuspended in PBS, and immediately subjected to flow cytometry (BD FACSCalibur). Detached cells were analyzed on the fluorescence channel FL4 for liposomes labeled with DiD. The mean fluorescent intensity with a tight spread of  $5 \times 10^3$  cells was recorded per liposomal formulation.

### **2.6.10 Uptake Studies**

For the assessment of targeted uptake by fluorometry, cells cultured overnight in 96-well plates ( $80 \times 10^3$  cells/well) were incubated with liposomes labeled with DiD (400  $\mu$ M PL) at 37° C for 24 hr, washed with PBS 3x, freeze-thawed 3x, and lysed with 80% isopropyl alcohol (IPA) and 1% Triton X-100. Lysed samples along with standards using labeled liposomes added to the plates were read on a fluorescent microplate reader (Wallac Victor). Measurements were read with excitation and emission band-pass filters as follow: DiD 644:665 nm and doxorubicin 485/20:590/35 nm. Cell count was estimated based on a hemacytometer and MTT assay ((3-(4,5-Dimethylthiazol-2-yl)-2,5-diphenyltetrazolium bromide), showing negligible cell detachment or toxicity under these conditions between groups.

### **2.6.11 Animal Study with EGFR-Targeted Paclitaxel Immunoliposomes**

Liposomal paclitaxel (MM310) was obtained from Merrimack Pharmaceuticals (Cambridge, MA) and functionalized with cetuximab via the sequential micelle transfer - conjugation method as previously described, yielding EGFR-targeted paclitaxel immunoliposomes with 10 cetuximab-Fab' per liposome. Through the UCSF Preclinical Therapeutics Core (San Francisco, CA), MDA-MB-231 orthotopic tumor xenograft model / SCID-beige mice (n = 10 per treatment condition) with an average 100 mm<sup>3</sup> tumor volume were treated by tail vein intravenous injection at a paclitaxel dose of 2.5 mg/kg every 4<sup>th</sup> day for a total of 6 times starting on day 28 post-tumor implantation. Other treatment groups included saline, free paclitaxel, free irinotecan, and liposomal irinotecan; irinotecan groups were treated at a dose of 10 mg/kg weekly for a total of 3 times. Animals were sacrificed 40 days after first treatment.

### **2.6.12 Statistical Analysis**

Treatment effects of tumor volume were analyzed by two-way ANOVA via SPSS Statistics 20 (IBM) using two factors, treatment group and day. Effects of treatment groups were compared to each other for 28-67 days post-tumor implantation.

## Chapter 3: Uptake Efficiency and Effect

### 3.1 Abstract

In the field of receptor-targeted lipid nanoparticles such as immunoliposomes against HER2 and EGFR, uptake efficiency and effect have been primarily focused on general cell-specificity, internalization, and cytotoxicity in the delivery of drugs. The studies in this chapter wish to extend the understanding on the uptake efficiency of immunoliposomes relative to ligand surface density, receptor expression level, mono-targeting, as well as dual-targeting to multiple receptors, and ultimately the consequential biological activity in the delivery of drugs.

For HER2-overexpressing and EGFR-overexpressing cell lines, the receptor-mediated uptake studies confirmed the observation where increasing ligand density per liposome increases targeted uptake until saturation (trastuzumab, F5 scFv, and cetuximab). For ligand surface densities at optimum binding and higher, as well as high liposomal concentration in incubation, there is roughly a 1:1 ratio of ligands to expressed receptors for MCF-7/HER2, BT-474, SK-BR-3, and MDA-468 cells. In addition, the accumulation of liposomes and ligands for anti-HER2 and anti-EGFR dual-targeted immunoliposomes were roughly additive of their mono-targeted counterparts in BT-474 and MKN-7 cells. No antagonistic effects were observed from the additional of a non-targeted ligand in all cell lines except for SK-BR-3 cells unless beyond 10 anti-EGFR ligand per liposome, where anti-EGFR ligands decreased overall uptake. Despite the additive uptake effect, dual-targeted liposomal delivery of doxorubicin to cell lines

expressing HER2 and EGFR was only slightly better in the inhibition of cell proliferation. The development of anti-HER2 and anti-EGFR dual-targeted immunoliposomes provides a useful system to broaden the potential number of targetable cell types in a simplified formulation and increase the delivery of drugs.

### 3.2 Introduction

In the last few decades, research has shown that the attachment of receptor-targeting ligands to liposomes offers cell-specificity, improved cellular uptake, and an effective targeted drug delivery technique against HER2-expressing and EGFR-expressing cells *in vitro* and *in vivo*. Many aspects in the delivery of receptor-mediated lipid nanoparticles to cells in regards to uptake efficiency and effect are still unknown. Increasing the surface density of ligands per liposomes correlates to increased targeted uptake in cells until a plateau, after which additional ligands may decrease binding and internalization(34-37). In HER2-overexpressing human breast cancer cells, cell binding and internalization of anti-HER2 immunoliposomes increased at higher surface density of conjugated ligands, reaching a plateau at ~40 trastuzumab-Fab'/liposome(35) and a plateau at ~30 F5 scFv/liposome(34). Similarly in EGFR-overexpressing human breast cancer cells, a plateau was reached at ~30-40 cetuximab-Fab'/liposome(36).

We wished to study whether the optimum ligand density for cell association at saturation is a limitation of ligand density on the liposomes or receptor expression level. A more extensive look on the relationship between ligand valence and binding will be mathematically covered in Chapter 5. During the studies, we introduced the attachment of a second targeting ligand to the immunoliposomes. Anti-HER2 and anti-EGFR dual-

targeted immunoliposomes not only allowed us to examine the antagonistic effects of a non-specific ligand possibly from sterical hindrance on cells expressing only one of the receptors, but also the potential benefits from dual-targeting receptors where both are expressed on the cells. Combination therapy with anti-HER2 mAb 4D5 and anti-EGFR mAb cetuximab have been shown to augment the inhibition of cell proliferation in ovarian carcinoma cells(95). In addition, dual-targeted liposomes against CD19 and CD20 have been demonstrated to increase uptake and improve cytotoxicity in B lymphoma cells(96).

Dual-targeting liposomes against HER2 and EGFR may improve the delivery of immunoliposomes to cell lines expressing both receptors by increasing the number of available targets to where the liposomes can bind. By increasing the number of available targets, multi-targeted drug delivery systems can also be effective for a larger array of tumor types compared to mono-targeted systems. Due to the difficulty of clinically approving multiple formulations as specialized anticancer medicine, clinical applications as well as manufacturing processes can be simplified with a single broader targeting formulation.

As described in Chapter 2, we formulated a series of anti-HER2, anti-EGFR, and dual-targeted immunoliposomes at varying ligand densities (trastuzumab, F5 scFv, and cetuximab). Cell association, uptake, and cytotoxicity studies were performed on a panel of human breast cancer cell lines that express either or both HER2 and EGFR at different expression levels.

### 3.3 Results and Discussion

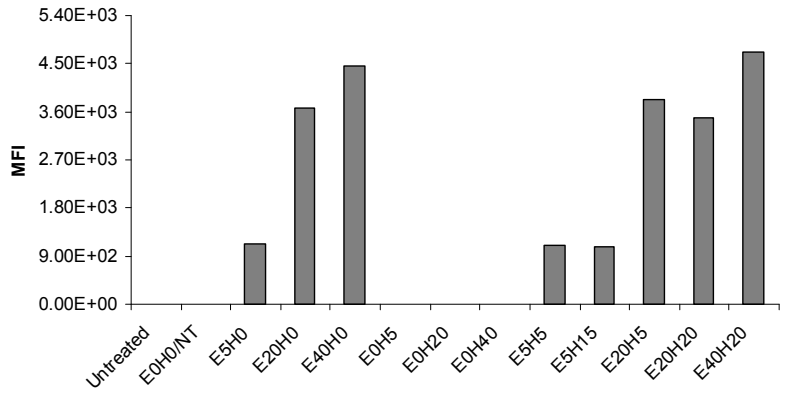
#### 3.3.1 Cell Association of HER2-Targeted, EGFR-Targeted, and Dual-Targeted Immunoliposomes in HER2-Expressing and EGFR-Expressing Cell Lines

To determine the optimum ligand densities and ligand combinations for HER2-targeted, EGFR-targeted, and dual-targeted immunoliposomes in HER2-expressing and EGFR-expressing cell lines, the targeted binding of immunoliposomes labeled with DiD was evaluated by flow cytometry. Cells were incubated with liposomes of varying ligand densities of anti-HER2 F5 scFv (0-40 ligands/liposomes), anti-EGFR cetuximab-Fab' (0-40 ligands/liposomes), and combinations of both for dual-targeting at 37° C for 4 hr (75  $\mu$ M phospholipid (PL)). The mean fluorescent intensity with a tight spread of  $5 \times 10^3$  cells was recorded per liposomal formulation.

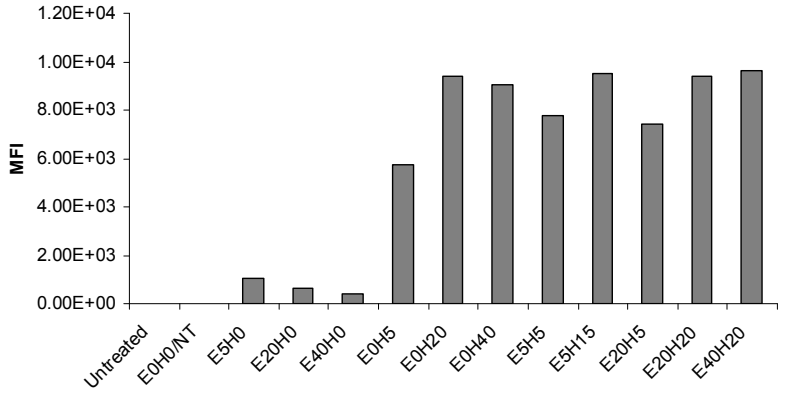
In EGFR-overexpressing MDA-468 cells, maximum binding was confirmed at ~20-40 anti-EGFR cetuximab-Fab' per liposome (~500 fold > non-targeted liposomes, NT) (Figure 3.1). There were negligible binding for anti-HER2 F5 scFv-conjugated immunoliposomes (ILS) at all ligand densities (= NT), and correspondingly no additive binding effects for dual-targeted immunoliposomes (~500 fold > NT). In HER2-overexpressing BT-474 cells, maximum binding was confirmed at ~15-20 F5 scFv per liposome (~400 fold > NT) (Figure 3.1). Binding was low but significant for cetuximab-ILS (~20-40 fold > NT). EGFR has been documented to be moderately expressed in BT-474 cells(123). In comparison to mono-targeted immunoliposomes, dual-targeted immunoliposomes offered no additive binding effects for combinations with 15+ F5 scFv per liposome (~400 fold > NT), but appeared to be additive for combinations with 5 F5 scFv per liposome (~300 fold vs. ~200 fold > NT).

In HER2 and EGFR moderately expressing MKN-7 cells, binding was low but significant for HER2-targeted and EGFR-targeted immunoliposomes in comparison to non-targeted liposomes (~300 fold > NT) (Figure 3.1). Similarly to liposomal cell association in MDA-468 and BT-474 cells, maximum binding was observed at ~20 cetuximab-Fab' per liposome for EGFR-targeted immunoliposomes and ~15-20 F5 scFv per liposome for HER2-targeted immunoliposomes in MKN-7 cells. Dual-targeted immunoliposomes resulted in higher binding than their mono-targeted counterparts (~500 fold > NT), indicating possible synergistic or additive effects. The cell association studies were quick preliminary tests for targeted functionality and were further investigated in the dose-uptake studies.

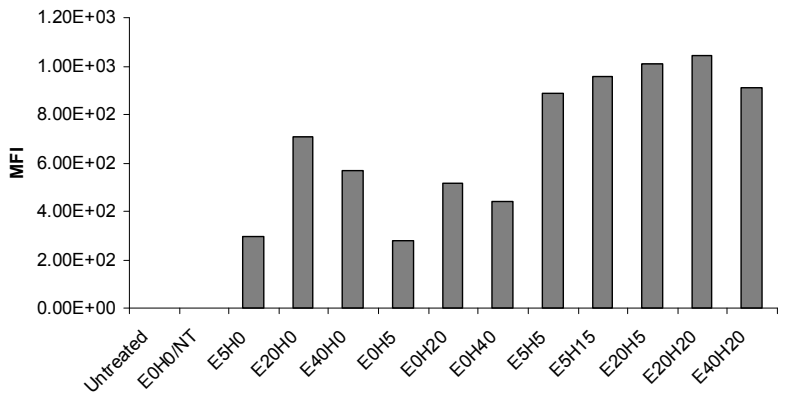
For mono-targeted immunoliposomes against HER2 and EGFR, the optimum ligand densities for maximum binding were in line with previous research(34-37), ~20-40 cetuximab-Fab' per liposome for EGFR-targeted immunoliposomes and ~15-20 F5 scFv per liposome for HER2-targeted immunoliposomes. At maximum cell association, these results also provide a baseline to compare to dual-targeted immunoliposomes for potential additive, synergistic, or antagonistic effects. Because MDA-468 cells overexpress EGFR but negligible HER2, binding was only observed with EGFR-targeted immunoliposomes. Dual-targeted immunoliposomes resulted in similar cell association as EGFR-targeted immunoliposomes, confirming negligible HER2 binding as well as a lack of antagonistic effects from additional non-targeted functional groups or sterical hindrance.



A



B



C

**Figure 3.1 Cell association of HER2-targeted, EGFR-targeted, and dual-targeted immunoliposomes (ILS) of varying ligand densities.** *A.* in MDA-468, *B.* BT-474, and *C.* MKN-7 cells: Cells were incubated with liposomes labeled with DiD at 37° C for 4 hr and analyzed by flow cytometry (mean fluorescent intensity [MFI] with a tight spread of  $5 \times 10^3$  cells). For ExHy ILS, *x* and *y* specify the number of ligands per liposome against EGFR (cetuximab-Fab') and HER2 (F5 scFv), respectively. Non-targeted (NT)



Although BT-474 cells overexpress HER2, they also moderately express EGFR, corroborating with our results for high HER2-targeted and low EGFR-targeted cell association. Interestingly, potential additive effects were observed with dual-targeted liposomes only with low F5 scFv densities. Again, no antagonistic binding effects were observed for dual-targeted immunoliposomes. MKN-7 cells express moderate levels of both HER2 and EGFR, and accordingly moderate cell association with immunoliposomes targeting either receptor was observed. Dual-targeted immunoliposomes resulted in higher cell association than all mono-targeted counterparts. Hence, immunoliposomes with dual-targeting to HER2 and EGFR may increase cell association with targeted cells when conditions are not optimum, in the case of low F5 scFv densities in BT-474 cells and moderately HER2-expressing and EGFR-expressing MKN-7 cells. Based on these results, ligand densities were chosen for uptake studies for further investigation.

### **3.3.2 Uptake of HER2-Targeted Immunoliposomes and Trastuzumab in Relationship to Receptor Expression Level**

To investigate whether the accumulation of trastuzumab is higher when attached to immunoliposomes or as a free antibody in HER2-overexpressing cell lines, an uptake study was conducted and evaluated by fluorometry. MCF-7/HER2 and BT-474 cells were oversaturated with trastuzumab labeled with Alexa Fluor 488 (40 nM) or immunoliposomes labeled with DiD (23 trastuzumab-Fab' per liposome, 375  $\mu$ M PL). After a 4 hr incubation, the total accumulation of trastuzumab as an IgG and trastuzumab-Fab' from the immunoliposomes were comparable in MCF-7/HER2 cells,  $5-7 \times 10^5$  ligands per cell ( $P < 0.1$ ) (Table 3.1). Although the accumulation was significantly

different in BT-474 cells,  $0.8-1.2 \times 10^6$  trastuzumab ligands per cell ( $P < 0.002$ ), they were in the same range. Results from a dose-uptake study in BT-474 cells for F5 scFv-ILS in the next section also yielded similar uptake levels,  $1.0 \times 10^6$  ligands per cell at valence of 15 ligands per liposomes, which is comparable to the amount of ligands delivered from trastuzumab-ILS ( $P < 0.14$ ) and free trastuzumab ( $P < 0.07$ ). These results suggest that multiple ligands on the liposomes may contribute the uptake of the lipid nanoparticles. If only a few ligands are required for uptake, it is more likely that the accumulation of liposomes would be closer to the free trastuzumab accumulation range and hence the ligands delivered from the liposomes would be many folds higher (up to 15-20 fold).

	BT-474		MCF-7/HER2	
	Lg/Cell	LS/Cell	Lg/Cell	LS/Cell
Trastuzumab	$8.0 \times 10^5 \pm 5.5 \times 10^4$	NA	$6.4 \times 10^5 \pm 6.1 \times 10^4$	NA
Trastuzumab-ILS (23 Lg/LS)	$1.2 \times 10^6 \pm 7.6 \times 10^4$	$5.2 \times 10^4 \pm 3.3 \times 10^3$	$5.5 \times 10^5 \pm 4.4 \times 10^4$	$2.4 \times 10^4 \pm 1.9 \times 10^3$
F5 scFv-ILS (15 Lg/LS)	$1.0 \times 10^6 \pm 1.1 \times 10^5$	$6.8 \times 10^4 \pm 7.3 \times 10^3$		

**Table 3.1 Uptake studies of trastuzumab, trastuzumab-conjugated and F5 scFv-conjugated immunoliposomes (ILS) in BT-474 and MCF-7/HER2 cells.** Cells were incubated with trastuzumab labeled with Alexa Fluor 488 or liposomes labeled with DiD or DiO at 37° C for 4 hr, lysed, and analyzed by fluorometry. Ligand (Lg) and liposomes (LS) were oversaturated to ensure maximum uptake (40 nM ligand, 375 μM PL). In MCF-7/HER2 cells, lg/cell was not significantly different ( $P < 0.1$ ). In BT-474 cells, lg/cell were not significant different comparing F5 scFv to trastuzumab-ILS ( $P < 0.14$ ) and free trastuzumab ( $P < 0.07$ ), but later two are significant different ( $P < 0.002$ ). Phospholipid (PL)

HER2 is overexpressed in the human breast cancer cell lines BT-474 ( $10^6$  HER2/cell)(44, 124) and MCF-7/HER2 ( $10^6$  HER2/cell)(44, 125). Regardless as a free antibody or conjugated as an antibody fragment onto liposomes, the total accumulation of the trastuzumab ligands is close to a 1:1 ratio of ligands to HER2 expressed on BT-474

and MCF-7/HER2 cells. This raises an interesting question in the targeted delivering of drugs, whether it is more efficient as an antibody-drug conjugate such as trastuzumab emtansine (Roche) or drug-encapsulated liposomal formulations? Typical immunoliposomes (100 nm) can encapsulate  $15-40 \times 10^3$  drug molecules per liposome, but require 15-40 ligands per liposome for optimum delivery(4). Hence, the total maximum accumulation of liposomal particles compared to antibody-drug particles can be 1-2 magnitudes less due to the rate limiting 1:1 ratio of ligands to HER2 expressed. However in a controlled environment *in vitro*, immunoliposomes still offer roughly a 3 magnitude advantage in drug delivery over antibody-drug conjugates (assuming 1:1 ratio) due to the high drug-loading efficiency and large payload of liposomal delivery. The advantage may be even higher *in vivo* due to other benefits from liposomal delivery compared to antibody-bound delivery, such as increased drug stability, prolonged circulation, and enhanced permeability and retention effect. The 1:1 ratio uptake of ligands to HER2 expressed will be revisited and supported through a binding model in Chapter 5.

### **3.3.3 Dose-Uptake of HER2-Targeted and EGFR-Targeted Immunoliposomes of Varying Ligand Densities**

To evaluate the targeted uptake of HER2-targeted and EGFR-targeted immunoliposomes relative to ligand density, ligand combinations, and lipid concentration, dose-uptake studies were performed with increasing concentrations of liposomes labeled with DiO at 37° C for 4 hr. Immunoliposomes consisted of varying ligand densities of anti-HER2 F5 scFv (0-15 ligands/liposomes), anti-EGFR cetuximab-Fab' (0-20 ligands/liposomes), and combinations of both for dual-targeting. Similar

studies using immunoliposomes labeled with DiD, loaded with doxorubicin, and slightly different ligand combinations were also evaluated and yielded comparable results (data not shown).

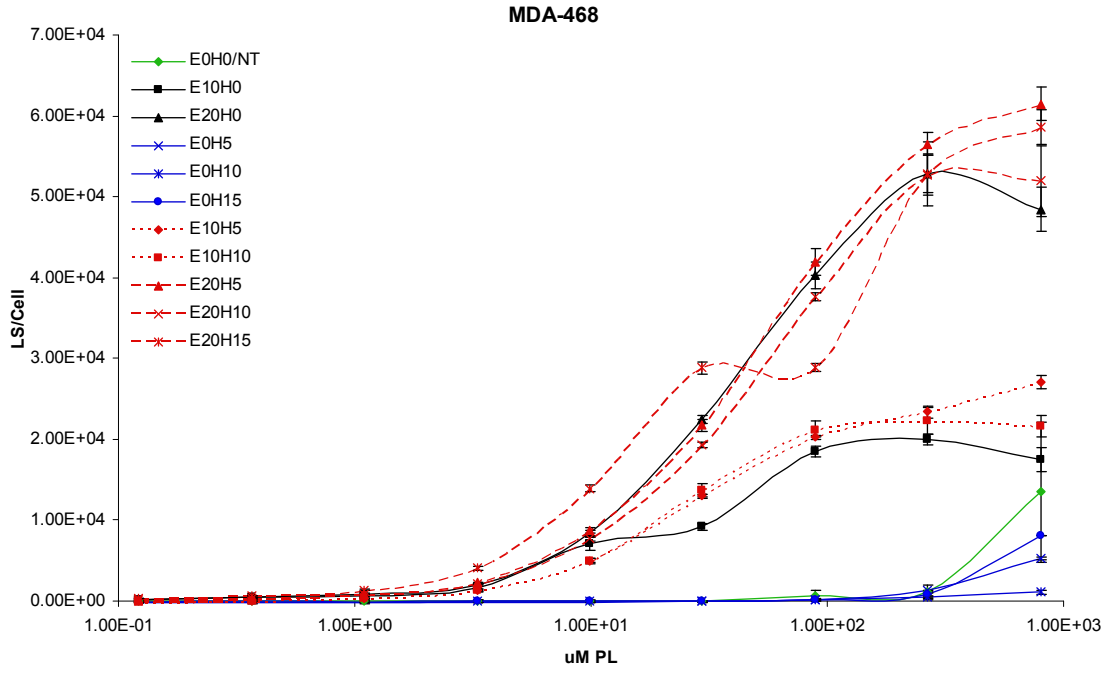
In MDA-468 cells, immunoliposomes with higher cetuximab-Fab' per liposome densities correlated with higher targeted uptake (Figure 3.2). 20 cetuximab-Fab' per liposome reached a plateau at ~300  $\mu$ M PL, resulting in  $\sim 5 \times 10^5$  liposomes and  $\sim 10^6$  cetuximab-Fab' per cell (Table 3.2). Similarly, there was an accumulation of  $\sim 10^6$  cetuximab-Fab' per cell in all cases for dual-targeted immunoliposomes with 20 cetuximab-Fab' and 0-15 F5 scFv per liposome. Immunoliposomes with varying F5 scFv densities had no significant uptake compared to non-targeted liposomes.

In HER2-overexpressing SK-BR-3 cells, immunoliposomes with high F5 scFv per liposome densities correlated with high targeted uptake (Figure 3.2). 10-15 F5 scFv per liposome reached a plateau at ~200  $\mu$ M PL, resulting in  $\sim 2-3 \times 10^5$  liposomes and  $\sim 3 \times 10^6$  F5 scFv per cell. Similarly, there was an accumulation of  $\sim 2-3 \times 10^6$  F5 scFv per cell in all cases for dual-targeted immunoliposomes with 10-15 F5 scFv and 0-20 cetuximab-Fab' per liposome. Immunoliposomes with varying cetuximab-Fab' densities had no significant uptake compared to non-targeted liposomes. There is higher uptake of anti-HER2 targeted immunoliposomes in SK-BR3 cells than in BT-474 cells; this will be revisited in Chapter 5.

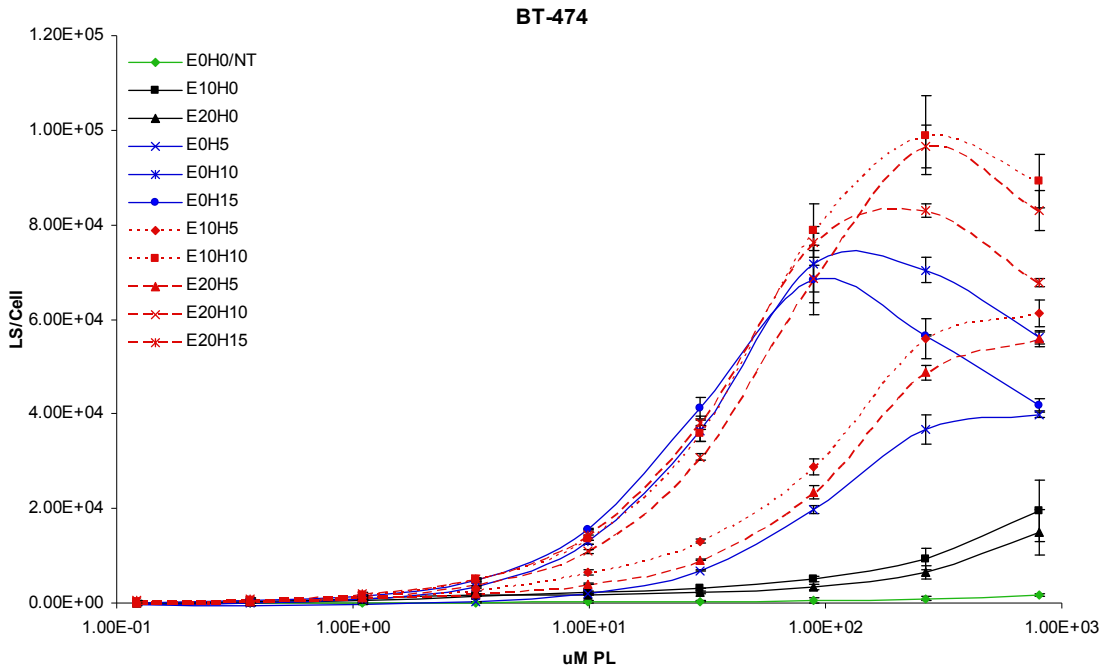
The MDA-468 human breast cancer cell line overexpresses roughly  $10^6$  EGFR per cell (126, 127) but negligible HER2, and the SK-BR-3 human breast cancer cell line overexpresses  $2-3 \times 10^6$  HER2 per cell (128, 129) but negligible EGFR. At the plateau, there is roughly a 1:1 ratio of ligands to receptors for both cell lines with their respective

overexpressed receptors. Similar to the cell association studies in MDA-468 cells, non-specific anti-HER2 ligands did not interfere with targeted uptake. In the case of anti-HER2 and anti-EGFR dual-targeted immunoliposomes, uptake was not significantly different compared to anti-EGFR immunoliposomes of similar cetuximab-Fab' densities ( $P < 0.95$  for E20Hy;  $P < 0.53$  for E10Hy).

Interestingly in SK-BR-3 cells, non-specific anti-EGFR ligands can interfere with targeted uptake in an antagonistic manner beyond 10 anti-EGFR ligands per liposome. At 10 anti-EGFR ligands per liposome, there is no significant effect. Although mono-targeted cetuximab-immunoliposomes had no significant uptake compared to non-targeted liposomes, in the case of anti-HER2 and anti-EGFR dual-targeted immunoliposomes with 20 cetuximab-Fab' per liposome, uptake was lower for all combinations with F5 scFv compared to mono-targeted counterparts. These results provide evidence that the addition of non-specific ligands may interfere with the uptake of some cell lines such as SK-BR-3, but not others like MDA-468, at high enough of ligand valence. It could also be due to the larger size of Fab' compared to scFv.

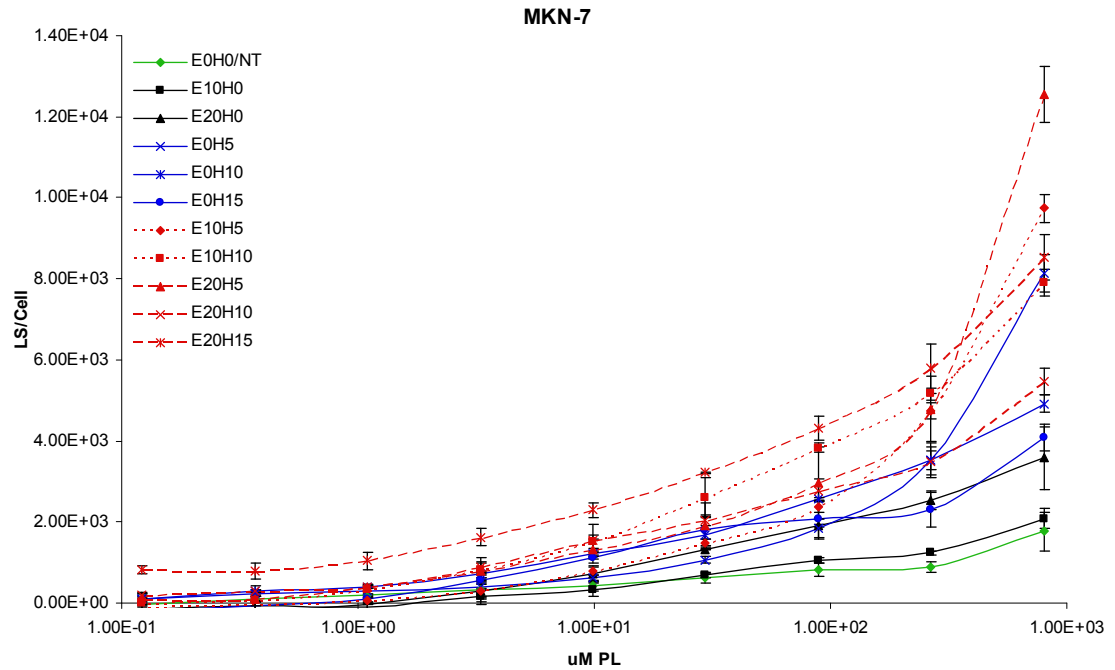


A

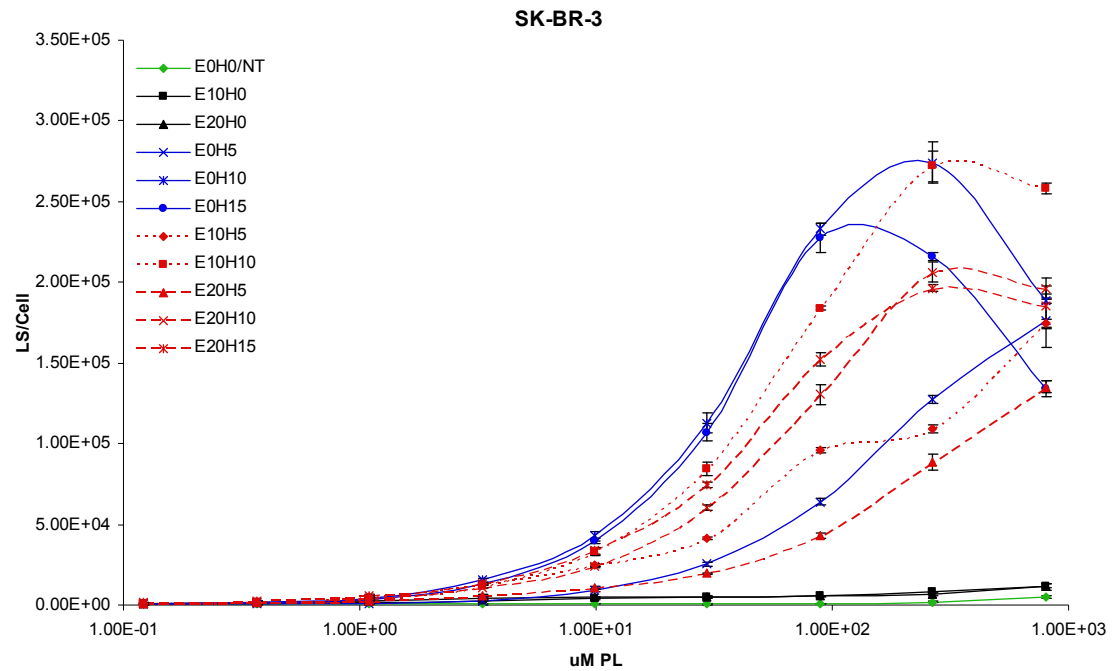


B

Continued on next page...



C



D

**Figure 3.2 Dose-uptake studies of HER2-targeted, EGFR-targeted, and dual-targeted immunoliposomes (ILS) of varying ligand densities. A. in MDA-468, B. BT-474, C. MKN-7, and D. SK-BR-3 cells:** Cells were incubated with liposomes (LS) labeled with DiO at 37° C for 4 hr, lysed, and analyzed by fluorometry. For ExHy ILS,  $x$  and  $y$  specify the number of ligands per liposome against EGFR (cetuximab-Fab') and HER2 (F5 scFv), respectively. Phospholipid (PL), non-targeted (NT)

### 3.3.4 Additive Dose-Uptake Effect of Anti-HER2 and Anti-EGFR Dual-Targeted Immunoliposomes

To investigate the effects of true dual-targeting, dose-uptake studies were continued on cell lines expressing moderate to high levels of both HER2 and EGFR. In BT-474 cells ( $10^6$  HER2 per cell and moderate levels of EGFR(44, 124)), F5 scFv-ILS reached a plateau at  $\sim 100$ - $200$   $\mu$ M PL, resulting in  $\sim 7 \cdot 10^4$  liposomes and  $\sim 1 \cdot 10^6$  F5 scFv per cell (Figure 3.2). At the plateau, there is again roughly a 1:1 ratio of ligands to receptors, similar ratios seen from trastuzumab as an IgG and trastuzumab-Fab' from the immunoliposomes (Table 3.1). Immunoliposomes with varying cetuximab-Fab' densities exhibited low uptake ( $\sim 2 \cdot 10^4$  liposomes/cell), but significantly higher compared to non-targeted liposomes. In the case of anti-HER2 and anti-EGFR dual-targeted immunoliposomes, uptake was significantly higher compared to anti-HER2 immunoliposomes of similar F5 scFv densities ( $P < 4 \cdot 10^{-3}$  for ExH15;  $P < 8 \cdot 10^{-5}$  for ExH10;  $P < 9 \cdot 10^{-5}$  for ExH5).

Interestingly, the accumulation of liposomes and ligands for dual-targeted immunoliposomes were roughly additive of their mono-targeted counterparts in BT-474 cells (Table 3.2). Dual-targeted immunoliposomes with 15 F5 scFv and 20 cetuximab-Fab' resulted in  $8.3 \cdot 10^4$  liposomes per cell, which is also the additive accumulation of mono-targeted 15 F5 scFv-ILS ( $6.8 \cdot 10^4$  liposomes/cell) and 20 cetuximab-ILS ( $1.5 \cdot 10^4$  liposomes/cell). Similarly, dual-targeted immunoliposomes resulted in  $1.2 \cdot 10^6$  F5 scFv per cell, which is also the additive accumulation of mono-targeted F5 scFv ( $1 \cdot 10^6$  F5 scFv/cell) and cetuximab-ILS ( $2 \cdot 10^5$  F5 scFv/cell, extrapolated from  $3 \cdot 10^5$  cetuximab-



Fab' assuming 15:20 ratio). The additive accumulation of liposomes and ligands for dual-targeted immunoliposomes from their mono-targeted counterparts were close for all ratios, 0-15 F5 scFv and 0-20 cetuximab-Fab' per liposome.

In MKN-7 cells (moderate levels of both HER2 and EGFR), HER2-targeted and EGFR-targeted immunoliposomes did not reach an uptake plateau for any ligand densities (Figure 3.2). Immunoliposomes exhibited low uptake ( $<2 \times 10^4$  liposomes/cell), but significantly higher compared to non-targeted liposomes, except for 10 cetuximab-Fab' per liposome. In the case of dual-targeted immunoliposomes, uptake was significantly higher compared to anti-EGFR or anti-HER2 immunoliposomes of similar ligand densities, in line with previous cell association studies ( $P < 10^{-6}$  for ExH15, ExH10, ExH5, E20Hy, & E10Hy). Similar to the BT-474 cell line, the accumulation of liposomes and ligands for dual-targeted immunoliposomes were roughly additive of their mono-targeted counterparts (Table 3.2). Dual-targeted immunoliposomes with 15 F5 scFv and 20 cetuximab-Fab' resulted in  $\sim 9 \times 10^3$  liposomes per cell, which is the additive accumulation of mono-targeted 15 F5 scFv-ILS ( $4 \times 10^3$  liposomes/cell) and 20 cetuximab-ILS ( $4 \times 10^3$  liposomes/cell). Similarly, dual-targeted immunoliposomes resulted in  $\sim 1.3 \times 10^5$  F5 scFv per cell, which is the additive accumulation of mono-targeted F5 scFv ( $6.1 \times 10^5$  F5 scFv/cell) and cetuximab-ILS ( $5.4 \times 10^5$  F5 scFv/cell, extrapolated from  $7.2 \times 10^5$  cetuximab-Fab' assuming 15:20 ratio). The additive accumulation of liposomes and ligands for dual-targeted immunoliposomes from their mono-targeted counterparts were close for all ratios, 0-15 F5 scFv and 0-20 cetuximab-Fab' per liposome.

**A**

BT-474	LS/Cell		Anti-EGFR Lg/Cell		Anti-HER2 Lg/Cell	
	Max	Sum	Max	Sum	Max	Sum
E0H0/NT	1.7E3 ± 3.6E2					
E10H0	2.0E4 ± 6.6E3		2.0E5 ± 6.6E4			
E20H0	1.5E4 ± 4.8E3		3.0E5 ± 9.6E4			
E0H5	4.0E4 ± 6.0E2				2.0E5 ± 3.0E3	
E0H10	7.2E4 ± 8.0E3				7.2E5 ± 8.0E4	
E0H15	6.8E4 ± 7.3E3				1.0E6 ± 1.1E5	
E10H5	6.1E4 ± 2.8E3	5.9E4	6.1E5 ± 2.8E4	5.9E5	3.1E5 ± 1.4E4	3.0E5
E10H10	9.9E4 ± 8.4E3	9.1E4	9.9E5 ± 8.4E4	9.1E5	9.9E5 ± 8.4E4	9.1E5
E20H5	5.6E4 ± 1.8E3	5.5E4	1.1E6 ± 3.5E4	1.1E6	2.8E5 ± 8.8E3	2.7E5
E20H10	9.7E4 ± 4.6E3	8.7E4	1.9E6 ± 9.2E4	1.7E6	9.7E5 ± 4.6E4	8.7E5
E20H15	8.3E4 ± 1.4E3	8.3E4	1.7E6 ± 2.7E4	1.7E6	1.2E6 ± 2.1E4	1.2E6

**B**

MKN-7	LS/Cell		Anti-EGFR Lg/Cell		Anti-HER2 Lg/Cell	
	Max	Sum	Max	Sum	Max	Sum
E0H0/NT	1.8E3 ± 4.7E2					
E10H0	2.1E3 ± 2.5E2		2.1E4 ± 2.5E3			
E20H0	3.6E3 ± 7.8E2		7.2E4 ± 1.6E4			
E0H5	8.1E3 ± 4.5E2				4.1E4 ± 2.3E3	
E0H10	4.9E3 ± 2.2E2				4.9E4 ± 2.2E3	
E0H15	4.1E3 ± 3.3E2				6.1E4 ± 5.0E3	
E10H5	9.8E3 ± 3.4E2	1.0E4	9.8E4 ± 3.4E3	1.0E5	4.9E4 ± 1.7E3	5.1E4
E10H10	7.9E3 ± 3.3E2	7.0E3	7.9E4 ± 3.3E3	7.0E4	7.9E4 ± 3.3E3	7.0E4
E20H5	1.3E4 ± 6.9E2	1.2E4	2.5E5 ± 1.4E4	2.3E5	6.3E4 ± 3.4E3	5.9E4
E20H10	5.5E3 ± 3.4E2	8.5E3	1.1E5 ± 6.8E3	1.7E5	5.5E4 ± 3.4E3	8.5E4
E20H15	8.5E3 ± 5.7E2	7.7E3	1.7E5 ± 1.1E4	1.5E5	1.3E5 ± 8.5E3	1.2E5

**C**

MDA-468	LS/Cell		Anti-EGFR Lg/Cell		Anti-HER2 Lg/Cell	
	Max	Sum	Max	Sum	Max	Sum
E0H0/NT	1.4E4 ± 8.6E3					
E10H0	2.0E4 ± 5.8E2		2.0E5 ± 5.8E3			
E20H0	5.3E4 ± 2.3E3		1.1E6 ± 4.6E4			
E0H5	5.3E3 ± 2.0E2				2.6E4 ± 1.0E3	
E0H10	1.1E3 ± 2.2E2				1.1E4 ± 2.2E3	
E0H15	8.0E3 ± 2.0E2				1.2E5 ± 2.0E3	
E10H5	2.7E4 ± 8.5E2	2.5E4	2.7E5 ± 8.5E3	2.5E5	1.4E5 ± 4.2E3	1.3E5
E10H10	2.2E4 ± 1.6E3	2.1E4	2.2E5 ± 1.6E4	2.1E5	2.2E5 ± 1.6E4	2.1E5
E20H5	6.1E4 ± 2.0E3	5.8E4	1.2E6 ± 4.1E4	1.2E6	3.1E5 ± 1.0E4	2.9E5
E20H10	5.3E4 ± 2.6E3	5.4E4	1.1E6 ± 5.2E4	1.1E6	5.3E5 ± 2.6E4	5.4E5
E20H15	5.9E4 ± 2.2E3	6.1E4	1.2E6 ± 4.3E4	1.2E6	8.8E5 ± 3.2E4	9.1E5

**Table 3.2 Accumulation of liposomes (LS) and ligands (Lg) from HER2-targeted, EGFR-targeted, and dual-targeted immunoliposomes (ILS).** *A.* in BT-474, *B.* MKN-7, and *C.* MDA-468 cells from dose-uptake studies: *Max* is the maximum measured accumulation; *Sum* is the total calculated accumulation from mono-targeted immunoliposomes counterparts. For ExHy ILS, *x* and *y* specify the number of ligands per liposome against EGFR (cetuximab-Fab') and HER2 (F5 scFv), respectively. Non-targeted (NT)

The dose-uptake experiments were also evaluated on Scatchard plots for cooperativity, which compares the binding affinity with the extent of receptor occupancy (Figure 3.3). Although Scatchard plots are traditionally used to assess binding, uptake and binding for lipid nanoparticles are directly and proportionally linked with internalizing surface ligands. For all cases where mono-targeted immunoliposomes were incubated with a receptor overexpressing cell line (ie, anti-EGFR in MDA-468, anti-HER2 in BT-474, & anti-HER2 in SK-BR-3), the plot concave downwards indicating positive cooperativity. This implies that the equilibrium dissociation constant increases with occupancy. For all cases where mono-targeted immunoliposomes were incubated with a receptor moderately expressing cell line (ie, anti-EGFR in BT-474, both anti-EGFR and anti-HER2 in MKN-7, lesser extent with anti-EGFR in SK-BR-3), the plot concave upwards indicating negative cooperativity. The equilibrium dissociation constant hence decreases with occupancy. Interestingly, for BT-474 cells, dual-targeted immunoliposomes changes the curvilinear profile, with cooperativity being negative at low concentrations and linear to positive at higher concentrations. The cooperativity for all the liposomal samples is apparent, indicating other possible associating interactions such as multivalent binding.

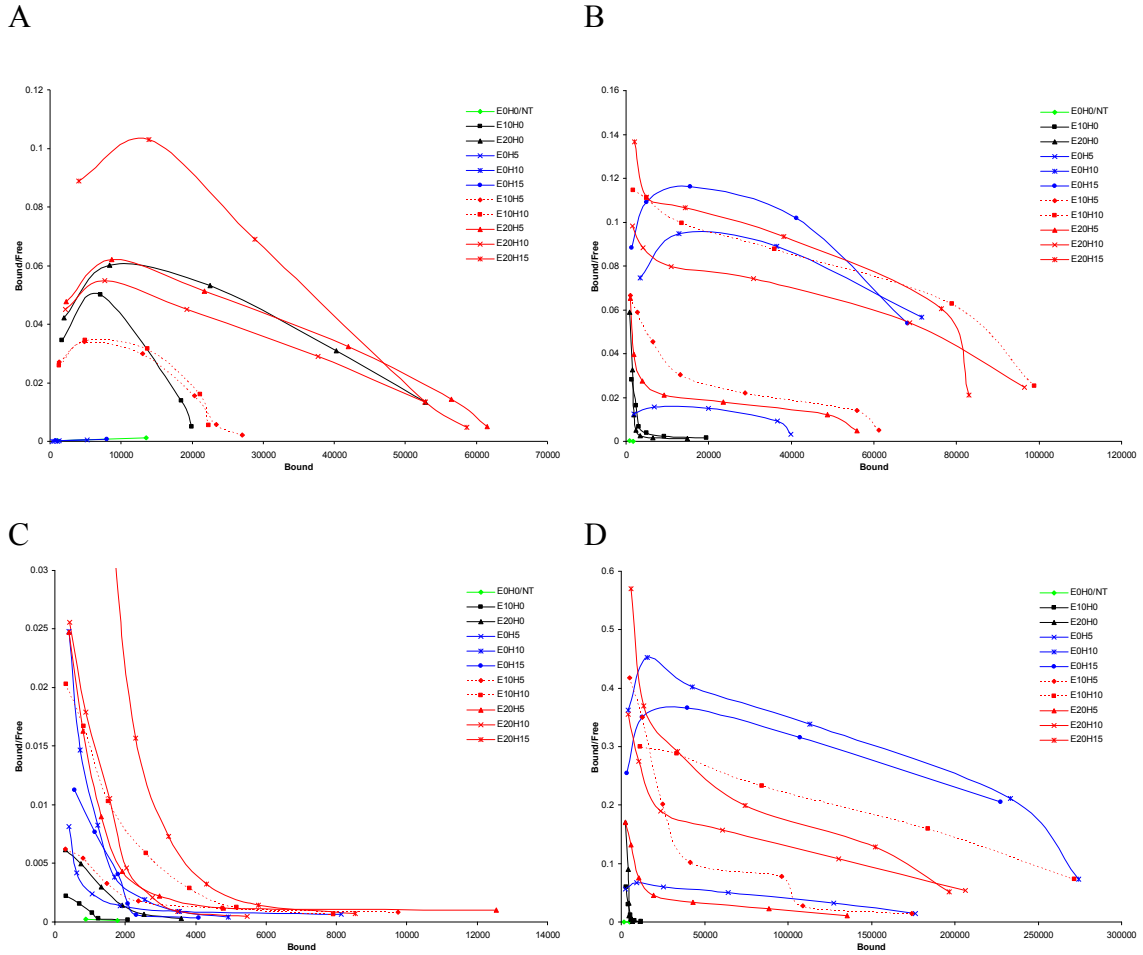


**Figure 3.3** Scatchard plots for dose-uptake studies of HER2-targeted, EGFR-targeted, and dual-targeted immunoliposomes (ILS) of varying ligand densities. **A.** in MDA-468, **B.** BT-474, **C.** MKN-7, and **D.** SK-BR-3 cells: Uptake was assumed to be comparable to cell association; free liposomal concentration was adjusted by subtracting the total bound concentration from the initial liposomal concentration. For ExHy ILS,  $x$  and  $y$  specify the number of ligands per liposome against EGFR (cetuximab-Fab') and HER2 (F5 scFv), respectively. Non-targeted (NT)

In HER2-overexpressing and EGFR-overexpressing human breast cancer cell lines, increasing the density of ligands per liposomes increased targeted uptake until saturation. After which point, increased ligand density may decrease uptake, maintaining a 1:1 ratio of ligands to receptors. The equal ligands to receptors ratio may be explained by multivalent binding and receptor crosslinking. In such ideal situations with both high receptor expression on the cells and high affinity constants for ligands to receptors, it

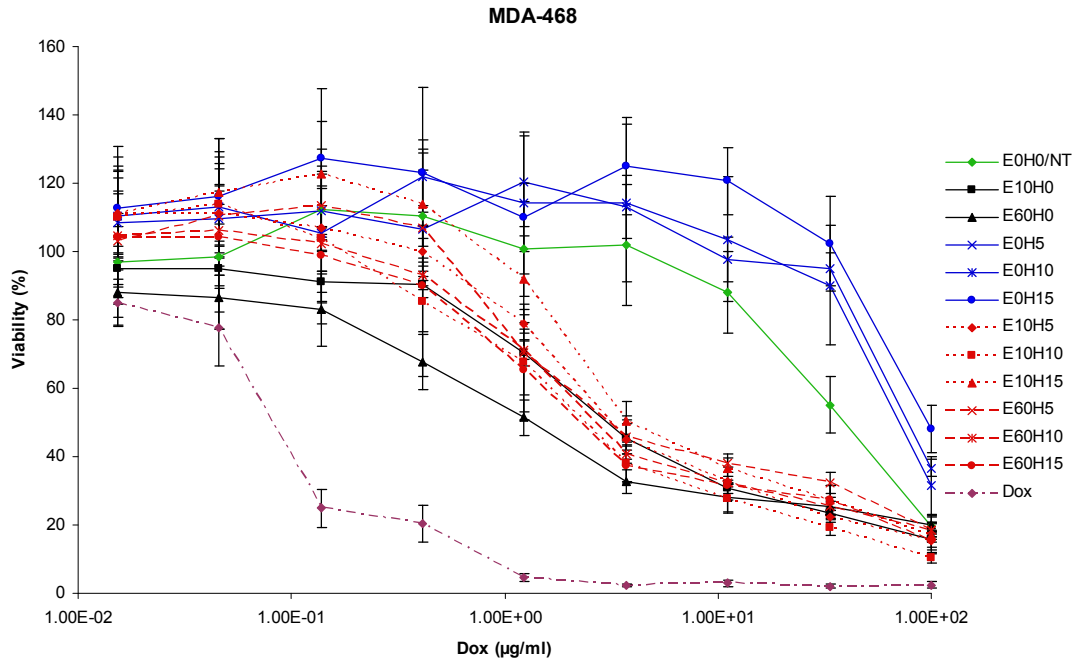
may be possible that multiple ligands are binding to multiple receptors during the process of receptor-mediated endocytosis. In essence, a liposome is behaving as a multivalent ligand that can multivalent bind and crosslink monovalent receptors expressed on the cells. HER2 have been shown to form clusters in cell membranes which may even increase the chances of crosslink binding(130, 131). In addition, per surface area, there are more receptors available per ligand. Assuming an average cell diameter of 10  $\mu\text{m}$  with  $10^6$  receptors and an average liposome diameter of 100 nm with 20 ligands, the receptor to ligand per surface area ratio is 5, meaning that for every ligand there are 5 receptors available to bind. Crosslink multivalent binding of liposomes to clustered receptors is a possible and plausible outcome, and is furthered examined in Chapter 5.

For cell lines that express both receptors such as BT-474 and MKN-7, anti-HER2 and anti-EGFR dual-targeted immunoliposomes can increase the overall accumulation of liposomes and ligands beyond the saturation point of mono-targeted immunoliposomes. In addition, the uptake is roughly additive of their mono-targeted counterparts. Because the uptake of dual-targeted immunoliposomes appears to be additive instead of synergistic, the overall accumulation is only marginally higher (folds, not magnitudes), and hence may result only in marginally increased benefits from increased accumulation. The main advantage may be more of a simplified multi-targeting formulation, where the immunoliposomes can target multiple receptors, and hence effective with more cell lines and accordingly heterogeneous receptor expressing tumors. Only in the SK-BR-3 cell line that the addition of a non-targeting functional group may be antagonistic to uptake at high anti-EGFR ligand valence. Despite that, uptake was only marginally lower.

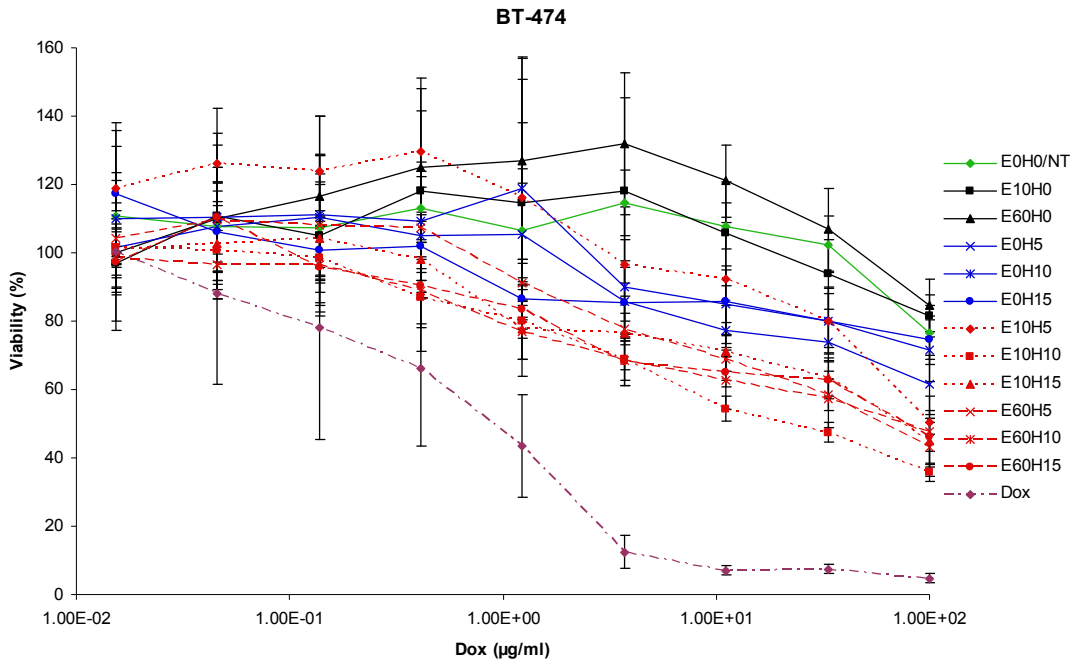
### **3.3.5 Cytotoxicity Studies of Doxorubicin-Encapsulated HER2-Targeted, EGFR-Targeted, and Dual-targeted Immunoliposomes**

In parallel to the dose-uptake studies, cytotoxicity studies with doxorubicin-encapsulated HER2-targeted, EGFR-targeted, and dual-targeted immunoliposomes were also examined for any correlations between increased targeted uptake and toxicity benefits of dual-targeted drug delivery. In MDA-468 cells, immunoliposomes with higher cetuximab-Fab' per liposome ligand densities (0-60 ligands/liposome) correlated with higher cell death (Figure 3.4). Immunoliposomes with varying F5 scFv densities (0-15 ligands/liposome) had no significant cytotoxicity compared to non-targeted liposomes. In the case of anti-HER2 and anti-EGFR dual-targeted immunoliposomes, cell viability was not significantly lower to anti-EGFR immunoliposomes of similar cetuximab-Fab' densities ( $P < 0.6$  for E10Hy;  $P < 0.99$  for E60Hy). Results were in agreement with the dose-uptake studies, higher uptake resulting in higher toxic effect in cells.

In BT-474 cells, immunoliposomes with varying F5 scFv per liposome densities (5-15 ligands/liposome) yielded significant cytotoxicity compared to non-targeted liposomes, but no significant difference among each other (Figure 3.4). Immunoliposomes with varying cetuximab-Fab' densities (0-60 ligands/liposome) resulted in no significant cell viability. In the case of anti-HER2 and anti-EGFR dual-targeted immunoliposomes, cell growth inhibition was significantly better compared to anti-HER2 immunoliposomes of similar F5 scFv only in two cases where cetuximab was also high: E60H10 ( $P < 10^{-6}$ ) and E60H15 ( $P < 9 \times 10^{-4}$ ). Compared to the dose-uptake studies, the degree of toxic effect is not as pronounced as targeted uptake.

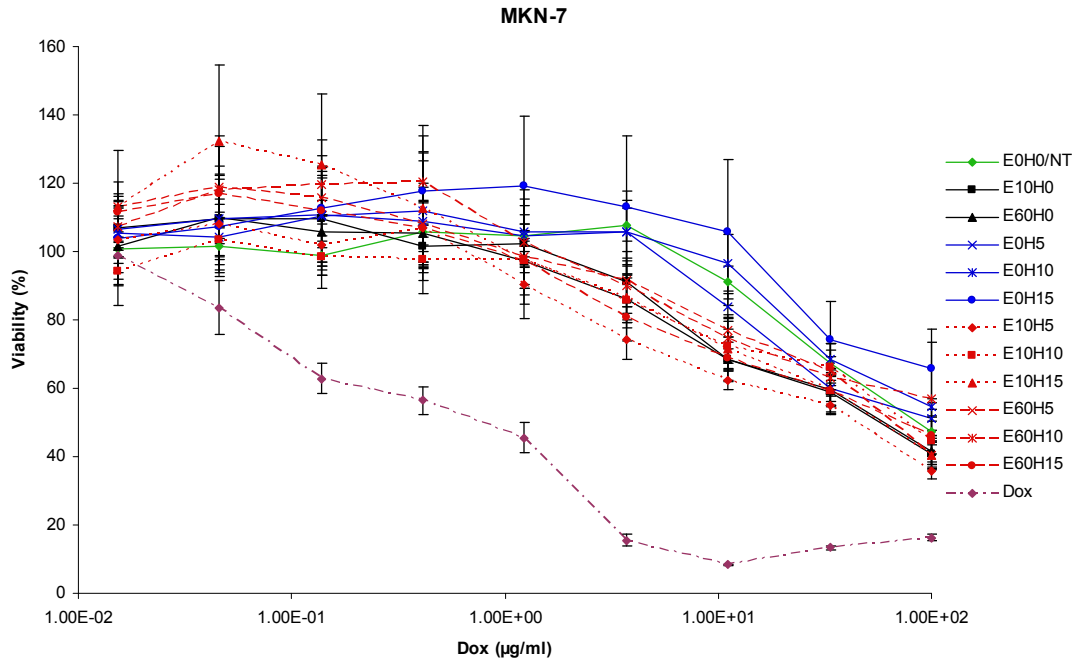


A

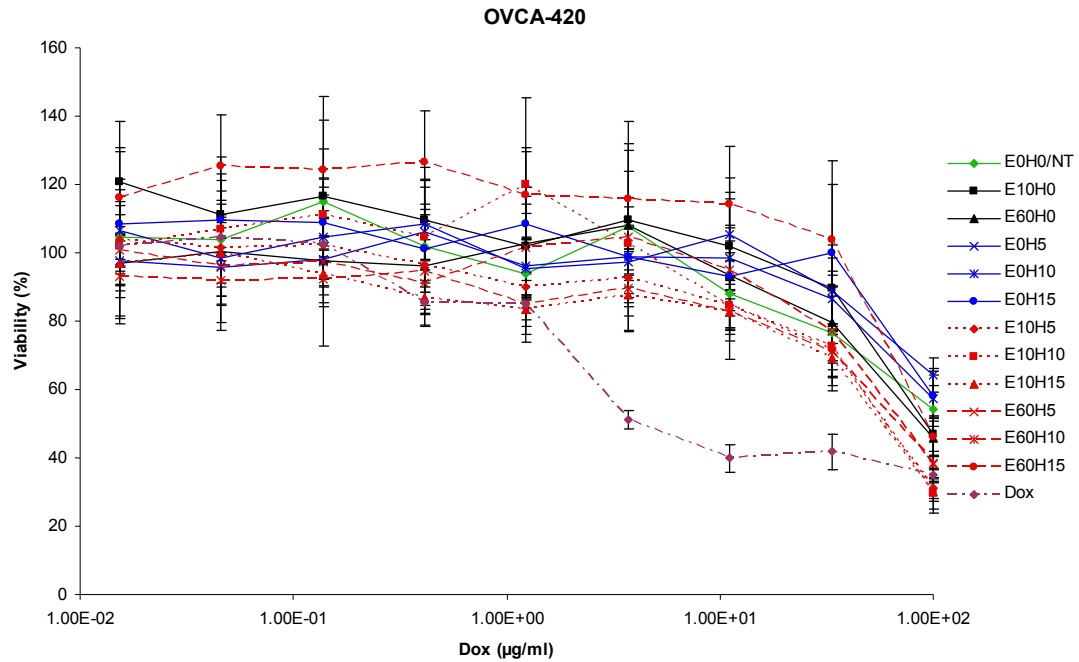


B

Continued on next page...



C



D

**Figure 3.4 Cytotoxicity studies of doxorubicin-encapsulated HER2-targeted, EGFR-targeted, and dual-targeted immunoliposomes (ILS).** *A.* in MDA-468, *B.* BT-474, *C.* MKN-7, and *D.* OVCA-420 cells: Cells were incubated with liposomes at 37° C for 4 hr and evaluated for cell viability by MTT assay after 3 days. For ExHy ILS,  $x$  and  $y$  specify the number of ligands per liposome against EGFR (cetuximab-Fab') and HER2 (F5 scFv), respectively. Non-targeted (NT), doxorubicin (Dox)



In MKN-7 cells, immunoliposomes with varying cetuximab-Fab' per liposome ligand densities (10-60 ligands/liposome) yielded higher cytotoxicity compared to non-targeted liposomes ( $P < 10^{-4}$ ), but no significant difference among each other (Figure 3.4). Immunoliposomes with varying F5 scFv densities (0-15 ligands/liposome) resulted in no significant cell growth inhibition ( $P < 1$ ). In the case of anti-HER2 and anti-EGFR dual-targeted immunoliposomes, cell viability was not significant compared to any mono-targeted immunoliposomes ( $0.01 < P < 1$ ). Compared to the dose-uptake studies, the degree of toxic effect again is not as pronounced as targeted uptake. In OVCA-420 cells which moderately express both EGFR and HER2, immunoliposomes with varying F5 scFv per liposome (0-15 ligands/liposome) and cetuximab-Fab' per liposome (0-60 ligands/liposome) ligand densities for mono-targeting had no significant cytotoxicity compared to non-targeted liposomes (Figure 3.4). However, similar to BT-474 cells, anti-HER2 and anti-EGFR dual-targeted immunoliposomes yielded enhanced cytotoxicity for a few cases cases: E60H10, E60H15, & E10F15;  $P < 10^{-6}$ ). Results were in agreement with the dose-uptake studies (data not shown).

For these cytotoxicity studies *in vitro*, free doxorubicin is the most effective since it easily and quickly penetrate the cell membrane and internalized into the nucleus, the site of action. On the contrary, free doxorubicin is not as effective as liposomal doxorubicin *in vivo* since free doxorubicin has a fast clearance rate and liposomal doxorubicin are passively targeted to the tumors through the enhanced permeability and retention effect. Cytotoxicity studies *in vitro* with less membrane diffusible drugs such as topotecan and vinorelbine are more effective in a targeted liposomal formulation compared to free form. Cytotoxicity studies were conducted with doxorubicin as it is the

staple drug for liposomal delivery. Changing to more membrane less permeable drugs will likely increase the resolution for the cytotoxicity studies.

In comparison to the cytotoxicity studies with doxorubicin, the targeted uptake studies with anti-HER2 and anti-EGFR immunoliposomes resulted in higher resolution, showing differences between ligand densities and the additive effects of using dual-targeted immunoliposomes. The additive and possible synergistic effects of using dual-targeting ligands only significantly enhanced the cell growth inhibition with doxorubicin for a few formulations where both anti-EGFR and anti-HER2 ligands were of high density in the BT-474 and OVA-420 cell lines. As discussed earlier, the uptake of dual-targeted immunoliposomes appears to be additive instead of synergistic where the accumulation is only marginally higher, and hence it is expected that the biological effect of drug delivery was only marginally better if at all. The main advantage was evident in the cocktail-targeting approach, where the immunoliposomes can target multiple receptors, and hence effective with more cell lines. The same dual-targeting liposomal formulations were used with all the cell lines with no observed antagonistic effects with cell viability, even in the case of SK-BR-3 cells (data not shown). Hence, the dozen formulations can be reduced to one.

### **3.4 Conclusion**

For HER2-overexpressing and EGFR-overexpressing cell lines, the receptor-mediated cell association studies confirmed the observation where increasing ligand density per liposome increases targeted uptake until saturation (trastuzumab, F5 scFv, and cetuximab). At the optimum ligand density and higher valence, there is roughly a 1:1

ratio of ligands (F5 scFv and cetuximab-Fab') to receptor for MCF-7/HER2, BT-474, SK-BR-3, and MDA-468 cells. There was also comparable accumulation of free trastuzumab as trastuzumab-Fab' delivered from immunoliposomes in MCF-7/HER2 and BT-474 cells.

In addition, the accumulation of liposomes and ligands for anti-HER2 and anti-EGFR dual-targeted immunoliposomes were roughly additive of their mono-targeted counterparts in BT-474 and MKN-7 cells. No antagonistic effects were observed from the additional of a non-targeted ligand in all cell lines except for SK-BR-3 at high anti-EGFR ligand valence, where anti-EGFR ligands decreased overall uptake. Despite the additive uptake effect, dual-targeted liposomal delivery of doxorubicin to cell lines expressing HER2 and EGFR only significantly enhanced the cell growth inhibition compared to mono-targeted liposomal delivery for a few liposomal formulations where both anti-EGFR and anti-HER2 ligands were of high valency. Although significant, the improvement was minimal and hence not valuable on a purely increased of cellular drug accumulation standpoint. Dual-targeting lipid nanoparticles can still be beneficial as a system to target heterogeneous cancers.

### **3.5 Materials and Methods**

#### **3.5.1 Materials**

HER2-targeted, EGFR-targeted, and dual-targeted liposomal formulations and their ligands are described in Chapters 2. Cell culture media, fetal calf serum, penicillin-streptomycin, gentamycin, trypsin, and phosphate buffered saline (PBS) were purchased from the UCSF Cell Culture Facility (San Francisco, CA). Glycine and thiazolyl

blue tetrazolium bromide were purchased from Sigma-Aldrich (St. Louis, MO).

Doxorubicin (Bedford Laboratories) was purchased from the UCSF Pharmacy (San Francisco, CA).

### **3.5.2 Cell Lines**

MDA-468 and BT-474 human breast cancer cell lines were obtained from the American Type Culture Collection (Rockville, MD), MKN-7 and SK-BR-3 human breast cancer cell lines from the UCSF Cell Culture Facility (San Francisco, CA), and MCF-7/HER2(125) human breast cancer cell line from the UCSF Preclinical Therapeutics Core (San Francisco, CA). MDA-468 cells were maintained in Leibovitz's L-15 medium without NaHCO<sub>3</sub>, BT-474 and MKN-7 cells in RPMI-1640 medium, SK-BR-3 in McCoy's 5A medium, and MCF-7/HER2 in DEM H-21 medium with gentamycin (200 µg/ml). All media were supplemented with 10% fetal calf serum and 1% penicillin-streptomycin. All cells were cultured as monolayer at 37° C in 5% CO<sub>2</sub> except in the absence of CO<sub>2</sub> for MDA-468 cells.

### **3.5.3 Cell Association Studies**

For the assessment of targeted binding by flow cytometry, cells cultured overnight in 24-well plates (75-100\*10<sup>3</sup> cells/well) were incubated with liposomes labeled with DiD or DiO (0-750 µM PL) at 37° C for 1-11 hr, washed with PBS 3x, detached with trypsin, resuspended in PBS, and immediately subjected to flow cytometry (BD FACSCalibur). Detached cells were analyzed on fluorescence channels FL4 and FL1 for

liposomes labeled with DiD and DiO, respectively. The mean fluorescent intensity with a tight spread of  $5 \times 10^3$  cells was recorded per liposomal formulation.

### **3.5.4 Uptake and Dose-Uptake Studies**

For the assessment of targeted uptake by fluorometry, cells cultured overnight in 96-well plates ( $50 \times 10^3$  cells/well) were incubated with liposomes labeled with DiD (75 or 375  $\mu$ M PL) or ligands labeled with Alexa Fluor 488 (40 nM) at 37° C for 4 hr, stripped with an acid wash (50 mM glycine, 150 mM NaCl, pH 3) at 4° C for 5 min, washed with PBS 2x, freeze-thawed 3x, and lysed with 80% isopropyl alcohol (IPA) and 1% Triton X-100. For the assessment of targeted dose-uptake by fluorometry, cells cultured overnight in 96-well plates ( $50 \times 10^3$  cells/well) were incubated with liposomes labeled with DiD or DiO (800  $\mu$ M PL with 1/3 dilutions) at 37° C for 4 hr, washed with PBS 3x, freeze-thawed 3x, and lysed with 80% IPA and 1% Triton X-100. Lysed samples along with standards using labeled liposomes and ligands added to the plates were read on a fluorescent microplate reader (Biotek Synergy HT or Wallac Victor). Measurements were read with excitation and emission band-pass filters as follow: DiO 485/20:528/20 nm, DiD 644:665 nm, Alexa Fluor 488 485/20:528/20 nm, and doxorubicin 485/20:590/35 nm. Cell count was estimated based on a hemacytometer and MTT assay ((3-(4,5-Dimethylthiazol-2-yl)-2,5-diphenyltetrazolium bromide), showing negligible cell detachment or toxicity under these conditions between groups.

### **3.5.5 Cytotoxicity Studies**

For cytotoxicity studies, cells cultured overnight in 96-well plates ( $10 \times 10^3$  cells/well) were incubated with doxorubicin-load liposomes (100  $\mu\text{g/ml}$  with 1/3 dilutions) at 37° C for 4 hr, washed with PBS, and grown in medium for 3 additional days. Cell viability was analyzed by MTT assay. Bars of standard deviations were adjusted for the error of propagation.

### **3.5.6 Statistical Analysis**

For dose-uptake studies, the uptake of liposomes was analyzed by two-way ANOVA via SPSS Statistics 20 (IBM) using two factors, liposomal formulation and incubated liposomal concentration. For cytotoxicity studies, cell growth inhibition was analyzed by two-way ANOVA via SPSS Statistics 20 (IBM) using two factors, liposomal formulation and incubated drug concentration. For group comparisons, the largest P value was selected to generalize the overall group. For mean comparisons, student's t-test was applied.

## Chapter 4: Analysis of Intracellular Sorting

### 4.1 Abstract

In the area of receptor-targeted lipid nanoparticles such as immunoliposomes (ILS), the intracellular sorting of the nanoparticles is not well defined. The choice of the targeted receptor offers cell-specificity and receptor-mediated uptake, but it may also determine the intracellular routing and ultimately the biological effect. Ligands targeting HER2 and EGFR were investigated alone and as targeting functional groups attached to the surface of liposomes as they traffic through endosomal compartments in cells by confocal microscopy and colocalization analysis. In addition, recycling and hence exocytosis assessments through flow cytometry and pathway-targeted cell growth inhibition through doxorubicin delivery were evaluated. Ligand choice, such as anti-HER2 trastuzumab & F5 scFv and anti-EGFR EGF, TGF $\alpha$ , & cetuximab, as well as pathway transregulation and pathway saturation were examined.

Evidence suggested that the intracellular sorting of receptor-mediated lipid nanoparticles to the degradative and the recycling endosomal pathways may be governed by the sorting of the targeted receptor. When a recycling ligand such as trastuzumab was attached to liposomes, the immunoliposomes accumulated higher in the recycling endosomes than in the late endosomes. Since the pathway of trastuzumab can be diverted towards the degradative pathway with geldanamycin, the pathway of trastuzumab-conjugated immunoliposomes also similarly diverted. For EGFR-targeting, EGF-conjugated liposomes like EGF accumulated more in late endosomes than the recycling

endosomes and TGF $\alpha$ -conjugated liposomes like TGF $\alpha$  accumulated more in the recycling endosomes than the late endosomes. F5 scFv-conjugated and cetuximab-conjugated immunoliposomes were also investigated, showing comparable distribution between the endosomal compartments. Unlike the exocytosis of recycled ligands, evidence suggested that lipid nanoparticles settle in endosomal compartments without exocytosis. Finally, early assessments in bioactivity advantages for targeted intracellular pathways were examined but inconclusive. However due to the increased endocytosis and accumulation of ligand-conjugated lipid nanoparticles into cells compared to free ligands such as trastuzumab, data suggested that targeted liposomal drug delivery has a large intracellular drug delivery advantage over antibody-drug conjugates, as high as 5200 fold increase.

## **4.2 Introduction**

Upon receptor-mediated endocytosis, receptor-bounded ligands are sorted in the early endosomes to the recycling or the degradative endosomal pathways. While receptors in the recycling endosomes are returned to the cell surface, receptors in the degradative pathway are routed to the late endosomes and lysosomes for degradation. For example, transferrin, the major iron-carrying protein, has been long studied to internalize with the transferrin receptor and then both ligand and receptor are continuously recycled back to the cell surface largely undegraded(70-75). The fates of EGFR and HER2 are less certain. Both receptors and their associated ligands may play pivotal roles in intracellular sorting. Not only do the relationship of the targeted



receptors and ligands determine the sorted pathway, but other mechanisms may dictate routing such as transregulation and pathway saturation.

The pathways of a few EGFR-binding and HER2-binding ligands have been documented. EGF and TGF $\alpha$  are the key EGFR binding ligands. Although both growth factors are structurally related in size and structure and have comparable affinity constants and function, EGFR-EGF complexes are largely degraded while EGFR-TGF $\alpha$  complexes are regularly recycled(76-78). Similar to transferrin, TGF $\alpha$  dissociates from the receptor-ligand complex at a much higher pH than EGF, and is more rapidly recycled with a substantial portion undegraded compared to EGF(77). The intracellular trafficking of recently discovered monoclonal antibodies such as anti-EGFR cetuximab and matuzumab are still uncertain, with research showing contradictory evidence of EGFR downregulation and lack thereof(78, 80, 81). Although anti-HER2 trastuzumab induces receptor-mediated endocytosis, the antibody subsequently recycles passively with no downregulation of surface HER2(79). F5 single-chain variable fragments (scFv), selected from an antibody phage library by panning HER2-overexpressing cells, efficiently bind HER2, triggering receptor-mediated endocytosis and inducing downstream signaling through HER2(38). The intracellular trafficking like F5 scFv is still unknown.

In addition, the intracellular pathway of receptors can be modulated by receptor transregulation and pathway saturation. With EGFR, protein kinase C stimulation of threonine 654 with phorbol myristate acetate shifts the pathway from degradative to recycling for EGF(86-88). With HER2, chaperone heat shock protein 90 inhibition by geldanamycin shifts the default recycling to degradative sorting for trastuzumab(79).

Hence, one can regulate the intracellular pathway by inducing the receptors prior to incubation with ligands. The degradative endosomal pathway is saturable not only for ligands but also large carriers such as viruses(76, 87-89). In essence, for complexes with preferential degradative pathway sorting, eventually the cargo delivered to late endosomes gets saturated, diverting the remaining receptor and cargo to recycling endosomes.

In the area of receptor-targeted lipid nanoparticles such as immunoliposomes, the intracellular sorting of the nanoparticles is not well defined. The choice of the targeted receptor offers cell-specificity and receptor-mediated uptake, but it may also determine the intracellular routing and ultimately the biological effect. For viruses like the AAV2, higher bioactivity was evident when the virus sorted to recycling endosomes and away from the degradative endosomes prone of nucleotide digestion(89). The resulted pathway and the consequential biological activity in the delivery of drugs may differ from viruses and potentially nucleotides. First, the intracellular sorting of receptor-mediated lipid nanoparticles to the degradative and the recycling endosomal pathways may be governed by the sorting of the targeted receptor. Second, lipid nanoparticles diverted from the degradative to the recycling endosomal pathway may enhance biological activity for membrane impermeable, pH-sensitive molecules such as nucleotides and large hydrophobic drugs. Essentially, molecules that are easily denatured and have difficulty escaping the late endosomes may benefit from recycling endosomal targeting, where the pH is more neutral and the lack of digestive enzymes. Stable, resilient molecules and drugs may not gain any advantages from diverting away from the late endosomes since endosomal escape may be more rate limiting.

Pathway sorting of ligands and possibly ligand-conjugated lipid nanoparticles also can determine the sorting of the receptors. When ligands like transferrin and TGF $\alpha$  recycle, their corresponding receptors also recycle instead of being downregulated and degraded. Hence one potential advantage of recycling receptors, with the quick turnaround, is that more free recycled receptors are made available to bind and internalize more extracellular ligands or ligand-conjugated lipid nanoparticles. This can potentially increase the accumulation of liposomal drug delivery since there is always a high accessible supply of surface receptors.

Through confocal microscopy and immunocytochemistry, we investigated whether the uptake and intracellular sorting of ligand-conjugated lipid nanoparticles to either the degradative or the recycling endosomal pathways is determined by the targeted receptor EGFR and HER2. We studied the relationship of the targeted receptors to the resulted pathways, other mechanisms that may dictate routing such as transregulation and pathway saturation, and ultimately the consequential biological activity in the delivery of drugs.

## **4.3 Results and Discussion**

### **4.3.1 Endosomal Colocalization Analysis of HER2-Targeted and EGFR-Targeted Liposomes and Ligands**

Immunocytochemistry, an immunolabeling technique that uses antibodies that target specific peptides or protein antigens in the cell via specific epitopes, was applied to label Rab7 found on late endosomes and Rab11 found on recycling endosomes in cells for visualization by confocal microscopy. Endosomal trafficking is controlled by several

Rab proteins, small guanosine triphosphate-binding proteins(57, 58). The Rab family is the largest branch of the Ras superfamily with more than 60 members found in mammalian cells. Rab proteins reside in particular types of endosomes and function by recruiting specific effector proteins. Rab proteins distinguish certain intracellular compartments and are involved in vesicle budding, vesicular movement, membrane tethering, membrane docking, and membrane fusion(64, 65). Rab7 is primarily localized on the late endosomes and has been shown to be essential for lysosomes biogenesis(66). Rab11 is primarily localized on the recycling endosomes(67), and has been extensively studied for its involvement in transferrin receptor recycling(68, 69). Tagged Rab proteins as markers are useful for the isolation and localization of nanoparticles within the late endosomes and the recycling endosomes.

Colocalization analysis between fluorescently labeled molecules in optical microscopy is a useful technique to assess the degree of spatial coincidence, and hence potential interactions, among subcellular species(132). Colocalization studies using confocal microscopy and immunocytochemistry were used to study the intracellular trafficking of fluorescently labeled liposomes and ligands through the endosomal compartments. Liposomes and ligands were incubated with cells and chased at different time points. Micrographs captured by confocal microscopy (1 megapixel) were processed with ImageJ using plug-ins from MacBiophotonics and analyzed by the Costes method for colocalization threshold and to calculate the percentage of colocalized pixels. TetraSpeck fluorescent microsphere standards (Life Technologies) were used as controls for instrumentation adjustment and colocalization analysis. Endosomal labeling was

initially confirmed by the trafficking of transferrin labeled with Alexa Fluor 546 in a series of cells.

As an example of colocalization analysis, the colocalization of TetraSpeck microspheres 500 nm in size (roughly the size of endosomes), initially at 100% colocalization when self-overlaid, decreased approximately 18% per pixel<sup>2</sup> shift relative to the original position (Figure 4.1). When the frame had shifted for a total of 5 pixel<sup>2</sup>, only 9% of the microspheres are still colocalized. Since the microspheres are stained with four different fluorescent dyes, they are valuable as controls. Microscopy settings were adjusted so the microspheres were confirmed ~100% colocalized at the relevant spectrums. For the intracellular trafficking studies, 3-10 images of cells with at least 3 z-slices per sample from 1-3 studies were analyzed and averaged to calculate the percentage of pixels representing liposomes and ligands colocalized to pixels representing the endosomal compartments.

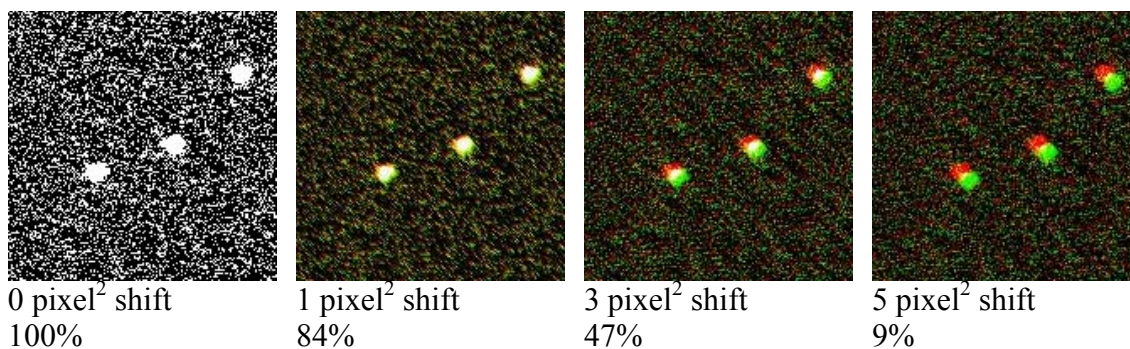


**Figure 4.1 Colocalization analysis of pixel shifted TetraSpeck fluorescent microspheres.** Micrograph of microspheres (500 nm) captured by confocal microscopy (1 megapixel), initially at 100% colocalization when self-overlaid, was shifted 1-5 pixel<sup>2</sup> and analyzed by the Costes method for colocalization threshold and to calculate the percentage of pixels representing the microspheres still colocalized to the original position, resulting in approximately ~18% change in colocalization per pixel<sup>2</sup> shift. Percentages represent colocalization. Pixels representing microspheres (red or green) are labeled white for colocalized pixels.

### 4.3.2 Trafficking of Trastuzumab and Trastuzumab-Conjugated Immunoliposomes

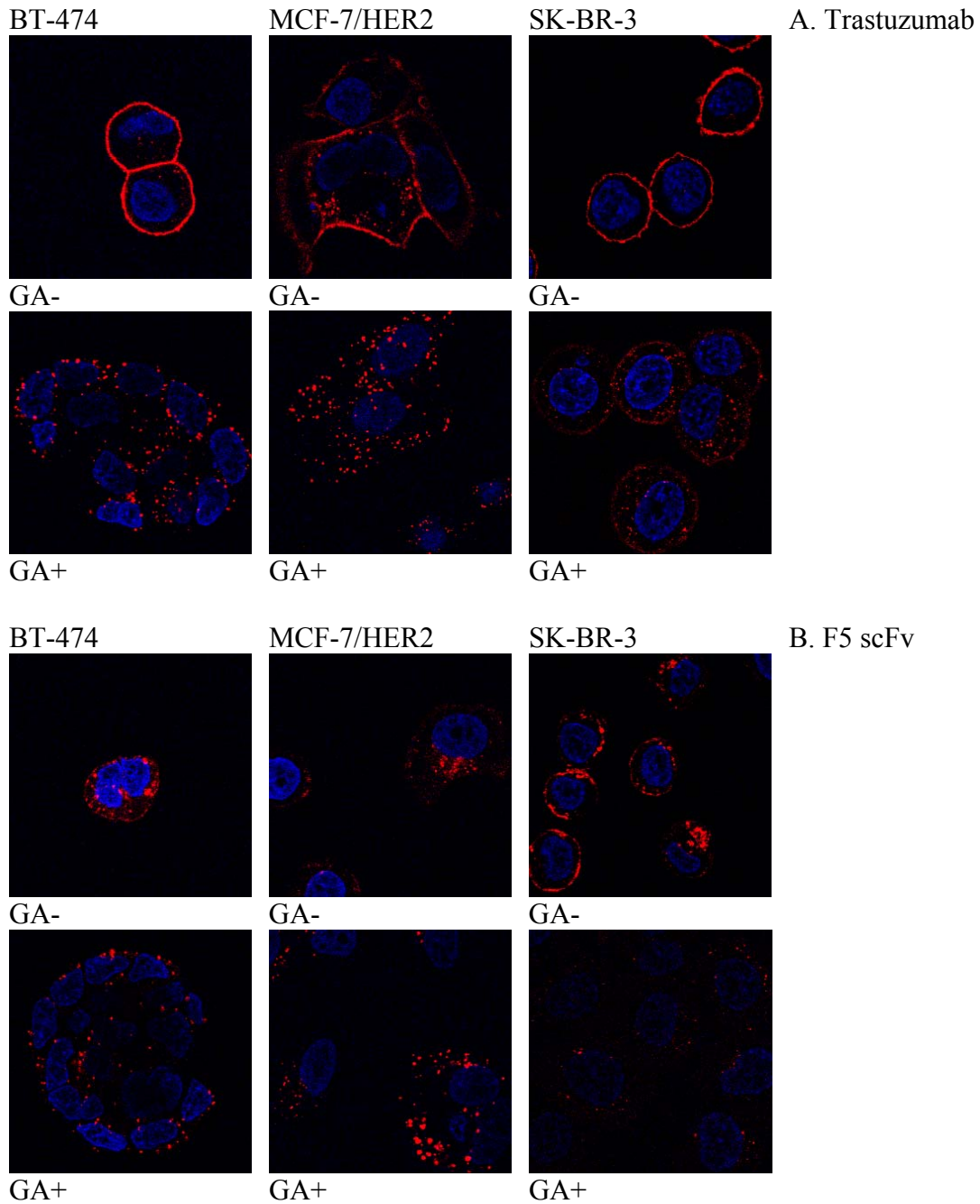
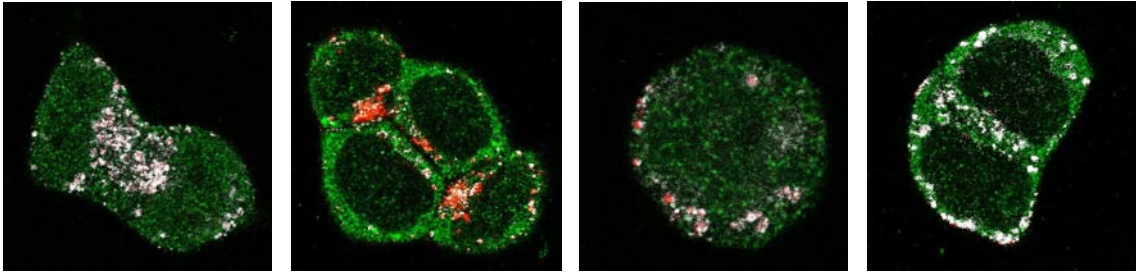


**Figure 4.2 Cellular uptake of anti-HER2 trastuzumab and F5 scFv-PEG-DSPE in BT-474, MCF-7/HER2, and SK-BR-3 cells visualized by microscopy.** Cells, pre-incubated with(+) or without(-) geldanamycin (GA), were incubated with **A.** trastuzumab labeled with Alexa Fluor 488 (red) or **B.** F5 scFv-PEG-DSPE labeled with Alexa Fluor 488 (red) at 37° C for 10 min with 3 hr chase and visualized by confocal microscopy. Nucleus was post-stained with DAPI (blue).

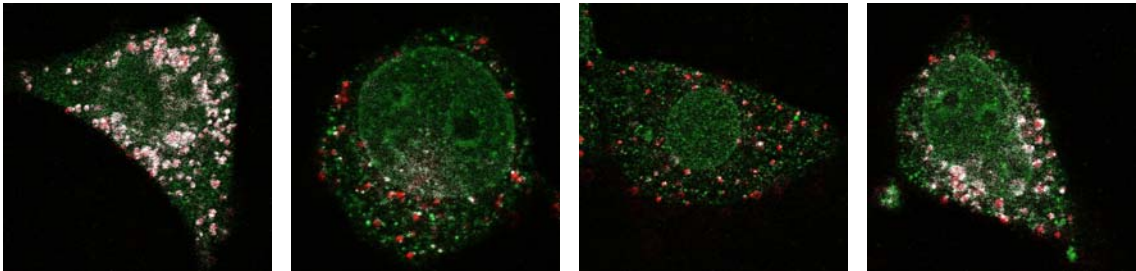
To access the intracellular trafficking of trastuzumab in HER2-overexpressing cells, trastuzumab labeled with Alexa Fluor 488 was incubated with BT-474, MCF-7/HER2, or SK-BR-3 cells for 10 min with a 3-4 hr chase, subjected to immunocytochemistry, and visualized by confocal microscopy. Trastuzumab remained mostly surface-bound throughout, with very few IgG internalized in the intracellular compartments (Figure 4.2). ImageJ analysis of z-slices of BT-474 cells estimated approximately ~100% IgG remained surface-bound at 30-60 min incubation and decreased to  $92 \pm 3\%$  after 3 hr incubation. However when pre-incubated with geldanamycin, trastuzumab was shifted from the surface to the intracellular compartments. Geldanamycin, an inhibitor of chaperone heat shock protein 90, is known to transregulate HER2-trastuzumab complexes and shift the default recycling to degradative sorting(79). Through colocalization analysis of trastuzumab with fluorescently labeled late endosomes and recycling endosomes by immunocytochemistry, trastuzumab transregulated with geldanamycin was predominately found colocalized in the degradative compartments, favoring the late endosomes to the recycling endosomes 3:2-4:1 (Figure 4.3; Table 4.1). In the absence of geldanamycin, the colocalization of trastuzumab in endosomes was negligible throughout since trastuzumab remained mostly extracellular.

RE (Rab11), GA-      LE (Rab7), GA-      RE (Rab11), GA+      LE (Rab7), GA+

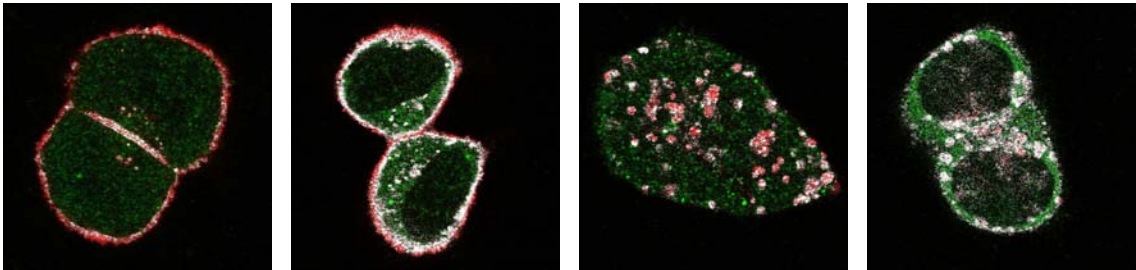
A. Trastuzumab-ILS in BT-474 cells



B. Trastuzumab-ILS in MCF-7/HER2 cells



C. Trastuzumab in BT-474 cells



D. Trastuzumab in MCF-7/HER2 cells

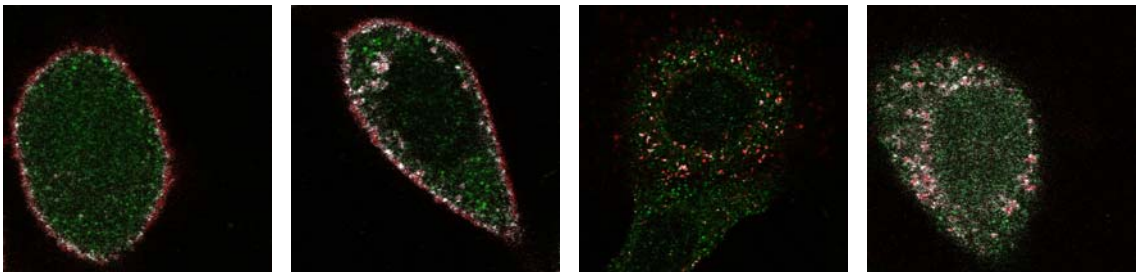


**Figure 4.3 Endosomal colocalization analysis of trastuzumab-conjugated immunoliposomes (ILS) and trastuzumab in HER2-expressing cells.** Cells, pre-incubated with/out geldanamycin (GA±), were incubated with trastuzumab-ILS labeled with DiD in **A.** BT-474 and **B.** MCF-7/HER2 cells or trastuzumab labeled with Alexa Fluor 488 in **C.** BT-474 and **D.** MCF-7/HER2 cells at 37° C for 10 min with 3 hr chase and visualized by confocal microscopy. Rab11 and Rab7 were labeled by immunocytochemistry for the recycling endosomes (RE) and the late endosomes (LE), respectively (green). Z-slices were analyzed by the Costes method for colocalization threshold and to calculate the percentage of pixels representing liposomes or ligands (red) colocalized to pixels representing the endosomal compartments (colocalized pixels, white).



	GA		MCF-7/HER2	BT-474
Trastuzumab-ILS	-	RE	57±6	64±5
	-	LE	44±5	37±10
	+	RE	40±9	46±5
	+	LE	59±4	63±8
Trastuzumab	-	RE	NE	NE
	-	LE	NE	NE
	+	RE	38±4	24±10
	+	LE	62±6	76±5
F5 scFv-ILS	-	RE	46±5	
	-	LE	54±7	
	+	RE	48±6	
	+	LE	52±10	
F5 scFv	-	RE	37±5	
	-	LE	63±5	
	+	RE	39±8	
	+	LE	61±5	

(Average of 1-3 studies, 3-10 samples per study, 3 z-slices per sample)

**Table 4.1 Colocalization percentage of HER2-targeted immunoliposomes (ILS) and ligands in the recycling endosomes (RE) and the late endosomes (LE) of BT-474 and MCF-7/HER2 cells.** Cells, pre-incubated with/out geldanamycin (GA±), were incubated with trastuzumab-ILS, trastuzumab, F5 scFv-ILS, or F5 scFv-PEG-DSPE at 37° C for 10 min with 3-4 hr chase and captured by confocal microscopy. Z-slices were analyzed by the Costes method for colocalization threshold and to calculate the percentage of pixels representing liposomes or ligands colocalized to pixels representing the endosomal compartments labeled by immunocytochemistry. Intracellular values were not evaluable (NE) for trastuzumab due to high signal interference from surface-binding, with approximately 92 ± 3% surface-bound.

When trastuzumab was incubated with cells for 4 hr without a chase, more trastuzumab was found to be endocytosed, but evenly distributed between the recycling endosomes and the late endosomes. Most ligands still remained surface-bound (92 ± 3%). When ligands are surface-bound, colocalization analysis was complicated due to signal interference, and as a result not evaluable. When pre-incubated with geldanamycin, trastuzumab again was predominately found colocalized in the degradative compartments with the distribution unchanged. The results are in line with the literature where trastuzumab was found to recycle passively with internalized HER2, except when down-regulated with geldanamycin which improved degradative

sorting(79). As expected, trastuzumab favors the recycling pathway over the degradative pathway, except after transregulation with geldanamycin.

Similarly, the intracellular trafficking of trastuzumab-conjugated immunoliposomes was examined in HER2-overexpressing cells. Trastuzumab-ILS labeled with DiD was incubated with BT-474 and MCF-7/HER2 cells for 10 min with a 3-4 hr chase, subjected to immunocytochemistry, and visualized by confocal microscopy. Unlike surface-bound trastuzumab, trastuzumab-ILS was immediately found predominately endocytosed to the intracellular compartments (Figure 4.3). Once internalized, colocalization analysis revealed that immunoliposomes colocalized more in the recycling endosomes than the late endosomes 3:2 (Table 4.1). When pre-incubated with geldanamycin, trastuzumab-ILS shifted from the recycling pathway to the degradative pathway by 20%, with colocalization in the recycling endosomes to the late endosomes 2:3. Geldanamycin appeared to induce the same degradative sorting effect for trastuzumab-ILS as it does for trastuzumab. When trastuzumab-ILS was incubated with cells for 4 hr without a chase, immunoliposomes were evenly distributed between the recycling endosomes and the late endosomes. In addition, the pre-incubation of geldanamycin resulted in no significant shift between the recycling pathway and the degradative pathway.

In terms of intracellular pathways, trastuzumab-ILS favors the recycling compartments over the degradative compartments, except reversed after transregulation with geldanamycin. Both trastuzumab-ILS and trastuzumab appear to be sorted in similar intracellular pathways favoring the recycling endosomes over the late endosomes, except do not appear to readily recycle to the surface and be exocytosed like trastuzumab.

Trastuzumab-ILS remains colocalized in the recycling endosomes and late endosomes for an indefinite amount of time. Immunoliposomes incubated at 10 min without a chase were observed on the cell membrane, coating the surface like trastuzumab. However after internalization, surface-coating has yet been observed again.

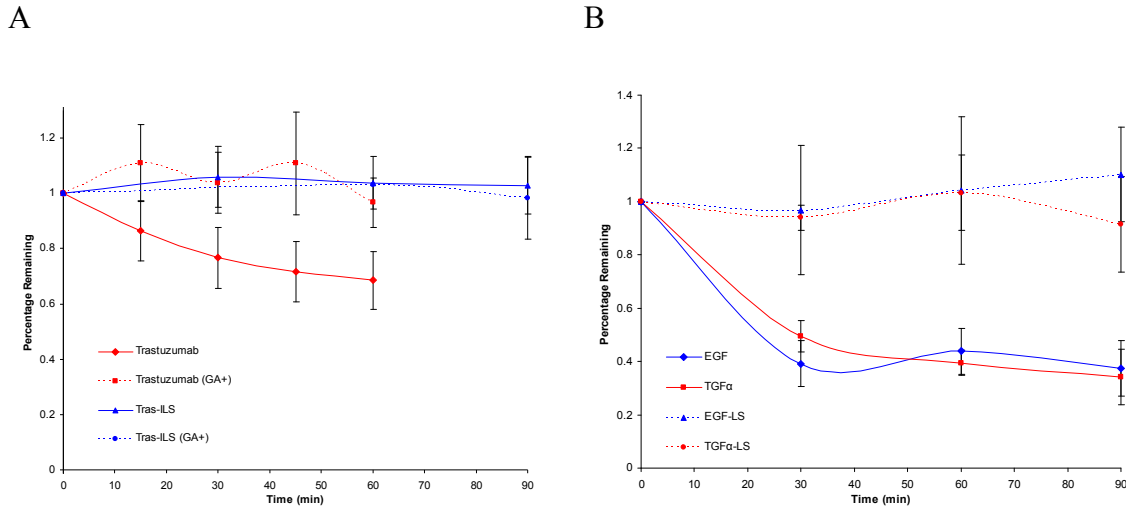


**Figure 4.4 Ligand and liposomal recycling assessments by flow cytometry.** **A.** Geldanamycin-pretreated or untreated (GA $\pm$ ) HER2-expressing SK-BR-3 cells incubated with trastuzumab labeled with Alexa Fluor 488 or trastuzumab-conjugated immunoliposomes (Tras-ILS) labeled with DiD were pulsed for 15 min at 37 $^{\circ}$  C and then chased for the indicated intervals and examined by fluorometry. Only internalized trastuzumab efficiently recycles in the absence of geldanamycin. **B.** EGFR-expressing MDA-468 cells incubated with EGF and TGF $\alpha$  labeled with Alexa Fluor 488 or EGF-conjugated and TGF $\alpha$ -conjugated immunoliposomes labeled with DiD were pulsed for 15 min at 37 $^{\circ}$  C and then chased for the indicated intervals and examined by fluorometry. Liposomes are not exocytosed.

Flow cytometry experiments modified from Austin's protocol(79) where SK-BR-3 cells incubated with fluorescently labeled trastuzumab or trastuzumab-ILS for 15 min and chased confirmed that trastuzumab but not immunoliposomes recycled out of the cells as evident of the decrease in fluorescent signal of cells with time only for cells incubated with trastuzumab (Figure 4.4). In addition, the presence of geldanamycin significantly minimized the drop of fluorescent signal for cells incubated with trastuzumab as evidence of degradative sorting. The difference of trastuzumab remaining

in cells with and without geldanamycin was about 20-30% after a one hour chase, similar to the percent change of colocalization of trastuzumab-ILS in the recycling endosomes to late endosomes upon transregulation as determined by colocalization analysis. In addition, subcellular fractionation studies where organelles from liposomal chased studies up to 4 hr were separated by density gradients revealed that liposomes remain in density gradients typical of endosomes as determined by western blotting instead of density gradients typical of free liposomes or free drug (data not shown). Hence, no liposomal endosomal escape or release of doxorubicin to the cytosol during 4 hour incubation was observed. This is also evident by the lack of nuclear staining from doxorubicin by microscopy in the same time frame. Liposomes are believed to remain intact in endosomal organelles during our colocalization experiments.

#### **4.3.3 Delivery of Trastuzumab-Conjugated Immunoliposomes Compared to Trastuzumab Conjugates**

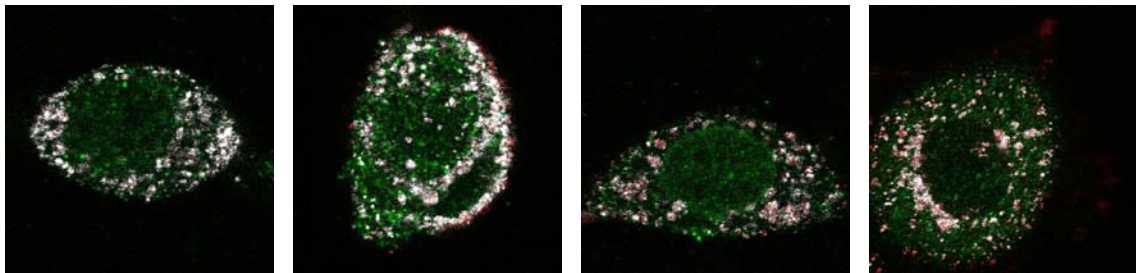
While trastuzumab remains mostly surface-bound, as high as  $92 \pm 3\%$  after 3 hr incubation, trastuzumab-conjugated immunoliposomes are mostly internalized. Regardless as a free antibody or conjugated as an antibody fragment onto liposomes, the total accumulation of the trastuzumab ligands is close to a 1:1 ratio of ligands to HER2 expressed on BT-474 and MCF-7/HER2 cells. An antibody-drug conjugate such as trastuzumab emtansine (Roche) typically contains 4-6 drug molecules per antibody. Assuming  $10^6$  HER2 per cell, approximately  $5 \times 10^6$  drug molecules would associate with a cell, while only 8% of that ( $4 \times 10^5$  drug molecules) would be intracellular. Typical immunoliposomes (100 nm) can encapsulate  $15-40 \times 10^3$  drug molecules per liposome

with roughly  $7 \times 10^5$  liposomes per cell taken up by cells such as BT-474 cells (Chapter 3). At  $30 \times 10^3$  drug molecules per liposome, approximately  $2.1 \times 10^9$  drug molecules per cell are internalized. Per cell basis, this equals to 420 fold increase of drugs associated to cells favoring targeted liposomal drug delivered over antibody-drug conjugates, and 5200 fold increase of drugs delivery to cells intracellularly. The large drug payload greatly favors immunoliposomes over antibody-drug conjugates.

#### 4.3.4 Trafficking of F5 scFv and F5 scFv-Conjugated Immunoliposomes

RE (Rab11), GA-      LE (Rab7), GA-      RE (Rab11), GA+      LE (Rab7), GA+

A. F5 scFv-ILS in MCF-7/HER2 cells



B. F5 scFv-PEG-DSPE in MCF-7/HER2 cells

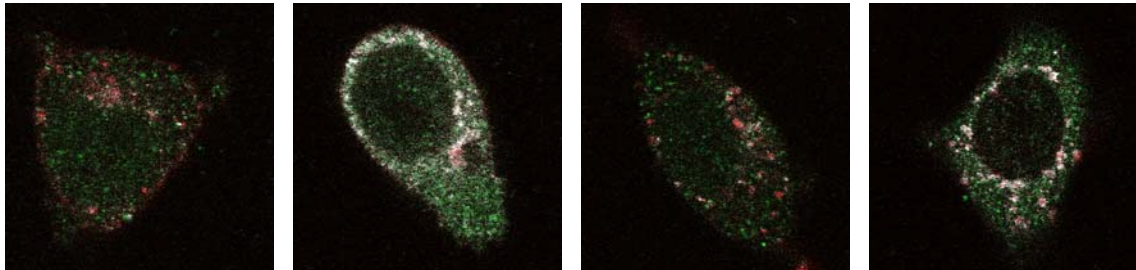


**Figure 4.5 Endosomal colocalization analysis of F5 scFv-conjugated immunoliposomes (ILS) and F5 scFv-PEG-DSPE in HER2-expressing MCF-7/HER2 cells.** Cells, pre-incubated with/out geldanamycin (GA $\pm$ ), were incubated with **A.** F5 scFv-ILS labeled with DiD or **B.** F5 scFv-PEG-DSPE labeled with Alexa Fluor 488 at 37° C for 10 min with 3 hr chase and visualized by confocal microscopy. Rab11 and Rab7 were labeled by immunocytochemistry for the recycling endosomes (RE) and the late endosomes (LE), respectively (green). Z-slices were analyzed by the Costes method for colocalization threshold and to calculate the percentage of pixels representing liposomes or ligands (red) colocalized to pixels representing the endosomal compartments (colocalized pixels, white).

Like trastuzumab, F5 scFv also has a high affinity for HER2. F5 scFv-PEG-DSPE labeled with Alexa Fluor 488 was incubated with BT-474, MCF-7/HER2, or SK-BR-3 cells for 10 min with a 3-4 hr chase, subjected to immunocytochemistry, and visualized by confocal microscopy. Unlike trastuzumab, the F5 scFv conjugates remained intracellular near perinuclear regions opposed to surface-bound trastuzumab (Figure 4.2). Colocalization analysis revealed a preference for localization in late endosomes over the recycling endosomes regardless with or without transregulation by geldanamycin (Figure 4.5; Table 4.1).

Similarly, F5 scFv-ILS labeled with DiD was incubated with BT-474 and MCF-7/HER2 cells for 10 min with a 3-4 hr chase, subjected to immunocytochemistry, and visualized by confocal microscopy. Like F5 scFv conjugates, F5 scFv-ILS was found mostly endocytosed to the intracellular compartments, but with a more even distribution between the late endosomes and the recycling endosomes (Figure 4.5; Table 4.1). When F5 scFv-ILS was incubated with cells for 4 hr without a chase, immunoliposomes colocalized more in the recycling endosomes than the late endosomes 3:2. Like F5 scFv, the pre-incubation of geldanamycin did not result in significant shift of sorting between the recycling pathway and the degradative pathway for F5 scFv-ILS.

Although both F5 scFv-ILS and trastuzumab-ILS are quickly internalized into HER2-overexpressing cells, there are differences in their trafficking. While trastuzumab-ILS has a higher preference for colocalization in the recycling endosomes than the late endosomes, the distribution of F5 scFv-ILS was more even between the endosomes. Unlike trastuzumab and trastuzumab-ILS, sorting was not affected from transregulation by geldanamycin for F5 scFv conjugates and F5 scFv-ILS. However, similar to

trastuzumab-ILS as well as other immunoliposomes, F5 scFv-ILS remains colocalized in the late endosomes and recycling endosomes for an indefinite amount of time. With a prolonged 4 hr incubation of F5 scFv-ILS, the degradative pathway appeared to be saturated, slightly shifting the ILS from the late endosomes to the recycling endosomes. The degradative pathway saturating effect has previously been documented with the oversaturation of ligands such as EGF and larger carriers like viruses. Unlike F5 scFv-ILS, pathway saturation was not as apparent with trastuzumab-ILS possibly because of their higher partiality for the recycling endosomes over the late endosomes.

#### 4.3.5 Trafficking of EGF, TGF $\alpha$ , EGF-Conjugated and TGF $\alpha$ -Conjugated

##### Liposomes

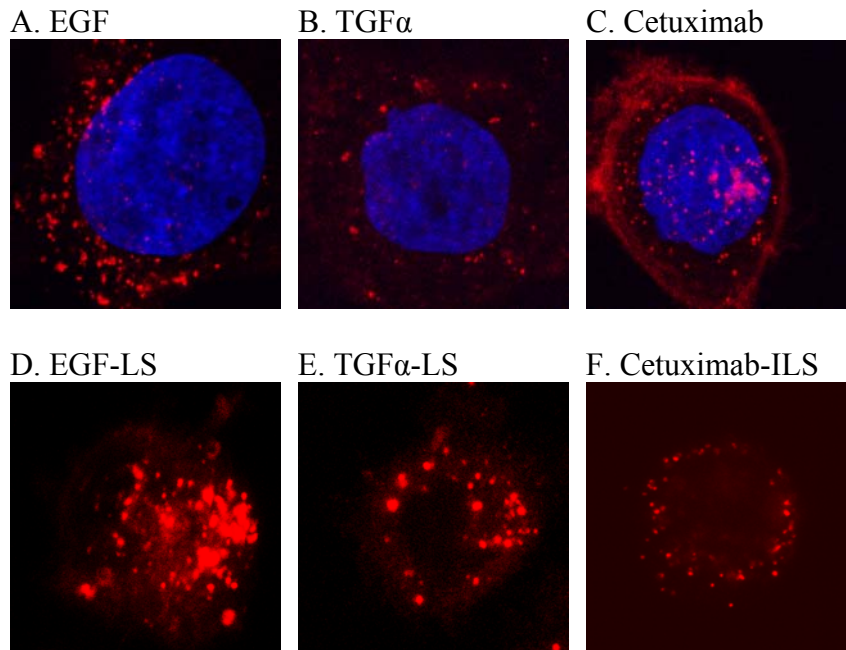


**Figure 4.6 Cellular uptake of anti-EGFR EGF, TGF $\alpha$ , cetuximab, and ligand-conjugated liposomes (LS) in MDA-468 cells visualized by microscopy.** Cells were incubated with **A.** EGF labeled with Alexa Fluor 488, **B.** TGF $\alpha$  labeled with Alexa Fluor 488, **C.** cetuximab labeled with Alexa Fluor 546, **D.** EGF-conjugated liposomes, **E.** TGF $\alpha$ -conjugated liposomes, or **F.** cetuximab-conjugated immunoliposomes (ILS) at 37° C for 1 hr and visualized by confocal microscopy; liposomes were labeled with DiI. Nucleus was post-stained with DAPI (blue) for ligands. Images are z-slice projections of single cells with internalized ligands or liposomes (red).

To investigate the trafficking of EGFR-targeted ligands with well-documented opposing intracellular sorting pathways to either degradation or recycling, EGF and TGF $\alpha$  were evaluated as ligands and targeting groups conjugated onto liposomes (LS). EGFR-EGF complexes are largely degraded while EGFR-TGF $\alpha$  complexes are regularly recycled(76-78). EGF and TGF $\alpha$  labeled with Alexa Fluor 488 were incubated with MDA-468 and MKN-7 cells for 10 min with a 3-4 hr chase, subjected to immunocytochemistry, and visualized by confocal microscopy. Both ligands were found endocytosed to the intracellular compartments (Figure 4.6). Colocalization analysis indicated that EGF favored the degradative pathway, predominately colocalized more in the late endosomes than the recycling endosomes 7:3 (Figure 4.7; Table 4.2). Contrarily, TGF $\alpha$  favored the recycling pathway, predominately colocalized more in the recycling endosomes than the late endosomes 7:3. When EGF and TGF $\alpha$  were incubated with cells for 4 hr without a chase, the pathway shifted more for EGF than TGF $\alpha$ . Trafficking to the recycling pathway improved for EGF, predominately colocalized more in the recycling endosomes than the late endosomes 3:2. TGF $\alpha$  still favored the recycling pathway but less, colocalized more in the recycling endosomes than the late endosomes 3:2.



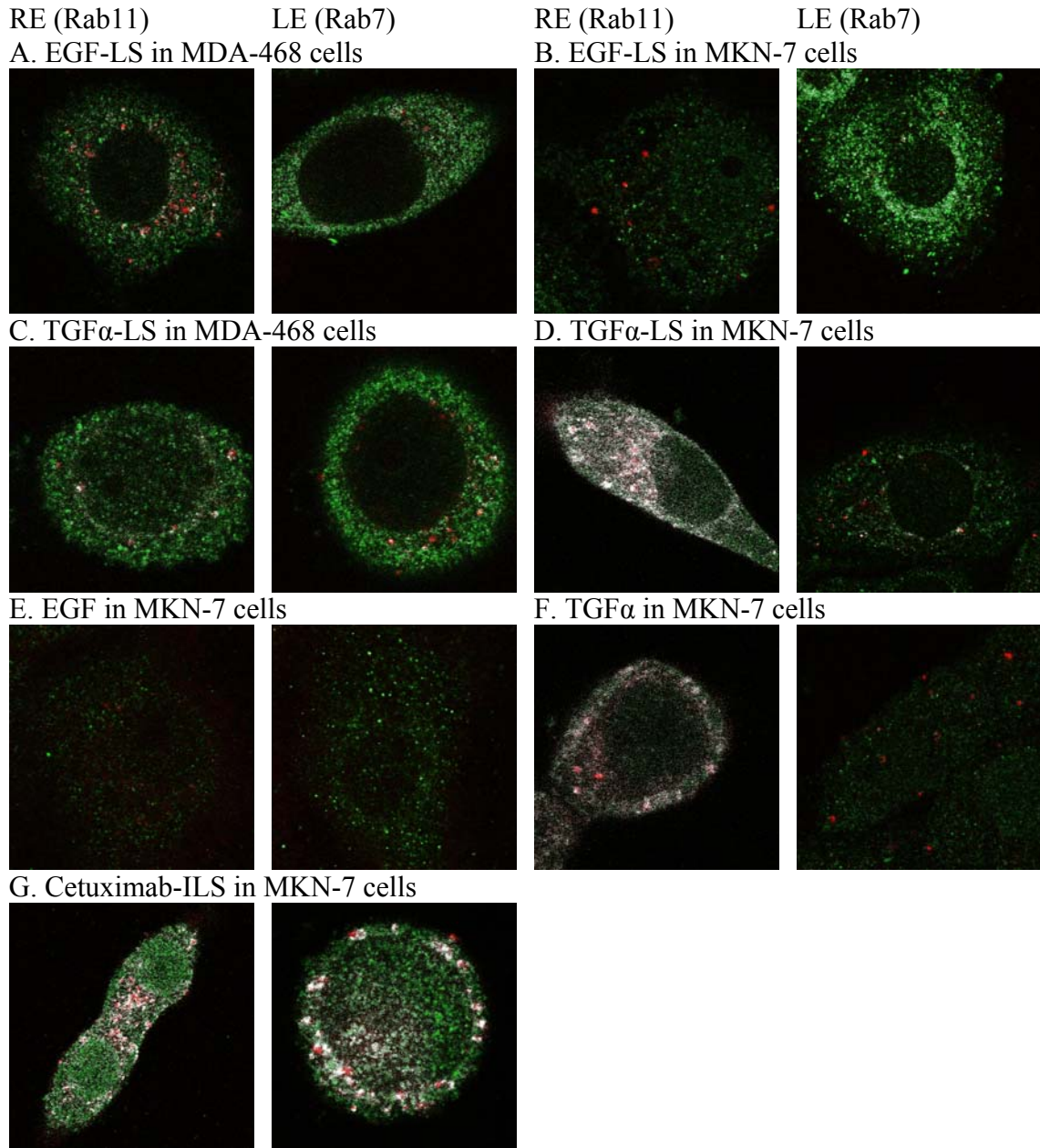


**Figure 4.7 Endosomal colocalization analysis of EGFR-targeted liposomes (LS) and ligands in EGFR-expressing cells.** Cells were incubated with EGF-LS labeled with DiD in **A.** MDA-468 and **B.** MKN-7 cells, TGF $\alpha$ -LS labeled with DiD in **C.** MDA-468 and **D.** MKN-7 cells, **E.** EGF labeled with Alexa Fluor 488 in MKN-7 cells, **F.** TGF $\alpha$  labeled with Alexa Fluor 488 in MKN-7 cells, or **G.** cetuximab-immunoliposomes (ILS) labeled with DiD in MKN-7 cells at 37° C for 10 min with 3 hr chase and visualized by confocal microscopy. Rab11 and Rab7 were labeled by immunocytochemistry for the recycling endosomes (RE) and the late endosomes (LE), respectively (green). Z-slices were analyzed by the Costes method for colocalization threshold and to calculate the percentage of pixels representing liposomes or ligands (red) colocalized to pixels representing the endosomal compartments (colocalized pixels, white).

The results are in line with the literature for the sorting of EGF and TGF $\alpha$ . EGF has been observed to predominately sort to the late endosomes until the degradative pathway is saturated, at which point EGF is shifted from the late endosomes to the recycling endosomes(76-78, 87-89). Unlike EGF, TGF $\alpha$  has been observed to recycle, with a more even distribution of sorting to the recycling pathway and the degradative pathway(76-78). Due to its recycling, TGF $\alpha$  may not as affected by the saturation of the degradative pathway. Studies in the literature have demonstrated minimal changes in the trafficking of TGF $\alpha$  as a function of concentration compared to the large changes for EGF. The minimal saturation of the degradative pathway was also apparent with trastuzumab-ILS, where like TGF $\alpha$ , there was a preference of accumulation in the recycling endosomes over the late endosomes.

Subsequently, EGF-conjugated and TGF $\alpha$ -conjugated liposomes labeled with DiD were incubated with MDA-468 and MKN-7 cells for 10 min with a 3-4 hr chase, subjected to immunocytochemistry, and visualized by confocal microscopy. Both EGFR-targeted liposomes were found endocytosed to the intracellular compartments (Figure 4.6). Like EGF, EGF-LS favored the degradative pathway, predominately colocalized more in the late endosomes than the recycling endosomes 7:3 (Figure 4.7; Table 4.2). Like TGF $\alpha$ , TGF $\alpha$ -LS favored the recycling pathway, predominately colocalized more in the recycling endosomes than the late endosomes 7:3. When EGF-conjugated and TGF $\alpha$ -conjugated liposomes were incubated with cells for 4 hr without a chase, the pathways shifted similar to those of their ligands, more for EGF-LS than TGF $\alpha$ -LS. Trafficking to the recycling pathway improved for EGF-LS, resulting in a more evenly distribution

between the recycling endosomes and the late endosomes. TGF $\alpha$ -LS still favored the recycling pathway, with the distribution unchanged.

For the two EGFR growth factors, the intracellular sorting of the ligand-conjugated liposomes are similar to their respective ligands. While EGF and EGF-conjugated liposomes favor sorting to the degradative pathway, TGF $\alpha$  and TGF $\alpha$ -conjugated liposomes favor sorting to the recycling pathway. With a prolonged 4 hr incubation, the degradative pathway appeared to be saturated, shifting both EGF and EGF-conjugated liposomes from the late endosomes to the recycling endosomes. Like TGF $\alpha$ , TGF $\alpha$ -conjugated liposomes are not as affected by the saturation of the degradative pathway. Combined with the results of HER2-targeting immunoliposomes with trastuzumab and F5 scFv, EGF-LS and TGF $\alpha$ -LS signifies the importance of ligand selection in regards to targeted intracellular pathways.

Despite evidence of liposomal accumulation in the recycling endosomes, there is still no evidence of liposomal exocytosis from the cells. Flow cytometry experiments where MDA-468 cells incubated with fluorescently labeled EGF, TGF $\alpha$ , EGF-LS, or TGF $\alpha$ -LS for 15 min and chased confirmed that immunoliposomes are not exocytosed out of the cells as evident of no decrease in fluorescent signal of cells with time (Figure 4.4). Approximately 60% of EGF and TGF $\alpha$  are recycled almost immediately. In this experiment, EGF recycling was observed to be high is due to the high incubation concentration (10 nM), which is in the range where the degradative pathway is saturated. Studies were also conducted at lower concentrations, but the cell association was undetectable by flow cytometry. Combined, flow cytometry and subcellular fractionation studies only provide confirmation of ligand recycling, not liposomal exocytosis.

		MKN-7	MDA-468
EGF-LS	RE	30±7	25±7
	LE	71±13	76±13
EGF	RE	25±11	
	LE	77±22	
TGF $\alpha$ -LS	RE	68±10	71±17
	LE	35±10	30±6
TGF $\alpha$	RE	68±20	
	LE	32±21	
Cetuximab-ILS	RE	40±10	
	LE	46±8	
Cetuximab	RE	NE	
	LE	NE	

(Average of 1-3 studies, 3-10 samples per study, 3 z-slices per sample)

**Table 4.2 Colocalization percentage of EGFR-targeted liposomes (LS) and ligands in the recycling endosomes (RE) and the late endosomes (LE) of MKN-7 and MDA-468 cells.** Cells were incubated with EGF-LS, EGF, TGF $\alpha$ -LS, TGF $\alpha$ , or cetuximab-immunoliposomes (ILS) at 37° C for 10 min with 3-4 hr chase and captured by confocal microscopy. Z-slices were analyzed by the Costes method for colocalization threshold and to calculate the percentage of pixels representing liposomes or ligands colocalized to pixels representing the endosomal compartments labeled by immunocytochemistry. Intracellular values were not evaluable (NE) for cetuximab due to high signal interference from surface-binding.

#### 4.3.6 Trafficking of Cetuximab and Cetuximab-Conjugated Immunoliposomes

Cetuximab, an anti-EGFR monoclonal antibody used for the treatment of colorectal cancer and head and neck cancer, also binds EGFR with high affinity. When cetuximab labeled with Alexa Fluor 546 or Alexa Fluor 488 was incubated with MDA-468 and MKN-7 cells for 10 min or longer and viewed by confocal microscopy, cetuximab can be seen present in both intracellular compartments as well as surface-bound pretty evenly (Figure 4.6; Figure 4.7). This is in contrast to trastuzumab which is found mostly surface-bound and EGF which is mostly intracellular. Cetuximab-conjugated immunoliposomes labeled with DiD was incubated with MDA-468 and MKN-7 cells for 10 min with a 3-4 hr chase, subjected to immunocytochemistry, and visualized by confocal microscopy. Similar to other ligand-targeting liposomes,

cetuximab-ILS was found mostly endocytosed to the intracellular compartments, but with a pretty even distribution between the late endosomes and the recycling endosomes (Table 4.2). When cetuximab-ILS was incubated with cells for 4 hr without a chase, the distribution of ILS in the intracellular compartments remained unchanged. Evidence suggests that cetuximab and cetuximab-ILS have no preferential pathway, being present in the late endosomes and recycling endosomes evenly, as well as cetuximab being present on the cell surface. This may explain the contradictory conclusions in the literature where cetuximab have been attributed both for and against EGFR downregulation(78, 80, 81).

#### **4.3.7 Cytotoxicity Studies of Pathway-Targeted Doxorubicin-Encapsulated HER2-Targeted and EGFR-Targeted Liposomes**

To investigate the relationship between intracellular pathway delivery and cell growth inhibition of trastuzumab-ILS encapsulated with doxorubicin in BT-474 and MCF-7/HER2 cells, cytotoxicity studies were examined and analyzed by MTT assay. For trastuzumab-ILS, pathway sorting was transregulated with geldanamycin. Since geldanamycin inhibits chaperone heat shock protein 90, which plays important roles in the regulation of cell cycle, cell growth, and cell survival, geldanamycin was first examined for cytotoxicity in BT-474 and MCF-7/HER2 cells.

Unfortunately, geldanamycin is highly toxic in both cell lines at concentrations higher than ~4 nM, well below the 1  $\mu$ M required for degradative sorting (Figure 4.8). When BT-474 and MCF-7/HER2 were examined for cytotoxicity with trastuzumab-ILS encapsulated with doxorubicin in the presence of geldanamycin at non-toxic

concentrations of 4-12 nM, the cell growth inhibition profiles were not affected by geldanamycin for both immunoliposomes and free drug. The results are not surprising since geldanamycin at the non-toxic concentration resulted in minimal intracellular accumulation of trastuzumab in BT-474 and MCF-7/HER2 cells when visualized by confocal microscopy. Hence, the experiments failed to examine any effects of intracellular sorting since the concentration required for pathway transregulation is highly toxic.

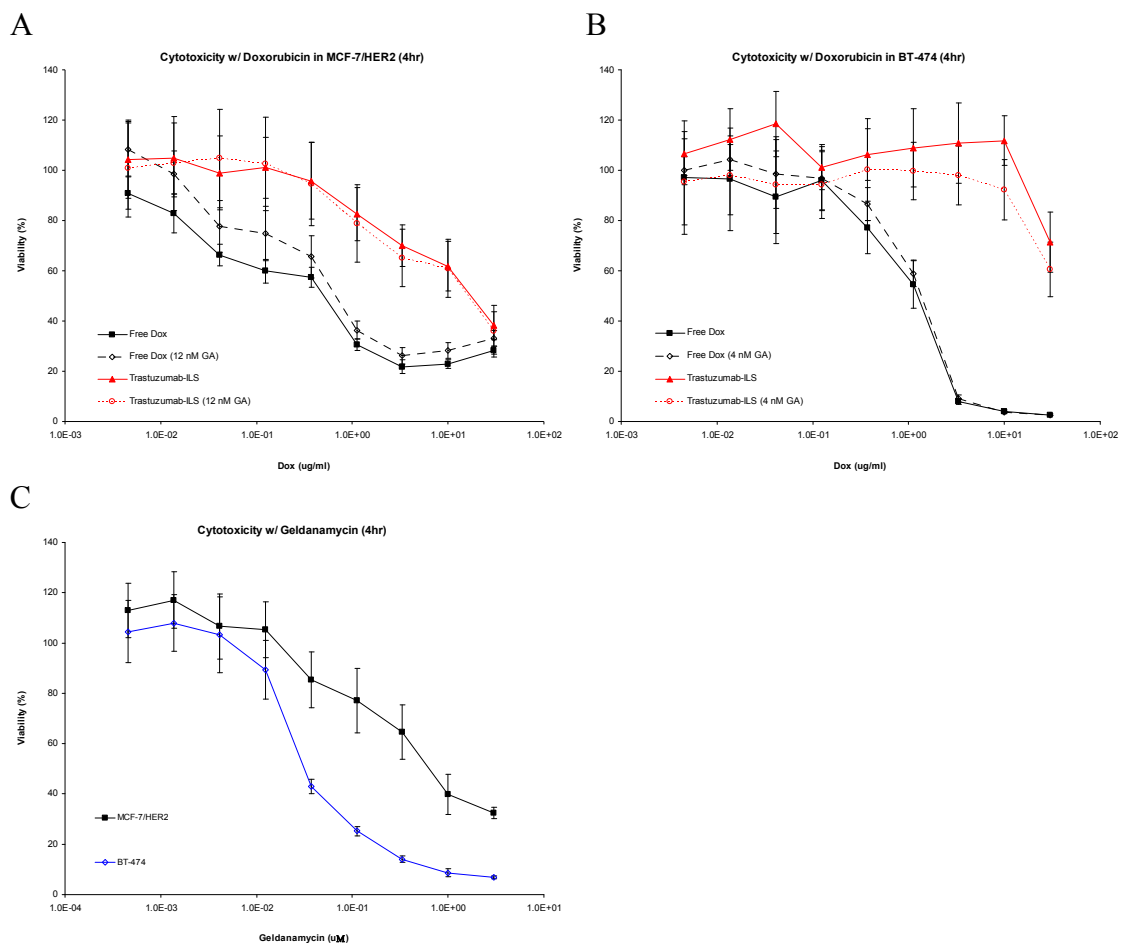


**Figure 4.8 Cytotoxicity studies of doxorubicin-encapsulated anti-HER2 trastuzumab-conjugated immunoliposomes (ILS) and geldanamycin (GA) in BT-474 and MCF-7/HER2 cells.** Cells, pre-incubated with/out GA, were incubated with doxorubicin-encapsulated trastuzumab-ILS in **A**. MCF-7/HER2 and **B**. BT-474 cells at 37° C for 4 hr and evaluated for cell viability by MTT assay after 3 days. **C**. Treatment with GA only was also similarly evaluated. Doxorubicin (Dox)

EGFR-targeted liposomes encapsulated with doxorubicin were also investigated for cell growth inhibition as a function of pathway sorting. In cytotoxicity experiments, EGF-LS and TGF $\alpha$ -LS encapsulated with doxorubicin in MDA-468 cells failed to show significant toxicity compared to non-targeted liposomes mostly likely due to their much lower uptake compared to previously examined immunoliposomes such as cetuximab-ILS. Phorbol myristate acetate has been shown transregulate EGFR, sorting degradative prone ligands to the recycling pathway(86-88). When MDA-468 cells were examined for cytotoxicity with cetuximab-ILS encapsulated with doxorubicin in the presence of phorbol myristate acetate, the cell inhibition profile was more toxic for cetuximab-ILS without transregulation ( $P < 10^{-6}$ ) (Figure 4.9). Uptake studies confirmed that the intracellular accumulation of doxorubicin was comparable for targeted liposomal delivery despite phorbol myristate acetate stimulation, so the observed change in toxicity may be a result of the intracellular pathway targeting and not changes in uptake concentration. In this case, the delivery of doxorubicin to the degradative pathway resulted in slightly higher toxicity than to the delivery to the recycling pathway. Targeted liposomal irinotecan was also similar examined, but yielded no significance differences compared to the non-targeted formulation.

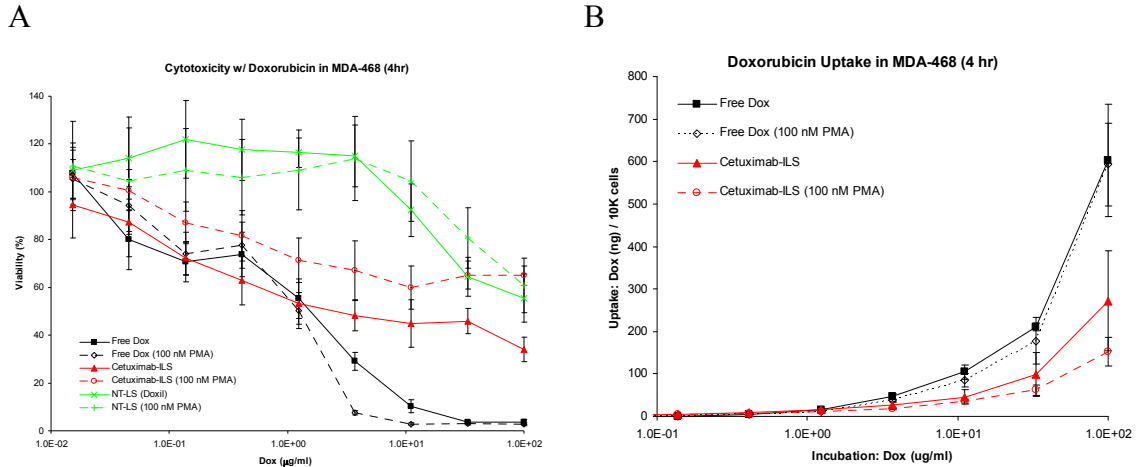


**Figure 4.9** Cytotoxicity and uptake studies of doxorubicin-encapsulated anti-EGFR cetuximab-conjugated immunoliposomes (ILS) and phorbol myristate acetate (PMA) in MDA-468 cells. Cells, pre-incubated with/out PMA, were incubated with doxorubicin-encapsulated cetuximab-ILS at 37° C for 4 hr and evaluated for **A.** cell viability by MTT assay after 3 days or **B.** uptake of doxorubicin (Dox) by fluorometry immediately. Non-targeted liposomes (NT-LS)

The relationship between intracellular pathway targeting and bioactivity needs to be further examined. Pathway transregulation with agents such as geldanamycin and phorbol myristate acetate may introduce undesirable variables to the experiments such as toxicity, drug resistance, etc. Ideally, ligands with high affinity but distinct pathways should be investigated. For EGF-LS and TGF $\alpha$ -LS, due to their low uptake, may benefit from the delivery of more potent drugs or drugs that are not readily released like doxorubicin. Ligands selected from scFv libraries with high affinities for HER2 and EGFR may also be evaluated for intracellular pathway preferences in parallel to cytotoxicity studies. In addition, ligands can also be selected from cellular association upon pathway transregulation. Another option is to look at wild-type vs. mutated receptors expressed on cells, since there are mutations of EGFR that are more selective towards either degradative or recycling sorting.



#### 4.4 Conclusion

In regards to the trafficking of lipid nanoparticles in intracellular compartments, ligand-conjugated liposomes appear to be governed by the sorting of the targeted receptor. When trastuzumab, a ligand known to recycle with HER2, is attached to liposomes, the ligand-conjugated liposomes prefer localization in the recycling endosomes over the late endosomes. While trastuzumab is recycled and remains mostly surface-bound, trastuzumab-ILS is internalized and retained in endosomal compartments. Trastuzumab-ILS favors accumulation in the recycling endosomes over the degradative endosomes 3:2, even though they do not appear to be exocytosed like trastuzumab. In addition since the pathway of trastuzumab can be shifted towards degradative sorting by the transregulation of geldanamycin, the pathway of trastuzumab-ILS can also be diverted. Geldanamycin induces a ~20% shift from the recycling pathway to the degradative pathway for trastuzumab-ILS. The distribution of F5 scFv-ILS is more even between the degradative endosomes and the recycling endosomes, and like trastuzumab-ILS is also retained in endosomal compartments. The pathway of F5 scFv-ILS is similar to that of F5 scFv-PEG-DSPE and is not affected by the stimulation of geldanamycin. Hence, the sorting in intracellular compartments for trastuzumab-ILS and F5 scFv-ILS are similar to their respective ligands, even though their ultimate destinations may be different.

The targeted intracellular sorting of EGFR-targeted ligands conjugated to liposomes also appear to be controlled by the sorting of the targeted receptor. EGF, TGF $\alpha$ , and liposomes conjugated with EGF and TGF $\alpha$  are all endocytosed to endosomal compartments for sorting. Like their respective ligands, EGF-conjugated liposomes favor

accumulation in the degradative endosomes, and TGF $\alpha$ -conjugated liposomes favor accumulation in the recycling endosomes, 7:3. For ligands and ligand-conjugated liposomes with a preference for the degradative pathway such as EGF, there is evidence of degradative pathway saturation upon which results in a shift from the degradative pathway to the recycling pathway. Cetuximab localizes on both the cell surface as well as endosomal compartments, and likewise cetuximab-ILS accumulates in both the late endosomes and the recycling endosomes evenly. The choice of the ligand and its targeted receptor play an important factor in the intracellular sorting of receptor-mediated lipid nanoparticles.

Even though recycled ligands are eventually exocytosed as apparent by flow cytometry, lipid nanoparticles were never observed to be exocytosed despite settling in the recycling endosomes. Investigations into the relationship between the targeted intracellular pathway and bioactivity in terms of cell growth inhibition with the delivery of doxorubicin were inconclusive. While transregulation with agents such as geldanamycin have been shown to divert sorting, these agents themselves can be highly toxic, interfering with cytotoxicity studies. Although EGF and TGF $\alpha$  are good candidates to investigate contrasting intracellular trafficking pathways as ligands and as EGFR-targeting groups for liposomal delivery, the overall delivery and uptake of encapsulated doxorubicin is low making them poor candidates for doxorubicin delivery. For anti-EGFR cetuximab-ILS, transregulation with phorbol myristate acetate to divert the delivery of doxorubicin away from the degradative endosomes suggest that cell growth inhibition for doxorubicin is more effective in the degradative compartments instead of the recycling ones. However due to the increased endocytosis and

accumulation of ligand-conjugated lipid nanoparticles into cells compared to free ligands such as trastuzumab, data suggested that targeted liposomal drug delivery has a large intracellular drug delivery advantage over antibody-drug conjugates.

## **4.5 Materials and Methods**

### **4.5.1 Materials**

HER2-targeted and EGFR-targeted liposomal formulations and their ligands are described in Chapter 2. Cell lines and growth conditions are described in Chapter 3. Rabbit polyclonal antibody to Rab11, mouse monoclonal antibody to Rab11, rabbit polyclonal antibody to Rab5, and goat polyclonal secondary antibody to rabbit IgG Cy3, mouse IgG Cy3, rabbit IgG FITC, and mouse IgG FITC were purchased from Abcam (Cambridge, MA). Rabbit polyclonal antibody to Rab7, mouse monoclonal antibody to Rab7, and mouse monoclonal antibody to Rab5 were purchased from Sigma-Aldrich (St. Louis, MO). Geldanamycin was purchased from InvivoGen (San Diego, CA).

### **4.5.2 Trafficking through the Endosomal Compartments**

Cells cultured overnight on 18 mm cell growth promoting glass cover slips in 12-well plates ( $25\text{-}50 \times 10^3$  cells/well) were incubated with liposomes labeled with DiD or ligands labeled with Alexa Fluor 488 at 37° C for 10 min – 4 hr and chased for up to 4 hr. For HER2-expressing cell lines BT-474, MCF-7/HER2, and MKN-7, cells were first incubated with  $\pm 1 \mu\text{M}$  geldanamycin at 37° C for 1 hr, followed by incubation with trastuzumab-ILS, trastuzumab-AF488, F5 scFv-ILS, or F5 scFv-AF488 (30  $\mu\text{M}$  PL or 20

nM ligand) for 10 min and chased with 20 nM trastuzumab for 3-4 hr, or by incubation with particles for 4 hr without chasing. For EGFR-expressing cell lines MDA-468 and MKN-7, cells were incubated with EGF-LS, EGF-AF488, TGF $\alpha$ -LS, TGF $\alpha$ -AF488, cetuximab-ILS, or cetuximab-AF488 for 10 min (30-150  $\mu$ M PL or 20 nM ligand) and chased with 20 nM cetuximab for 3-4 hr, or by incubation with particles for 4 hr without chasing. All incubation and washing steps were carried out in medium and PBS, respectively.

#### **4.5.3 Immunocytochemistry**

In preparation for immunocytochemistry, cells were washed with PBS, fixed with 4% formaldehyde in PBS for 15 min, and blocked and permeabilized in PBS with 1% bovine serum albumin (BSA), 5% goat serum, and 0.1% Triton X-100 for 1 hr. Permeabilized cells were incubated with primary antibodies in PBS with 1% BSA and 5% goat serum at 4° C overnight (rabbit polyclonal antibody to Rab7 or Rab11, 1:250; mouse monoclonal antibody to Rab7 or Rab11, 1:500), followed by incubation with secondary antibodies at room temperature for 1 hr (goat polyclonal secondary antibody to rabbit or mouse, IgG Cy3 or FITC, 1:500). All washing steps were carried out in PBS with 5% goat serum after each incubation. Cover slips were mounted in Vectashield mounting medium with DAPI (Vector Laboratories) and fluorescence was visualized by confocal microscopy.

#### **4.5.4 Confocal Microscopy**

Micrographs were captured on a Zeiss LSM 510 META NLO confocal microscope maintained by the UCSF Laboratory for Cell Analysis Core. All images were captured with a plan-apochromat 63x/1.4 oil differential interference contrast objective lens at 1 megapixel (1024x1024). TetraSpeck fluorescent microsphere standards (Life Technologies) were used as controls for instrumentation adjustment, adjusting pinholes to approximately 106  $\mu\text{m}$ . Z-slices were captured at thickness intervals of 0.5  $\mu\text{m}$ . Excitation and emission wavelength filters were as follow: FITC (488 nm, band-pass 500-530 nm), Cy3 (543 nm, band-pass 565-615 nm), DiD (633 nm, long-pass 650 nm), DAPI (400 nm, band-pass 390-465 nm). Images presented are a single section in the z-plane or z-slice projection where indicated. Colocalization images showing colocalized pixels as white were processed by ImageJ as described in the next section.

#### **4.5.5 Colocalization Analysis**

To study the intracellular trafficking of fluorescently labeled liposomes and ligands through the endosomal compartments, confocal microscopy micrographs were further processed to assess the degree of spatial coincidence between liposomes and ligands with the endosomal compartments labeled by immunocytochemistry.

Micrographs captured by confocal microscopy (1 megapixel) were processed with ImageJ using plug-ins from MacBiophotonics and analyzed by the Costes method for colocalization threshold and to calculate the percentage of colocalized pixels. In the colocalization threshold calculation, background and zero-zero pixels were subtracted,

and constant intensity for colocalized pixels was assumed. 3-10 images of cells with at least 3 z-slices per sample from 1-3 studies were analyzed and averaged to calculate the percent of pixels representing liposomes and ligands colocalized to pixels representing the endosomal compartments. TetraSpeck fluorescent microsphere standards (Life Technologies) were used as controls for instrumentation adjustment and colocalization analysis.

#### **4.5.6 Ligand and Liposomal Recycling Assessments by Flow Cytometry**

For the assessment of recycling by flow cytometry, cells cultured overnight in 24-well plates ( $75 \times 10^3$  cells/well) were incubated with liposomes labeled with DiD (75  $\mu$ M PL) or ligands labeled with Alexa Fluor 488 (10-20 nM) at 37° C for 15 min, stripped with an acid wash (50 mM glycine, 150 mM NaCl, pH 3) at 4° C for 1 min, chased with trastuzumab or cetuximab for the indicated intervals and immediately subjected to flow cytometry (BD FACSCalibur). The mean fluorescent intensity with a tight spread of  $5 \times 10^3$  cells was recorded. Cells incubated for 15 min without a chase was used as the baseline for 100% internalization. For transregulation studies, 1  $\mu$ M geldanamycin was also pretreated at 37° C for 1 hr.

#### **4.5.7 Cytotoxicity Studies**

For cytotoxicity studies, cells cultured overnight in 96-well plates ( $10 \times 10^3$  cells/well) were incubated with doxorubicin-load liposomes (30-100  $\mu$ g/ml with 1/3 dilutions) or geldanamycin (3  $\mu$ M with 1/3 dilutions) at 37° C for 4 hr, washed with PBS,

and grown in medium for 3 additional days. For transregulation experiments, cells were pre-incubated with geldanamycin (4-12 nM) for HER2-expressing cells or phorbol myristate acetate (100 nM) for EGFR-expressing cells for 1 hr before treatment. Cell viability was analyzed by MTT assay ((3-(4,5-Dimethylthiazol-2-yl)-2,5-diphenyltetrazolium bromide)). Bars of standard deviations were adjusted for the error of propagation.

#### **4.5.8 Uptake Studies**

For the assessment of targeted uptake by fluorometry, cells cultured overnight in 96-well plates ( $10 \times 10^3$  cells/well), pre-incubated with or without phorbol myristate acetate (100 nM) for 1 hr, were incubated with liposomes encapsulated with doxorubicin at 37° C for 4 hr, washed with PBS 3x, freeze-thawed 3x, and lysed with 80% isopropyl alcohol (IPA) and 1% Triton X-100. Lysed samples along with standards using free doxorubicin added to the plates were read on a fluorescent microplate reader (Wallac Victor). Measurements were read with excitation and emission band-pass filters as follow: doxorubicin 485/20:590/35 nm. Cell count was estimated based on a hemacytometer and MTT assay, showing negligible cell detachment or toxicity under these conditions between groups.

# **Chapter 5: Mathematical Insights on the Binding and Trafficking of Multivalent Lipid Nanoparticles**

## **5.1 Abstract**

The cell association and trafficking of multivalent lipid nanoparticles have been predominately optimized with experimental data. Studies, including ours, traditionally assess an array of variables, such as ligand types, ligand surface density, liposomal concentrations, incubation times, and temperature in relationship to cellular uptake. In this chapter, we rationalized and applied the crosslink multivalent binding model for multivalent lipid nanoparticles to monovalent receptors that fittingly corroborate our empirical results. With known inputs of ligand valence, ligand equilibrium dissociation constant, and total receptor expression level, the model can estimate targeted liposomal cell association using parameters described in our research. The optimal valence for optimum binding was predictable in this model. The model also predicted the antagonistic binding effects of lipid nanoparticles with high valences as observed in studies. Calculations suggest that lipid nanoparticles may bind with a high effective valence. For future binding optimization, the model pointed to the limitations of both ligand valence and ligand affinity. Finally, a compartmental model for the intracellular trafficking of multivalent lipid nanoparticles was reviewed for its shortcomings in applications to sorting of the slowly paced liposome.



## 5.2 Introduction

To better capture the dynamics between ligands and receptors on cells, many models for the cell surface receptor binding and trafficking of both ligands and receptors have been proposed(133-140). Translating the kinetic models of ligands with receptors to multivalent lipid nanoparticles with receptors may provide insight to the experimental data discussed in the previous chapters and as well as observations concluded in the literature. To begin, we start with a base case of the monovalent binding of ligand ( $L_g$ ) to receptor ( $R$ ) to form a ligand/receptor complex ( $C_{Lg}$ ) (Figure 5.1). Through mass action kinetics, the kinetics of ligand, receptor, and complex with time can be described as equation 5-1 with association and dissociation rate constants  $k_f$  and  $k_r$ , respectively. Unlike many ligands, lipid nanoparticles are multivalent. The first bond of a single ligand on a lipid nanoparticle to a single receptor on the cell surface can still be applied with the base model, but subsequent interactions must be considered and adjusted to more accurately model the avidity.

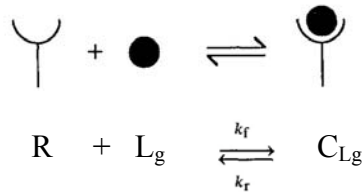


**Figure 5.1 Schematic of monovalent binding.** Ligand ( $L_g$ ) binds to receptor ( $R$ ) to form a ligand/receptor complex ( $C_{Lg}$ ).

$$\frac{dC_{Lg}}{dt} = k_f \cdot L_g \cdot R - k_r \cdot C_{Lg} \quad (5-1)$$

In regards to the receptor, the receptor can interact with other receptors and proteins, forming ternary complexes. The ErbB family of receptor tyrosine kinases such as EGFR and HER2 are known to form dimers. The affinity of ligands to single receptors compared to dimers, whether with one or more binding sites occupied, can greatly change the binding and internalizing kinetics, with the later, dimerization with higher binding site occupancy usually associated with higher affinity(133, 138, 141). For immunoglobulin receptors, the separation distance between the sites of a bivalent antibody is between 9 and 20 nm(135, 142, 143). For an immunoliposome with 20 surface ligands and an average diameter of 100 nm, the separation between ligands is approximately 40 nm assuming equal distribution. This distance can be slightly greater through a polymer linker attached to the ligand. Due to the spacing of the targeting groups on a lipid nanoparticle, it is unlikely for a single lipid nanoparticle to occupy both sites of a bivalent receptor or even occupy both dimerized receptors. Hence, we will assume that lipid nanoparticles with functional monovalent ligands can only occupy one site per single receptor or set of dimerized receptors. This allows us to simplify our model, treating the receptors as monovalent. Keep in mind that higher valence lipid nanoparticles are in the realms of possibility of bivalent receptor binding. Other ternary complex possibilities that receptors can interact with are G-proteins, coated-pit binding proteins, and cytoskeletal elements(133). We will assume none of these are rate-limiting or saturated in our model.

Relative to a ligand, lipid nanoparticles are large, increasing interaction with multiple components on a cell such as additional receptors, proteins, lipids, and macromolecules that may induce binding. Non-specific binding can skew a binding

model. Immunoliposomes are coated with a layer of polyethylene glycol, providing sterical stabilization that limits the non-specific binding and interaction with cells. Therefore, we will assume that non-specific binding is minimal, as also evident by low cell association for non-targeted liposomes surveyed in the previous chapters. Our studies mainly focused on targeting cancer cells that overexpressed receptors, specifically EGFR and HER2, and likewise will be the target of our model. Assuming an average cell diameter of 10  $\mu\text{m}$  with  $10^6$  receptors and an average liposome diameter of 100 nm with 20 ligands, the receptor to ligand per surface area ratio is 5, meaning that for every ligand there are 5 receptors available to bind. Crosslink multivalent binding of liposomes to multiple receptors is a possible and plausible outcome.

### 5.3 Crosslink Multivalent Binding Model of Multivalent Lipid Nanoparticles to Monovalent Receptors

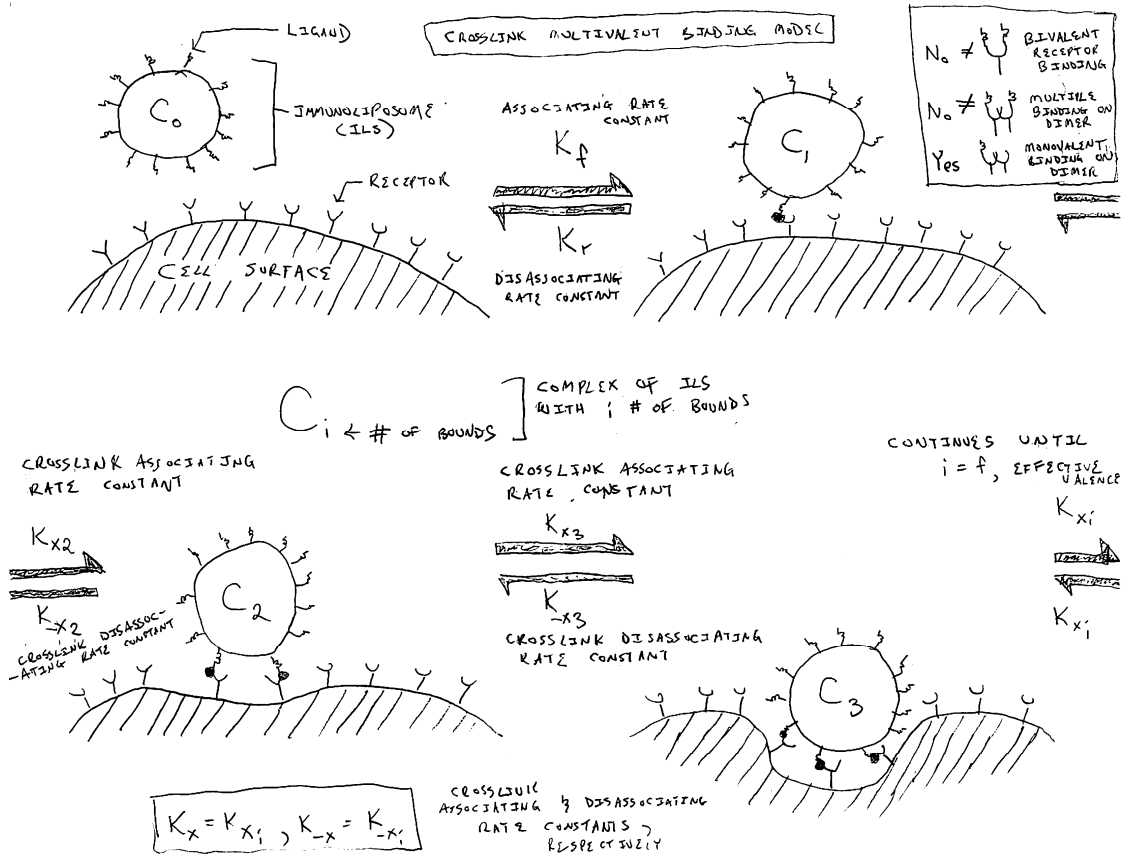
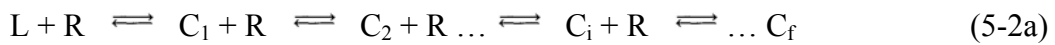


**Figure 5.2 Schematic of the crosslink multivalent binding model of multivalent lipid nanoparticles to monovalent receptors.** Let  $C_i$  be the concentration of a lipid nanoparticle bound to the cell surface via  $i$  of its  $v$  (valence) available surface-attached ligands ( $i = 0, 1, 2, \dots, f$ ) where  $f$  is the effective valence. First, a free lipid nanoparticle binds to a single receptor on the cell surface. Subsequently, the lipid nanoparticle binds to a second receptor. Simultaneous crosslink multivalent binding continues until the lipid nanoparticle reaches  $f$  bounds. It is assumed that the lipid nanoparticle can only form monovalent bounds with single receptors and receptor dimers. The crosslink association and dissociation constants are assumed to be constant for successive bindings.

The crosslink multivalent binding model for multivalent ligands to monovalent receptors, developed and reviewed by a number of investigators(134-136, 139, 140), will be applied to model the cell association of lipid nanoparticles (Figure 5.2). The general

idea is that a free lipid nanoparticle ( $L = C_0$ ) first binds to a single receptor (R) as described by the base monovalent binding model. Subsequently, a second ligand on the lipid nanoparticle binds to a second receptor with forward and reverse crosslinking constants ( $k_x$  and  $k_{-x}$ ), resulting in a complex consisting of a lipid nanoparticle bound to the surface by 2 ligands. Additional ligands simultaneously bind to the cell surface until the number of ligand-receptor bounds reach the effective valence ( $f$ ), essentially the effective number of ligands per liposome that can bind to a cell out of the total valence ( $v$ ). Consequently, the multivalent lipid nanoparticle with  $f$  crosslinked receptors will be internalized into the cell by receptor-mediated endocytosis. It is assumed that  $f \leq v$  due to sterical hindrance with the bound receptor and suboptimal positioning and spacing of the ligands(135). Let  $C_i$  be the concentration of a lipid nanoparticle bound to the cell surface via  $i$  of its  $v$  available surface-attached ligands ( $i = 0, 1, 2, \dots, f$ ), equations by mass action kinetics to describe the crosslink multivalent binding model building upon the monovalent binding model are as follow:



$$\frac{dL}{dt} = -v \cdot k_f \cdot L \cdot R + k_1 \cdot C_1 \quad (5-2b)$$

$$\frac{dC_1}{dt} = v \cdot k_f \cdot L \cdot R - k_1 \cdot C_1 - (f - 1) \cdot k_x \cdot C_1 \cdot R + 2 \cdot k_{-x} \cdot C_2 \quad (5-2c)$$

$$\frac{dC_i}{dt} = (f - i + 1) \cdot k_X \cdot C_{i-1} \cdot R - i \cdot k_{-X} \cdot C_i - (f - i) \cdot k_X \cdot C_i \cdot R + (i + 1) \cdot k_{-X} \cdot C_{i+1} \quad (5-2d)$$

$$i = 2, 3, \dots, f - 1$$

$$\frac{dC_f}{dt} = k_X \cdot C_{f-1} \cdot R - f \cdot k_{-X} \cdot C_f \quad (5-2e)$$

At steady-state, solutions for the number of free receptors per cell at equilibrium ( $R_{eq}$ ) and the number of cell associated liposomes per cell at equilibrium ( $C_{Beq}$ ) can be symbolic solved with the additional parameters (total receptors per cell ( $R_T$ ), free liposomal concentration in solution ( $L = L_o$ ), equilibrium dissociation constant ( $K_D = k_r/k_f$ ), and the crosslinking equilibrium constant ( $K_X = k_x/k_{-x}$ ):

$$R_T = R + \sum_{i=1}^f i \cdot C_i \quad (5-3a)$$

$$R_T = R_{eq} \cdot \left[ 1 + v \cdot \left( \frac{L_o}{K_D} \right) \cdot (1 + K_X \cdot R_{eq})^{f-1} \right] \quad (5-3b)$$

$$C_{ieq} = \left[ \frac{f!}{i! \cdot (f - i)!} \right] \cdot K_X^{i-1} \cdot \frac{v}{f} \cdot \left( \frac{L_o}{K_D} \right) \cdot R_{eq}^i \quad (5-3c)$$

$$C_{Beq} = \sum_{i=1}^f C_{ieq} = \frac{v}{K_X \cdot f} \cdot \left( \frac{L_o}{K_D} \right) \cdot \left[ (1 + K_X \cdot R_{eq})^f - 1 \right] \quad (5-3d)$$

### 5.3.1 High Receptor Expression Model

All parameters in our model are based on experimental data in our lab and in the literature, particularly for studies pertaining to anti-HER2 F5 scFv-conjugated immunoliposomes and BT-474 cells in the high receptor expression model. For our analysis at equilibrium (time < 4 hr), we will assume a constant free liposomal concentration in solution ( $L = L_o$ ), no liposomal and receptor depletion effects, and constant forward and reverse crosslinking constants ( $k_x$  and  $k_{-x}$ ) for additional receptor binding. The total receptors per cell ( $R_T$ ) is  $10^6$  for high receptor expressing cells (ie, BT-474 cells; adjusted to  $10^5$  and  $10^4$  for the intermediate and low receptor expression models, respectively). The free liposomal concentration in solution ( $L_o$ ) is  $10^6$  liposomes per cell (~70-100  $\mu$ M PL), which is approximately the saturating concentration observed at the optimal cell association. The equilibrium dissociation constant ( $K_D = k_r/k_f$ ) is 100 nM (111 nM for monovalent F5 scFv-ILS, 160 nM for F5 scFv)(34). The crosslinking equilibrium constant ( $K_X = k_x/k_{-x}$ ) is  $1/(70K \text{ \#/cell})$  for high receptor expressing cells, estimated from the maximum uptake of liposomes in dose-uptake studies assuming high crosslinking (Chapter 3). For the intermediate and low receptor expression models,  $K_X$  of  $1/(10K \text{ \#/cell})$  and  $1/(3K \text{ \#/cell})$  were estimated, respectively. Valence and effective valence in the range of 1-200 ligands per liposome were evaluated since that is the maximum Fab' valence per liposome stably construct in the lab. Since  $f \leq v$ , we assumed that if  $v < f$ , then  $f = v$  (equation 5-4). The number of free receptors per cell at equilibrium ( $R_{eq}$ ) and the number of cell associated liposomes per cell at equilibrium ( $C_{Beq}$ ) as a function of  $v$  and  $f$  were evaluated and plotted using Mathcad.

$$f = \begin{cases} v & \text{if } v < f \\ f & \text{otherwise} \end{cases}$$

(5-4)

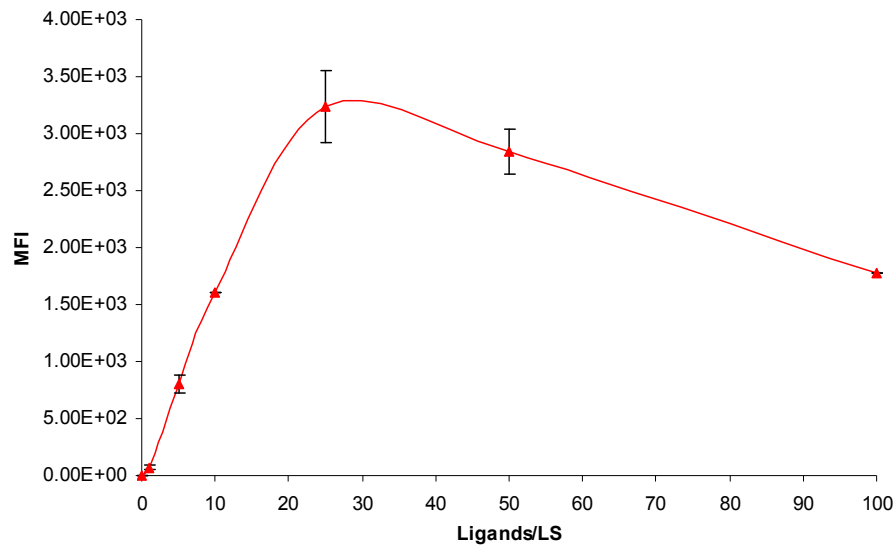


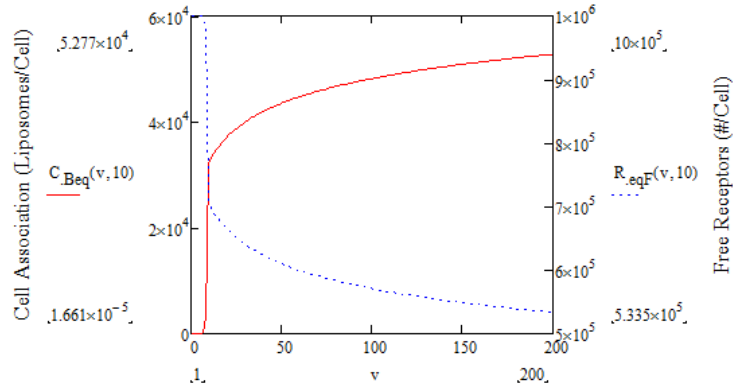
**Figure 5.3 Cell association of F5 scFv-conjugated immunoliposomes (ILS) with increasing valence in MCF-7/HER2 cells.** Cells were incubated with liposomes (LS) labeled with DiD (75  $\mu$ M PL) at 37° C for 1 hr and analyzed by flow cytometry (mean fluorescent intensity [MFI] with a tight spread of  $5 \times 10^3$  cells). Phospholipid (PL)

Predictions calculated from the crosslink multivalent binding model on the cell association of multivalent lipid nanoparticles to cells overall quite accurately describe our experimental data. We and many other investigators have observed optimal cell association of immunoliposomes to cells at  $v = 15-40$  antibody fragments per liposome(4, 33-37), as demonstrated with EGF-LS and TGF $\alpha$ -LS in Chapter 2 and F5 scFv-ILS in Figure 5.3. Since binding and uptake saturate in that range, we initially guessed an effective valence of  $f = 10 < v$  (Figure 5.4). Increasing the surface density of ligands per liposomes with  $f = 10$  correlated to increased targeted association in the high receptor

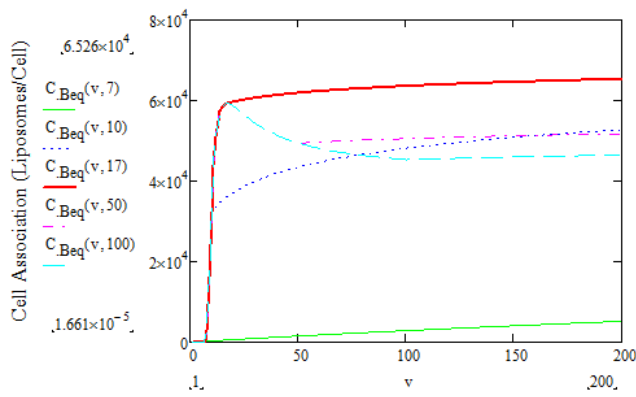


expression model until a plateau. Complementarily, the concentration of free receptors decreased as the concentration of liposomes was receptor-associated. These results fit quite in line with our observations.

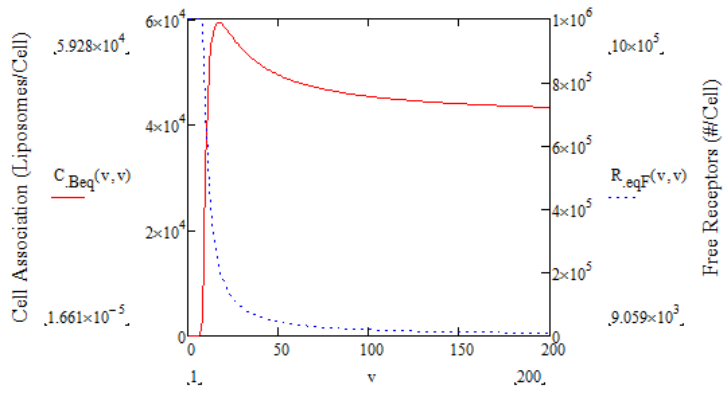
Various effective valences were also analyzed (Figure 5.4). At  $f \leq 7$  (ie,  $f = 7$ ), the binding is reasonably linear, increasing, and negligible in comparison to higher effective valences. This is similar to monovalent ligand binding and low receptor expressing models discussed later (Figure 5.6). At  $f = 8-17$  (ie,  $f = 10$ ), the overall bound concentration increases significantly, curves to saturation, and then maxes at  $f = 17$ . For  $f$  higher than 17 (ie,  $f = 50$  or  $100$ ), cell association subsequently decreases. A peak at  $f = 17$  supports that  $v = 15-40$  observed. Interesting, when  $v > f = 17$ , the overall binding starts to decrease.



A



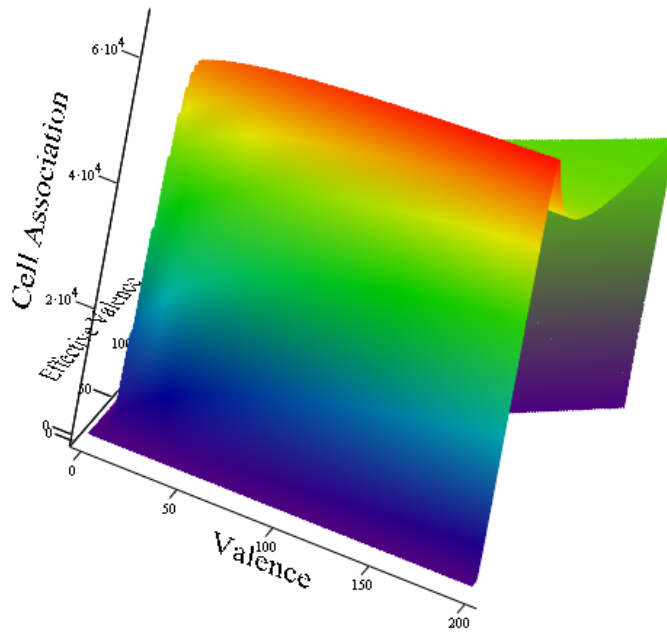
B



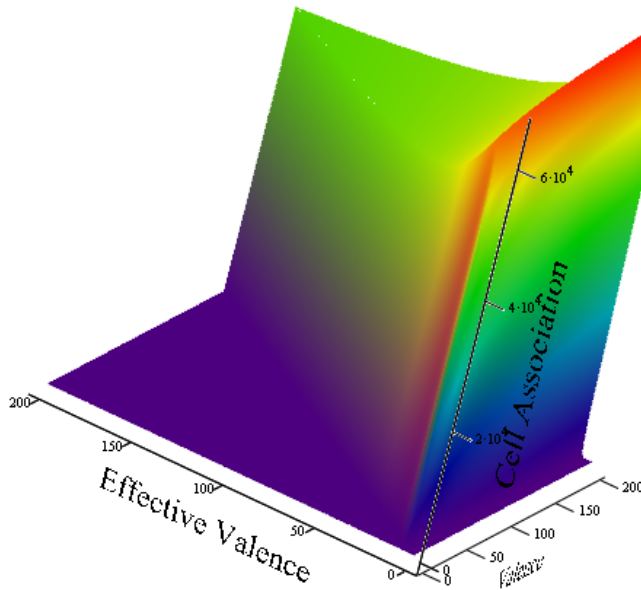
C

**Figure 5.4 Crosslink multivalent binding model predictions in high receptor expressing cells.** Plots of liposomal cell association ( $C_{\text{Beq}}$ ) and/or free receptors ( $R_{\text{eq}}$ ) as a function of valence ( $v$ ) in high receptor expressing cells ( $R_T = 10^6$  #/cell) with an effective valence ( $f$ ) of **A.**  $f = 10$  ligands per liposome, **B.**  $f = 7, 10, 17, 50, \& 100$ , and **C.**  $f = v$ . Values were evaluated in Mathcad with the additional parameters:  $10^6$  liposomes per cell in solution ( $L_o$ ),  $100$  nM equilibrium constant ( $K_D$ ),  $1/(70 \cdot 10^3)$  #/cells crosslinking equilibrium constant ( $K_X$ ). Assumed no liposomal and receptor depletion effects, and since  $f \leq v$ , if  $v < f$  then  $v = f$ .

The effective valence was initially assumed to be constant and much lower than  $v$  as observed for models of multivalent ligands. What if  $f$  is not constant, but increases as  $v$  increases? As previously mentioned, at  $v = 20$ , there are 5 receptors available in a given surface area per ligand, reducing to a reasonable 1:1 at  $v = 100$ . Hence, it is plausible that lipid nanoparticles can have a high  $f/v$  ratio. We plotted a scenario where  $f = v$ , which assumes that every ligand on the lipid nanoparticle efficiently binds to a receptor (Figure 5.4). The graph displays a familiar observation seen with experimental data, where increasing the valence beyond the optimal valence can decrease cell association (Figure 5.3). This will hold true not only for a model where  $f = v$ , but when  $v > f = 17$  (ie,  $f = 50$  &  $100$ , Figure 5.4) or when  $f$  increases with  $v$ . In addition at a high effective valence like when  $f \approx v$ , it supports our data in Chapter 3 where roughly a 1:1 ratio of ligands to expressed receptors was observed internalized at optimal valence. Plots of the cell association as a function of the full  $f$  and  $v$  range ( $f \leq v$ ) were also analyzed in our model (Figure 5.5), indicating that the optimal cell association can be no further optimized based purely on ligand surface density.



A

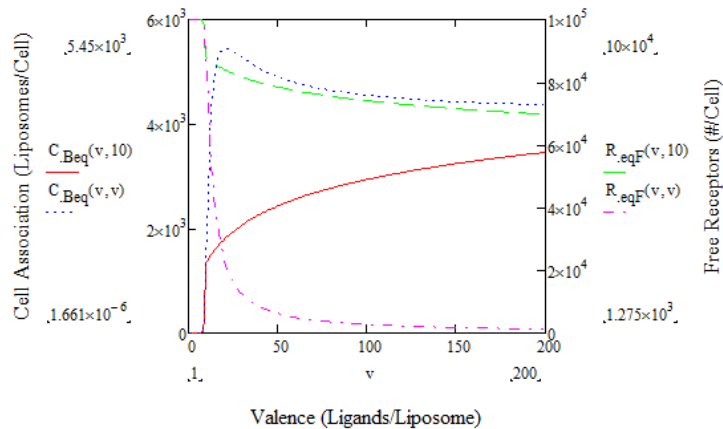


B

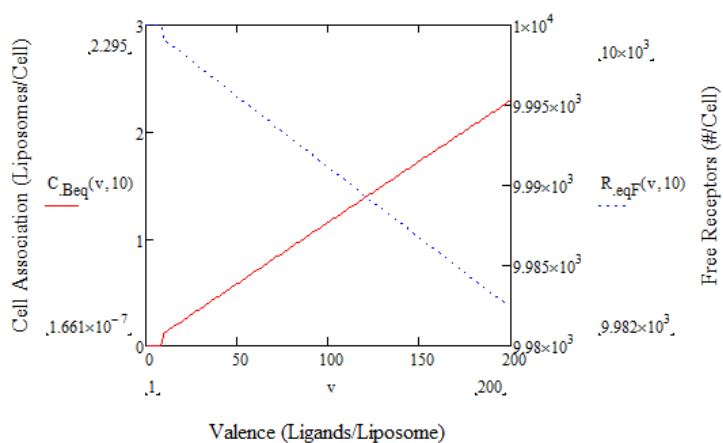
**Figure 5.5 Crosslink multivalent binding model predictions for all plausible valence and effective valence ( $f \leq v$ ) in high receptor expressing cells.** Surface plot of liposomal cell association ( $C_{Beq}$ , liposomes/cell) as a function of valence and effective valence (ligands/liposome) in high receptor expressing cells ( $R_T = 10^6$  #/cell). Values were evaluated in Mathcad with the additional parameters:  $10^6$  liposomes per cell in solution ( $L_o$ ), 100 nM equilibrium constant ( $K_D$ ),  $1/(70 \cdot 10^3$  #/cells) crosslinking equilibrium constant ( $K_X$ ). Assumed no liposomal and receptor depletion effects, and since  $f \leq v$ , if  $v < f$  then  $v = f$ . Color map is only for 3D visual aesthetics.

### 5.3.2 Intermediate and Low Receptor Expression Models

We also examined cases for the intermediate and low receptor expression models (Figure 5.6). We reduced the total receptors per cell availability, and likewise lowered and adjusted  $K_X$  to match our empirical data. It is expected that  $f$  will be much lower than cases for the high expression model and hence mainly examined  $f = 10$ . For the intermediate receptor expression model, when  $f = 10$ , binding was observed to increase with  $v$  reaching a steady plateau as free receptors concentration decreased. These results support the cell association of HER2/EGFR moderately expressing cell line MKN-7 (Chapter 3). We also examined  $f = v$ , but don't believe this is realistic due to the lower receptor availability. In reality,  $f$  will most likely have a lower limit than for cases of the high receptor expression model. In the case of the low receptor expression model, the cell association behavior appropriately resembles monovalent ligand binding, showing a linear non-crosslinking, non-cooperative binding with very low binding, similar to  $f = 1$  for the high receptor expression model.



A



B

**Figure 5.6 Crosslink multivalent binding model predictions in intermediate and low receptor expressing cells.** Plots of liposomal cell association ( $C_{\text{Beq}}$ ) and free receptors ( $R_{\text{eq}}$ ) as a function of valence ( $v$ ) in **A**, intermediate receptor expressing cells ( $10^5$  #/cell) and **B**, low receptor expressing cells ( $10^4$  #/cell) with an effective valence ( $f$ ) of 10 or  $v$  ligands per liposome. Values were evaluated in Mathcad with the additional parameters:  $10^6$  liposomes per cell in solution ( $L_0$ ), 100 nM equilibrium constant ( $K_D$ ),  $1/(10 \times 10^3$  #/cells) and  $1/(3 \times 10^3$  #/cells) crosslinking equilibrium constant ( $K_X$ ) for intermediate and low receptors model, respectively. Assumed no liposomal and receptor depletion effects, and since  $f \leq v$ , if  $v < f$  then  $v = f$ .

### 5.3.3 Data Fitting, Limitations, and Optimization

Concentrations of the calculated cell association closely approximate our dose-uptake experimental data in Chapter 3 at comparable liposomal incubation concentrations ( $L$  at  $89 \mu\text{M}$ ). For HER2 high-expressing BT-474 cells ( $R_T = 10^6$  receptors per cell), our model calculated the bound liposomes per cell concentration of  $5.9 \times 10^4$  for  $v = 15$ , where

in our dose-uptake studies we observed cellular uptake at  $6.8 \cdot 10^4 \pm 7 \cdot 10^3$  for  $v = 15$ . The estimated uptake is within 85% accuracy of empirical data. When the high receptor expression model was adjusted for SK-BR-3 cells (increasing to  $3 \cdot 10^6$  receptors per cell), the calculated concentration again appropriately increased. For SK-BR-3 cells, our model calculated bound liposomes per cell concentrations of  $2.3 \cdot 10^5$  for  $v = 10$  and  $2.2 \cdot 10^5$  for  $v = 15$ , where in our dose-uptake studies we observed cellular uptakes at  $2.3 \cdot 10^5 \pm 4 \cdot 10^3$  for  $v = 10$  and  $2.3 \cdot 10^5 \pm 9 \cdot 10^3$  for  $v = 15$ . The estimated values are within 95% accuracy of empirical data. Since  $v$  for optimum binding was calculated to be  $v = 11$  for SK-BR-3 cells, it is appropriate that the observed uptake in the dose-uptake studies was slightly higher for  $v = 10$  than for  $v = 15$ , as predicted from our model. Suitably, it also suggests that the optimum  $v$  decreases as the number of available receptor increases as expected. When  $R_T$  was lowered to  $5 \cdot 10^5$  receptors per cell, the optimum ligand valence was observed at  $\sim 30$  ligands per liposome, which would account for the full 15-40 ligands per liposome range observed for optimal uptake.

Assuming the equilibrium dissociation constants for monovalent lipid nanoparticles and their respective attached ligand are comparable as in the real example of F5 scFv, the crosslink multivalent binding model allows researchers to estimate the optimum valence and cell association by knowing the dissociation constants of the ligand and the receptor expression level of a cell. However based on the crosslink multivalent binding model for the cell association of multivalent lipid nanoparticles to high receptor expressing cells, our current systems may have already been optimized purely from experimental data. Varying monovalent ligand density beyond the 10+  $v$  range will not significantly alter the binding and uptake of lipid nanoparticles.

In addition, the model also predicted the limitations of ligand affinity as experimentally observed by Zhou and associates, where ultrahigh affinity anti-EGFR scFv is unnecessary for optimal nanoparticles targeting(93). Zhou empirically detected an increase of 24% in targeted liposomal cell association when comparing surface attached C10 scFv (264 nM  $K_D$ ) to 224 scFv (0.94 nM  $K_D$ ). Using the listed  $K_D$ 's, our model precisely predicted a 23.7% increase at  $v = 74$  (valence evaluated by the paper). Based on our model for F5 scFv, the affinity must be improved by an order of 5 magnitudes to merely increase cell association by 2-fold (Figure 5.7).

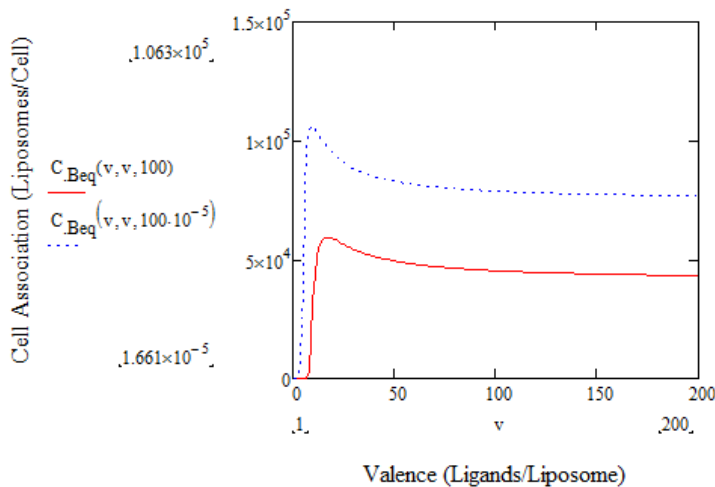


**Figure 5.7 Crosslink multivalent binding model prediction for increased affinity.** The equilibrium dissociation constant was decreased from 100 nM to  $100 \times 10^{-5}$  nM in the high reception expression model with  $f = v$ , resulting in approximately only 2-fold increase in cell association.

How can we then increase cell association? As evidence by equations 5-3b and 5-3d,  $C_{Beq}$  is exponentially proportional to  $R_{eq}$  which is exponentially proportional to  $R_T$ . Hence, increasing the total receptor will in effect increase the concentration of bound lipid nanoparticles. This hypothesis was experimentally examined in Chapter 3 with dual-targeted immunoliposomes, showing additive uptake effects. In addition, quite



simply, the liposomal uptake in cells directly correlates with expression level, ie SK-BR-3 cells > BT-474 cells. Still, the overall uptake, despite being higher, is not quite valuable in applications that rely mainly on increased accumulation for bioactivity since the increase is marginal. However, applications where the receptor expression level is uncertain, such as drug delivery to tumors since expressed receptors can be both heterogeneous and transient, may still be an avenue worth pursuing for dual-targeted systems.

In reality,  $R_T$  may significantly decrease if the receptors are downregulated as with the binding of certain degradative sorting ligands such as EGF. Certain receptors such as the transferrin receptor are continuously recycled. Chapter 4 investigated the intracellular sorting pathways of lipid nanoparticles to the degradative late endosomes and the recycling endosomes. In essence, the idea is that if the receptors and subsequently bound complexes are sorted away from the degradative pathway towards the recycling endosomes,  $R_T$  will not significantly decrease and  $R_{eq}$  will increase due to the quick recycling turnover. Mathematically, this will increase cell association. Lipid nanoparticles should accrue in the recycling endosomes, less likely to be degraded as in the late endosomes, and eventually escape from the endosomes. Experimentally, we were unable to demonstrate any increased benefits despite distinct sorting of the lipid nanoparticles. Whether lipid nanoparticles and their respective attached receptors recycle and then exocytose or not, are still inconclusive.

## 5.4 Compartmental Model of the Intracellular Trafficking of Multivalent Lipid Nanoparticles

After crosslink multivalent binding, lipid nanoparticles are receptor-mediated endocytosed and sorted in the early endosomes to either the recycling endosomes usually associated with exocytosis or the late endosomes destined for degradation. The intracellular trafficking of multivalent lipid nanoparticles can be assessed as a compartmental model (Figure 5.8). Equations can be developed by mass action kinetics.

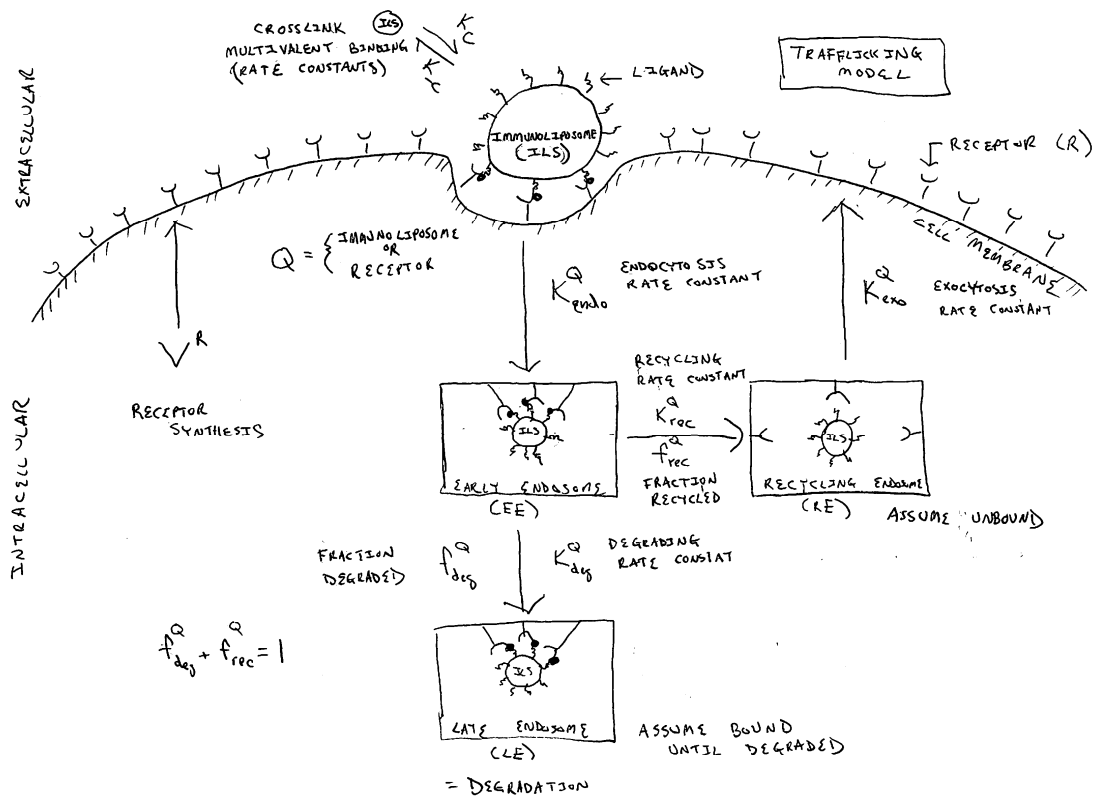


**Figure 5.8 Compartmental model of the intracellular trafficking of multivalent lipid nanoparticles.** First, a lipid nanoparticle crosslink multivalent binds to the cell surface. After receptor-mediated endocytosis, the lipid nanoparticle traffics to the early endosomes where it is sorted to either the late endosomes for degradation or the recycling endosomes. In the recycling endosomes, receptors and ligands are eventually exocytosed. However, there are no conclusive data supporting the exocytosis of lipid nanoparticles.

As discussed in Chapter 4, lipid-nanoparticles unlike ligands do not appear to efficiently traffic out the endosomal compartments. Beyond the quick targeted uptake of lipid nanoparticles and endosomal compartmental settling in either the late endosomes or the recycling endosomes, little other trafficking was observed. In fact, subcellular fractionation studies of organelles suggest that liposomes never escape the endosomes at 4 hr. The recycling and degrading rate constants hence may be extremely slow, possibly slower than endosomal escape mechanisms or drug release rates. While the kinetics such as recycling for ligands like trastuzumab can be evaluated within minutes, we were unable to observe exocytosis with lipid nanoparticles. If the rates are in the magnitudes of a few hours or days, a compartmental model will be complicated with other processes such as cell division, endosomal escape, and liposomal degradation.

In addition, data for the dissociation of receptors from the lipid nanoparticles in the endosomes have not been investigated. A possible scenario is that endocytosed receptors remained bound to the liposomes due to the increased avidity resulting from crosslink multivalent binding. In the end, we failed to establish a time appropriate model. In the future, focusing the trafficking on the receptors associated and dissociated from the lipid nanoparticles may be a more time manageable approach and may offer a more conclusive sorting model. The new design can be monitored by the chasing of endocytosed lipid nanoparticles with labeled ligands. Hence, subsequent ligand and receptor trafficking can be assessed in relationship to any exocytosed receptor effects from the lipid nanoparticles.

## 5.5 Conclusion

A crosslink multivalent binding model for the association of multivalent lipid nanoparticles to monovalent receptors was proposed that reasonably predicted the cell association of lipid nanoparticles analogously to our experimental data. Mathematically, the model in accordance with our research accurately calculated the optimum valence of 17 ligands per liposome for binding to cells with  $10^6$  receptors, which is in the 15 - 40 ligands per liposome range for maximum binding and uptake experimental observed. The optimum valence varies in relationship to the total receptors expressed. Supporting the common observation where lipid nanoparticles with a valence higher than the optimum can result in antagonistic cell association, the model suggests that lipid nanoparticles have a high effective valence, possibly equal to the valence. With known inputs of ligand valence, ligand equilibrium dissociation constant, and total receptor expression level, the model closely estimated the targeted liposomal uptake in high, intermediate, and low receptor expressing cells compared to experimental data, usually within 85% accuracy. Finally, the crosslink multivalent binding model confirmed that both the ligand density and ligand affinity avenues have both already been optimized. Other studies worth pursuing may be in the maintenance of a high surface receptor expression level. A compartmental model for the intracellular trafficking of multivalent lipid nanoparticles was also described, but was unable to accurately capture the sorting of lipid nanoparticles as currently investigated.

## 5.6 Methods

The number of free receptors per cell at equilibrium ( $R_{eq}$ ) and the number of cell associated liposomes per cell at equilibrium ( $C_{Beq}$ ) as a function of  $v$  and  $f$  were evaluated and plotted using Mathcad v14. Parameters and assumptions are listed in the chapter. Predicated data was compared to dose-uptake studies in Chapter 3 (Figure 5.9). The full Mathcad code will be release in a future publication.

**Figure 5.9 Mathcad data calculations for the crosslink multivalent binding model**

Data Fitting, examples

$$C_{Beq}(17, 17, R_T, K_D, K_X) = 5.928 \times 10^4 \quad \text{BT-474, max binding}$$

$$C_{Beq}(15, 15, R_T, K_D, K_X) = 5.853 \times 10^4$$

$$\frac{C_{Beq}(15, 15, R_T, K_D, K_X)}{68200} = 0.858 \quad \text{\% Accuracy to experimental data}$$

$$C_{Beq}(17, 17, 3 \cdot 10^6, K_D, K_X) = 2.067 \times 10^5 \quad \text{SK-BR-3 at } v=17, \text{ RT at 3M}$$

$$C_{Beq}(10, 10, 3 \cdot 10^6, K_D, K_X) = 2.297 \times 10^5 \quad \text{SK-BR-3 at } v=10$$

$$\frac{C_{Beq}(10, 10, 3 \cdot 10^6, K_D, K_X)}{233000} = 0.986 \quad \text{\% Accuracy to experimental data}$$

$$C_{Beq}(15, 15, 3 \cdot 10^6, K_D, K_X) = 2.168 \times 10^5 \quad \text{SK-BR-3 at } v=15$$

$$\frac{C_{Beq}(15, 15, 3 \cdot 10^6, K_D, K_X)}{227000} = 0.955 \quad \text{\% Accuracy to experimental data}$$

$$C_{Beq}(11, 11, 3 \cdot 10^6, K_D, K_X) = 2.332 \times 10^5 \quad \text{SK-BR-3, max binding}$$

$$\frac{C_{Beq}(17, 17, R_T, 94 \cdot 10^{-9}, K_X)}{C_{Beq}(17, 17, R_T, 264 \cdot 10^{-9}, K_X)} = 1.248 \quad \text{224 scFv vs C10 scFv, comparison of equilibrium dissociation constants, percentage increase}$$

$$\frac{C_{Beq}(74, 74, R_T, 94 \cdot 10^{-9}, K_X)}{C_{Beq}(74, 74, R_T, 264 \cdot 10^{-9}, K_X)} = 1.237 \quad \text{Valence of 74 from the literature}$$

## Chapter 6: Concluding Remarks

In this dissertation, I examined a series of ligands as targeted functional groups against HER2 and EGFR for liposomal drug delivery. Receptor-mediated uptake, both mono-targeted and dual-targeted to multiple receptors of different ligand valence, and the intracellular sorting of lipid nanoparticles were investigated to improve the delivery of drugs to cancer cells. I concluded my thesis with models to help explain my observations, as well as provide a basis to make predictions and to optimize targeted liposomal delivery in the future.

In Chapter 2, I described the design and development of receptor-targeted lipid nanoparticles through a new sequential micelle transfer - conjugation method and extended the micelle transfer method to growth factors. Through a combination of both techniques, I was able to construct anti-HER2 and anti-EGFR dual-targeted immunoliposomes with precise yet different ratios of ligand valence for comparative studies. The attachment of liposomes with EGF and TGF $\alpha$  increased cell association to EGFR-expressing cell lines with an optimum valence similar to other anti-EGFR and anti-HER2 antibody fragments. Through the sequential micelle transfer - conjugation method, liposomal paclitaxel was functionalized for EGFR-targeting and evaluated in mice, resulting in an enhancement of anti-tumor efficacy over both liposomal paclitaxel and free paclitaxel.

With the array of immunoliposomes formulated in Chapter 2, I was able to evaluate the uptake and effect of lipid nanoparticles in relationship to ligand valence, both mono-targeting and dual-targeting, on a small panel of breast cancer cell lines that express HER2 and EGFR of varying levels. The first relationship observed was that an

accumulation of ligands, whether free or conjugated to lipid nanoparticles, was comparable to the receptor expression on the cell. Both the 1:1 ligand to receptor ratio and the apparent cooperativity observed during uptake were possible signs of multivalent binding that lead to the binding modeling in Chapter 5. For cell lines that express both HER2 and EGFR, additive dose-uptake effects were observed with dual-targeted immunoliposomes. Despite the additive accumulation, cytotoxicity studies revealed significant but only marginally improvements in cell growth inhibition with doxorubicin delivery. Dual-targeted lipid nanoparticles can still be beneficial as a cocktail-targeting approach. Since the vehicle can target multiple receptors, the number of formulations can be reduced yet still be effective with a large selection of cancers.

Chapter 4 continued the investigation of the ligand-conjugated lipid nanoparticles to the intracellular level. Colocalization analysis revealed that ligand-conjugated lipid nanoparticles settle to endosomal compartments similar to their attached ligands. While liposomes attached with trastuzumab and TGF $\alpha$  were observed more in the recycling endosomes than in the late endosomes, those attached with EGF had a preference for the late endosomes. The attachment of cetuximab and F5 scFv to liposomes resulted in equal distributions to both endosomal compartments. Pathway transregulation was also evident with the pathway diversion of trastuzumab-conjugated immunoliposomes to favor accumulation in the late endosomes. Pathway saturation was apparent when late endosomal targeted lipid nanoparticles increased accumulation in the recycling endosomes. In the end, liposomes routed to the recycling endosomes were never observed to traffic beyond the endosomes nor to exocytose like recycled ligands. Pathway-targeted doxorubicin delivery was examined with inconclusive results.

Based on the observations in the previous chapters, two models were developed to help interpret and predict the binding and trafficking of lipid nanoparticles. The crosslink multivalent binding model accurately corroborated our experimental data. For high receptor expressing cells, it was able to predict both the ligand valence for optimum binding and the maximum cell association concentration. The model offered a possible answer that would explain the observation where high ligand valence can be antagonistic to cell association. In addition, the model was adjustable to intermediate and low receptor expressing scenarios. The compartmental model for the intracellular trafficking of multivalent lipid nanoparticles was also surveyed for its obstacles with liposomal non-trafficking beyond the endosomes.

With the apparent binding limitations from both ligand valence and ligand affinity exposed by the crosslink multivalent binding model of lipid nanoparticles to monovalent receptors, investigators may need to look towards more transitory optimization for targeted drug delivery. In a controlled environment *in vitro*, the targeted delivery of liposomal drugs to HER2 and EGFR overexpressing cells is already maximized. Increasing available receptor targets through increased targetable receptor types and faster receptor turnovers possibly from decreased receptor downregulation, and improved intracellular drug release will likely increase both drug accumulation and efficacy.



## References

1. D. C. Drummond, O. Meyer, K. Hong, D. B. Kirpotin, D. Papahadjopoulos, Optimizing liposomes for delivery of chemotherapeutic agents to solid tumors. *Pharmacological reviews* **51**, 691 (Dec, 1999).
2. D. Papahadjopoulos, A. Gabizon, *Sterically stabilized (Stealth®) liposomes: Pharmacological properties and drug carrying potential in cancer*. J. R. Philippot, F. Schuber, Eds., *Liposomes as Tools in Basic Research and Industry* (CRC Press, Boca Raton, FL, 1995), pp. 177-188.
3. P. A. Speth, Q. G. van Hoesel, C. Haanen, Clinical pharmacokinetics of doxorubicin. *Clinical pharmacokinetics* **15**, 15 (Jul, 1988).
4. C. O. Noble, D. B. Kirpotin, M. E. Hayes, C. Mamot, K. Hong, J. W. Park, C. C. Benz, J. D. Marks, D. C. Drummond, Development of ligand-targeted liposomes for cancer therapy. *Expert opinion on therapeutic targets* **8**, 335 (Aug, 2004).
5. T. M. Allen, L. Murray, S. MacKeigan, M. Shah, Chronic liposome administration in mice: effects on reticuloendothelial function and tissue distribution. *The Journal of pharmacology and experimental therapeutics* **229**, 267 (Apr, 1984).
6. G. Storm, C. Oussoren, P. J. Peters, Y. Barenholz, *Tolerability of liposomes in vivo*. G. Gregoriadis, Ed., *Liposome Technology* (CRC Press, Inc., Boca Raton, FL, 1993).
7. C. P. Carpenter, M. D. Woodside, E. R. Kinkead, J. M. King, L. J. Sullivan, Response of dogs to repeated intravenous injection of polyethylene glycol 4000 with notes on excretion and sensitization. *Toxicology and applied pharmacology* **18**, 35 (Jan, 1971).
8. T. M. Allen, C. Hansen, J. Rutledge, Liposomes with prolonged circulation times: factors affecting uptake by reticuloendothelial and other tissues. *Biochimica et biophysica acta* **981**, 27 (May 19, 1989).
9. D. Liu, A. Mori, L. Huang, Role of liposome size and RES blockade in controlling biodistribution and tumor uptake of GM1-containing liposomes. *Biochimica et biophysica acta* **1104**, 95 (Feb 17, 1992).
10. M. C. Woodle, K. K. Matthay, M. S. Newman, J. E. Hidayat, L. R. Collins, C. Redemann, F. J. Martin, D. Papahadjopoulos, Versatility in lipid compositions showing prolonged circulation with sterically stabilized liposomes. *Biochimica et biophysica acta* **1105**, 193 (Apr 13, 1992).
11. T. Allen, C. Hansen, D. E. Lopes de Menezes, Pharmacokinetics of long-circulating liposomes. *Advanced drug delivery reviews* **16**, 267 (September, 1995).
12. T. M. Allen, Long-circulating (sterically stabilized) liposomes for targeted drug delivery. *Trends in pharmacological sciences* **15**, 215 (Jul, 1994).
13. T. M. Allen, C. Hansen, Pharmacokinetics of stealth versus conventional liposomes: effect of dose. *Biochimica et biophysica acta* **1068**, 133 (Sep 30, 1991).
14. M. S. Webb, D. Saxon, F. M. Wong, H. J. Lim, Z. Wang, M. B. Bally, L. S. Choi, P. R. Cullis, L. D. Mayer, Comparison of different hydrophobic anchors

- conjugated to poly(ethylene glycol): effects on the pharmacokinetics of liposomal vincristine. *Biochimica et biophysica acta* **1372**, 272 (Jul 17, 1998).
15. M. S. Webb, T. O. Harasym, D. Masin, M. B. Bally, L. D. Mayer, Sphingomyelin-cholesterol liposomes significantly enhance the pharmacokinetic and therapeutic properties of vincristine in murine and human tumour models. *British journal of cancer* **72**, 896 (Oct, 1995).
  16. A. Gabizon, D. Papahadjopoulos, The role of surface charge and hydrophilic groups on liposome clearance in vivo. *Biochimica et biophysica acta* **1103**, 94 (Jan 10, 1992).
  17. J. Senior, J. C. Crawley, G. Gregoriadis, Tissue distribution of liposomes exhibiting long half-lives in the circulation after intravenous injection. *Biochimica et biophysica acta* **839**, 1 (Mar 29, 1985).
  18. J. H. Senior, Fate and behavior of liposomes in vivo: a review of controlling factors. *Critical reviews in therapeutic drug carrier systems* **3**, 123 (1987).
  19. F. M. Muggia, J. D. Hainsworth, S. Jeffers, P. Miller, S. Groshen, M. Tan, L. Roman, B. Uziely, L. Muderspach, A. Garcia, A. Burnett, F. A. Greco, C. P. Morrow, L. J. Paradiso, L. J. Liang, Phase II study of liposomal doxorubicin in refractory ovarian cancer: antitumor activity and toxicity modification by liposomal encapsulation. *Journal of clinical oncology : official journal of the American Society of Clinical Oncology* **15**, 987 (Mar, 1997).
  20. O. Lyass, B. Uziely, R. Ben-Yosef, D. Tzemach, N. I. Heshing, M. Lotem, G. Brufman, A. Gabizon, Correlation of toxicity with pharmacokinetics of pegylated liposomal doxorubicin (Doxil) in metastatic breast carcinoma. *Cancer* **89**, 1037 (Sep 1, 2000).
  21. F. Yuan, M. Dellian, D. Fukumura, M. Leunig, D. A. Berk, V. P. Torchilin, R. K. Jain, Vascular permeability in a human tumor xenograft: molecular size dependence and cutoff size. *Cancer research* **55**, 3752 (Sep 1, 1995).
  22. S. K. Hobbs, W. L. Monsky, F. Yuan, W. G. Roberts, L. Griffith, V. P. Torchilin, R. K. Jain, Regulation of transport pathways in tumor vessels: role of tumor type and microenvironment. *Proceedings of the National Academy of Sciences of the United States of America* **95**, 4607 (Apr 14, 1998).
  23. Y. Matsumura, H. Maeda, A new concept for macromolecular therapeutics in cancer chemotherapy: mechanism of tumoritropic accumulation of proteins and the antitumor agent smancs. *Cancer research* **46**, 6387 (Dec, 1986).
  24. H. Maeda, J. Wu, T. Sawa, Y. Matsumura, K. Hori, Tumor vascular permeability and the EPR effect in macromolecular therapeutics: a review. *Journal of controlled release : official journal of the Controlled Release Society* **65**, 271 (Mar 1, 2000).
  25. S. K. Huang, K. D. Lee, K. Hong, D. S. Friend, D. Papahadjopoulos, Microscopic localization of sterically stabilized liposomes in colon carcinoma-bearing mice. *Cancer research* **52**, 5135 (Oct 1, 1992).
  26. V. P. Torchilin, Passive and active drug targeting: drug delivery to tumors as an example. *Handbook of experimental pharmacology*, 3 (2010).
  27. A. Gabizon, M. Chemla, D. Tzemach, A. T. Horowitz, D. Goren, Liposome longevity and stability in circulation: effects on the in vivo delivery to tumors and

- therapeutic efficacy of encapsulated anthracyclines. *Journal of drug targeting* **3**, 391 (1996).
28. L. D. Mayer, P. Cullis, M. Bally, *Medical Applications of Liposomes*. D. Lasic, D. Papahadjopoulos, Eds., (Elsevier Science, B.V., New York, 1998).
  29. P. Sapra, T. M. Allen, Ligand-targeted liposomal anticancer drugs. *Progress in lipid research* **42**, 439 (Sep, 2003).
  30. T. M. Allen, Ligand-targeted therapeutics in anticancer therapy. *Nature reviews. Cancer* **2**, 750 (Oct, 2002).
  31. G. A. Niehans, T. P. Singleton, D. Dykoski, D. T. Kiang, Stability of HER-2/neu expression over time and at multiple metastatic sites. *Journal of the National Cancer Institute* **85**, 1230 (Aug 4, 1993).
  32. D. S. Salomon, R. Brandt, F. Ciardiello, N. Normanno, Epidermal growth factor-related peptides and their receptors in human malignancies. *Critical reviews in oncology/hematology* **19**, 183 (Jul, 1995).
  33. S. Zalipsky, B. Puntambekar, P. Boulikas, C. M. Engbers, M. C. Woodle, Peptide attachment to extremities of liposomal surface grafted PEG chains: preparation of the long-circulating form of laminin pentapeptide, YIGSR. *Bioconjugate chemistry* **6**, 705 (Nov-Dec, 1995).
  34. U. B. Nielsen, D. B. Kirpotin, E. M. Pickering, K. Hong, J. W. Park, M. Refaat Shalaby, Y. Shao, C. C. Benz, J. D. Marks, Therapeutic efficacy of anti-ErbB2 immunoliposomes targeted by a phage antibody selected for cellular endocytosis. *Biochimica et biophysica acta* **1591**, 109 (Aug 19, 2002).
  35. D. Kirpotin, J. W. Park, K. Hong, S. Zalipsky, W. L. Li, P. Carter, C. C. Benz, D. Papahadjopoulos, Sterically stabilized anti-HER2 immunoliposomes: design and targeting to human breast cancer cells in vitro. *Biochemistry* **36**, 66 (Jan 7, 1997).
  36. C. Mamot, D. C. Drummond, U. Greiser, K. Hong, D. B. Kirpotin, J. D. Marks, J. W. Park, Epidermal growth factor receptor (EGFR)-targeted immunoliposomes mediate specific and efficient drug delivery to EGFR- and EGFRvIII-overexpressing tumor cells. *Cancer research* **63**, 3154 (Jun 15, 2003).
  37. K. Maruyama, T. Takizawa, T. Yuda, S. J. Kennel, L. Huang, M. Iwatsuru, Targetability of novel immunoliposomes modified with amphipathic poly(ethylene glycol)s conjugated at their distal terminals to monoclonal antibodies. *Biochimica et biophysica acta* **1234**, 74 (Mar 8, 1995).
  38. M. A. Poul, B. Becerril, U. B. Nielsen, P. Morisson, J. D. Marks, Selection of tumor-specific internalizing human antibodies from phage libraries. *Journal of molecular biology* **301**, 1149 (Sep 1, 2000).
  39. B. Becerril, M. A. Poul, J. D. Marks, Toward selection of internalizing antibodies from phage libraries. *Biochemical and biophysical research communications* **255**, 386 (Feb 16, 1999).
  40. M. D. Sheets, P. Amersdorfer, R. Finnern, P. Sargent, E. Lindquist, R. Schier, G. Hemingsen, C. Wong, J. C. Gerhart, J. D. Marks, Efficient construction of a large nonimmune phage antibody library: the production of high-affinity human single-chain antibodies to protein antigens. *Proceedings of the National Academy of Sciences of the United States of America* **95**, 6157 (May 26, 1998).
  41. E. T. Boder, K. S. Midelfort, K. D. Wittrup, Directed evolution of antibody fragments with monovalent femtomolar antigen-binding affinity. *Proceedings of*

- the National Academy of Sciences of the United States of America* **97**, 10701 (Sep 26, 2000).
42. U. B. Nielsen, J. D. Marks, Internalizing antibodies and targeted cancer therapy: direct selection from phage display libraries. *Pharmaceutical science & technology today* **3**, 282 (Aug, 2000).
  43. D. Goren, A. T. Horowitz, S. Zalipsky, M. C. Woodle, Y. Yarden, A. Gabizon, Targeting of stealth liposomes to erbB-2 (Her/2) receptor: in vitro and in vivo studies. *British journal of cancer* **74**, 1749 (Dec, 1996).
  44. J. W. Park, K. Hong, D. B. Kirpotin, G. Colbern, R. Shalaby, J. Baselga, Y. Shao, U. B. Nielsen, J. D. Marks, D. Moore, D. Papahadjopoulos, C. C. Benz, Anti-HER2 immunoliposomes: enhanced efficacy attributable to targeted delivery. *Clinical cancer research : an official journal of the American Association for Cancer Research* **8**, 1172 (Apr, 2002).
  45. D. Aragnol, L. D. Leserman, Immune clearance of liposomes inhibited by an anti-Fc receptor antibody in vivo. *Proceedings of the National Academy of Sciences of the United States of America* **83**, 2699 (Apr, 1986).
  46. J. A. Harding, C. M. Engbers, M. S. Newman, N. I. Goldstein, S. Zalipsky, Immunogenicity and pharmacokinetic attributes of poly(ethylene glycol)-grafted immunoliposomes. *Biochimica et biophysica acta* **1327**, 181 (Jul 25, 1997).
  47. S. Zalipsky, Functionalized poly(ethylene glycol) for preparation of biologically relevant conjugates. *Bioconjugate chemistry* **6**, 150 (Mar-Apr, 1995).
  48. T. Ishida, D. L. Iden, T. M. Allen, A combinatorial approach to producing sterically stabilized (Stealth) immunoliposomal drugs. *FEBS letters* **460**, 129 (Oct 22, 1999).
  49. D. L. Iden, T. M. Allen, In vitro and in vivo comparison of immunoliposomes made by conventional coupling techniques with those made by a new post-insertion approach. *Biochimica et biophysica acta* **1513**, 207 (Aug 6, 2001).
  50. D. Kirpotin, J. W. Park, K. Hong, Y. Shao, R. Shalaby, G. Colbern, C. C. Benz, D. Papahadjopoulos, Targeting of Liposomes to Solid Tumors: The Case of Sterically Stabilized Anti-Her2 Immunoliposomes. *Journal of liposome research* **7**, 391 (1997).
  51. C. Mamot, D. C. Drummond, C. O. Noble, V. Kallab, Z. Guo, K. Hong, D. B. Kirpotin, J. W. Park, Epidermal growth factor receptor-targeted immunoliposomes significantly enhance the efficacy of multiple anticancer drugs in vivo. *Cancer research* **65**, 11631 (Dec 15, 2005).
  52. J. W. Park, K. Hong, D. B. Kirpotin, O. Meyer, D. Papahadjopoulos, C. C. Benz, Anti-HER2 immunoliposomes for targeted therapy of human tumors. *Cancer letters* **118**, 153 (Oct 14, 1997).
  53. J. N. Moreira, R. Gaspar, T. M. Allen, Targeting Stealth liposomes in a murine model of human small cell lung cancer. *Biochimica et biophysica acta* **1515**, 167 (Dec 1, 2001).
  54. C. Mamot, D. C. Drummond, K. Hong, D. B. Kirpotin, J. W. Park, Liposome-based approaches to overcome anticancer drug resistance. *Drug resistance updates : reviews and commentaries in antimicrobial and anticancer chemotherapy* **6**, 271 (Oct, 2003).

55. D. Sadava, A. Coleman, S. E. Kane, Liposomal daunorubicin overcomes drug resistance in human breast, ovarian and lung carcinoma cells. *Journal of liposome research* **12**, 301 (Nov, 2002).
56. C. Mamot, R. Ritschard, A. Wicki, W. Kung, J. Schuller, R. Herrmann, C. Rochlitz, Immunoliposomal delivery of doxorubicin can overcome multidrug resistance mechanisms in EGFR-overexpressing tumor cells. *Journal of drug targeting* **20**, 422 (Jun, 2012).
57. I. Mellman, Endocytosis and molecular sorting. *Annual review of cell and developmental biology* **12**, 575 (1996).
58. A. Sorkin, M. von Zastrow, Endocytosis and signalling: intertwining molecular networks. *Nature reviews. Molecular cell biology* **10**, 609 (Sep, 2009).
59. S. L. Schmid, Clathrin-coated vesicle formation and protein sorting: an integrated process. *Annual review of biochemistry* **66**, 511 (1997).
60. Q. Al-Awqati, Proton-translocating ATPases. *Annual review of cell biology* **2**, 179 (1986).
61. I. Mellman, R. Fuchs, A. Helenius, Acidification of the endocytic and exocytic pathways. *Annual review of biochemistry* **55**, 663 (1986).
62. M. Forgac, Structure and properties of the coated vesicle proton pump. *Annals of the New York Academy of Sciences* **671**, 273 (Nov 30, 1992).
63. A. Alexander, Endocytosis and intracellular sorting of receptor tyrosine kinases. *Frontiers in bioscience : a journal and virtual library* **3**, d729 (Jul 26, 1998).
64. A. Spang, Vesicle transport: a close collaboration of Rabs and effectors. *Current biology : CB* **14**, R33 (Jan 6, 2004).
65. M. Zerial, H. McBride, Rab proteins as membrane organizers. *Nature reviews. Molecular cell biology* **2**, 107 (Feb, 2001).
66. C. Bucci, P. Thomsen, P. Nicoziani, J. McCarthy, B. van Deurs, Rab7: a key to lysosome biogenesis. *Molecular biology of the cell* **11**, 467 (Feb, 2000).
67. M. Ren, G. Xu, J. Zeng, C. De Lemos-Chiarandini, M. Adesnik, D. D. Sabatini, Hydrolysis of GTP on rab11 is required for the direct delivery of transferrin from the pericentriolar recycling compartment to the cell surface but not from sorting endosomes. *Proceedings of the National Academy of Sciences of the United States of America* **95**, 6187 (May 26, 1998).
68. M. Trischler, W. Stoorvogel, O. Ullrich, Biochemical analysis of distinct Rab5- and Rab11-positive endosomes along the transferrin pathway. *Journal of cell science* **112 ( Pt 24)**, 4773 (Dec, 1999).
69. D. Duan, Y. Yue, Z. Yan, P. B. McCray, Jr., J. F. Engelhardt, Polarity influences the efficiency of recombinant adenoassociated virus infection in differentiated airway epithelia. *Human gene therapy* **9**, 2761 (Dec 10, 1998).
70. C. R. Hopkins, I. S. Trowbridge, Internalization and processing of transferrin and the transferrin receptor in human carcinoma A431 cells. *The Journal of cell biology* **97**, 508 (Aug, 1983).
71. C. R. Hopkins, Intracellular routing of transferrin and transferrin receptors in epidermoid carcinoma A431 cells. *Cell* **35**, 321 (Nov, 1983).
72. M. Karin, B. Mintz, Receptor-mediated endocytosis of transferrin in developmentally totipotent mouse teratocarcinoma stem cells. *The Journal of biological chemistry* **256**, 3245 (Apr 10, 1981).

73. J. N. Octave, Y. J. Schneider, R. R. Crichton, A. Trouet, Transferrin uptake by cultured rat embryo fibroblasts. The influence of temperature and incubation time, subcellular distribution and short-term kinetic studies. *European journal of biochemistry / FEBS* **115**, 611 (Apr, 1981).
74. J. D. Bleil, M. S. Bretscher, Transferrin receptor and its recycling in HeLa cells. *The EMBO journal* **1**, 351 (1982).
75. C. Harding, J. Heuser, P. Stahl, Receptor-mediated endocytosis of transferrin and recycling of the transferrin receptor in rat reticulocytes. *The Journal of cell biology* **97**, 329 (Aug, 1983).
76. A. R. French, G. P. Sudlow, H. S. Wiley, D. A. Lauffenburger, Postendocytic trafficking of epidermal growth factor-receptor complexes is mediated through saturable and specific endosomal interactions. *The Journal of biological chemistry* **269**, 15749 (Jun 3, 1994).
77. R. Ebner, R. Derynck, Epidermal growth factor and transforming growth factor-alpha: differential intracellular routing and processing of ligand-receptor complexes. *Cell regulation* **2**, 599 (Aug, 1991).
78. M. Perez-Torres, M. Guix, A. Gonzalez, C. L. Arteaga, Epidermal growth factor receptor (EGFR) antibody down-regulates mutant receptors and inhibits tumors expressing EGFR mutations. *The Journal of biological chemistry* **281**, 40183 (Dec 29, 2006).
79. C. D. Austin, A. M. De Maziere, P. I. Pisacane, S. M. van Dijk, C. Eigenbrot, M. X. Sliwkowski, J. Klumperman, R. H. Scheller, Endocytosis and sorting of ErbB2 and the site of action of cancer therapeutics trastuzumab and geldanamycin. *Molecular biology of the cell* **15**, 5268 (Dec, 2004).
80. T. Yoshida, I. Okamoto, T. Okabe, T. Iwasa, T. Satoh, K. Nishio, M. Fukuoka, K. Nakagawa, Matuzumab and cetuximab activate the epidermal growth factor receptor but fail to trigger downstream signaling by Akt or Erk. *International journal of cancer. Journal international du cancer* **122**, 1530 (Apr 1, 2008).
81. D. Patel, A. Lahiji, S. Patel, M. Franklin, X. Jimenez, D. J. Hicklin, X. Kang, Monoclonal antibody cetuximab binds to and down-regulates constitutively activated epidermal growth factor receptor vIII on the cell surface. *Anticancer research* **27**, 3355 (Sep-Oct, 2007).
82. W. S. Chen, C. S. Lazar, M. Poenie, R. Y. Tsien, G. N. Gill, M. G. Rosenfeld, Requirement for intrinsic protein tyrosine kinase in the immediate and late actions of the EGF receptor. *Nature* **328**, 820 (Aug 27-Sep 2, 1987).
83. E. Kornilova, T. Sorkina, L. Beguinot, A. Sorkin, Lysosomal targeting of epidermal growth factor receptors via a kinase-dependent pathway is mediated by the receptor carboxyl-terminal residues 1022-1123. *The Journal of biological chemistry* **271**, 30340 (Nov 29, 1996).
84. S. J. Kil, M. Hobert, C. Carlin, A leucine-based determinant in the epidermal growth factor receptor juxtamembrane domain is required for the efficient transport of ligand-receptor complexes to lysosomes. *The Journal of biological chemistry* **274**, 3141 (Jan 29, 1999).
85. S. J. Kil, C. Carlin, EGF receptor residues leu(679), leu(680) mediate selective sorting of ligand-receptor complexes in early endosomal compartments. *Journal of cellular physiology* **185**, 47 (Oct, 2000).

86. J. Bao, I. Alroy, H. Waterman, E. D. Schejter, C. Brodie, J. Gruenberg, Y. Yarden, Threonine phosphorylation diverts internalized epidermal growth factor receptors from a degradative pathway to the recycling endosome. *The Journal of biological chemistry* **275**, 26178 (Aug 25, 2000).
87. K. A. Lund, C. S. Lazar, W. S. Chen, B. J. Walsh, J. B. Welsh, J. J. Herbst, G. M. Walton, M. G. Rosenfeld, G. N. Gill, H. S. Wiley, Phosphorylation of the epidermal growth factor receptor at threonine 654 inhibits ligand-induced internalization and down-regulation. *The Journal of biological chemistry* **265**, 20517 (Nov 25, 1990).
88. L. K. Opresko, C. P. Chang, B. H. Will, P. M. Burke, G. N. Gill, H. S. Wiley, Endocytosis and lysosomal targeting of epidermal growth factor receptors are mediated by distinct sequences independent of the tyrosine kinase domain. *The Journal of biological chemistry* **270**, 4325 (Mar 3, 1995).
89. W. Ding, L. N. Zhang, C. Yeaman, J. F. Engelhardt, rAAV2 traffics through both the late and the recycling endosomes in a dose-dependent fashion. *Molecular therapy : the journal of the American Society of Gene Therapy* **13**, 671 (Apr, 2006).
90. R. J. Lee, P. S. Low, Delivery of liposomes into cultured KB cells via folate receptor-mediated endocytosis. *The Journal of biological chemistry* **269**, 3198 (Feb 4, 1994).
91. A. Gabizon, A. T. Horowitz, D. Goren, D. Tzemach, F. Mandelbaum-Shavit, M. M. Qazen, S. Zalipsky, Targeting folate receptor with folate linked to extremities of poly(ethylene glycol)-grafted liposomes: in vitro studies. *Bioconjugate chemistry* **10**, 289 (Mar-Apr, 1999).
92. G. Blume, G. Cevc, M. D. Crommelin, I. A. Bakker-Woudenberg, C. Kluft, G. Storm, Specific targeting with poly(ethylene glycol)-modified liposomes: coupling of homing devices to the ends of the polymeric chains combines effective target binding with long circulation times. *Biochimica et biophysica acta* **1149**, 180 (Jun 18, 1993).
93. Y. Zhou, D. C. Drummond, H. Zou, M. E. Hayes, G. P. Adams, D. B. Kirpotin, J. D. Marks, Impact of single-chain Fv antibody fragment affinity on nanoparticle targeting of epidermal growth factor receptor-expressing tumor cells. *Journal of molecular biology* **371**, 934 (Aug 24, 2007).
94. J. W. Park, K. Hong, P. Carter, H. Asgari, L. Y. Guo, G. A. Keller, C. Wirth, R. Shalaby, C. Kotts, W. I. Wood, et al., Development of anti-p185HER2 immunoliposomes for cancer therapy. *Proceedings of the National Academy of Sciences of the United States of America* **92**, 1327 (Feb 28, 1995).
95. D. Ye, J. Mendelsohn, Z. Fan, Augmentation of a humanized anti-HER2 mAb 4D5 induced growth inhibition by a human-mouse chimeric anti-EGF receptor mAb C225. *Oncogene* **18**, 731 (Jan 21, 1999).
96. K. Laginha, D. Mumbengegwi, T. Allen, Liposomes targeted via two different antibodies: assay, B-cell binding and cytotoxicity. *Biochimica et biophysica acta* **1711**, 25 (Jun 1, 2005).
97. S. Grant, L. Qiao, P. Dent, Roles of ERBB family receptor tyrosine kinases, and downstream signaling pathways, in the control of cell growth and survival. *Frontiers in bioscience : a journal and virtual library* **7**, d376 (Feb 1, 2002).

98. S. A. Eccles, The epidermal growth factor receptor/Erb-B/HER family in normal and malignant breast biology. *The International journal of developmental biology* **55**, 685 (2011).
99. E. M. Bublil, Y. Yarden, The EGF receptor family: spearheading a merger of signaling and therapeutics. *Current opinion in cell biology* **19**, 124 (Apr, 2007).
100. R. I. Nicholson, J. M. Gee, M. E. Harper, EGFR and cancer prognosis. *Eur J Cancer* **37 Suppl 4**, S9 (Sep, 2001).
101. J. J. Laskin, A. B. Sandler, Epidermal growth factor receptor: a promising target in solid tumours. *Cancer treatment reviews* **30**, 1 (Feb, 2004).
102. T. Heitner, A. Moor, J. L. Garrison, C. Marks, T. Hasan, J. D. Marks, Selection of cell binding and internalizing epidermal growth factor receptor antibodies from a phage display library. *Journal of immunological methods* **248**, 17 (Feb 1, 2001).
103. S. Paik, C. Park, HER-2 and choice of adjuvant chemotherapy in breast cancer. *Seminars in oncology* **28**, 332 (Aug, 2001).
104. N. Prenzel, O. M. Fischer, S. Streit, S. Hart, A. Ullrich, The epidermal growth factor receptor family as a central element for cellular signal transduction and diversification. *Endocrine-related cancer* **8**, 11 (Mar, 2001).
105. D. J. Slamon, G. M. Clark, S. G. Wong, W. J. Levin, A. Ullrich, W. L. McGuire, Human breast cancer: correlation of relapse and survival with amplification of the HER-2/neu oncogene. *Science* **235**, 177 (Jan 9, 1987).
106. D. J. Slamon, W. Godolphin, L. A. Jones, J. A. Holt, S. G. Wong, D. E. Keith, W. J. Levin, S. G. Stuart, J. Udove, A. Ullrich, et al., Studies of the HER-2/neu proto-oncogene in human breast and ovarian cancer. *Science* **244**, 707 (May 12, 1989).
107. A. D. Santin, S. Bellone, J. J. Roman, J. K. McKenney, S. Pecorelli, Trastuzumab treatment in patients with advanced or recurrent endometrial carcinoma overexpressing HER2/neu. *International journal of gynaecology and obstetrics: the official organ of the International Federation of Gynaecology and Obstetrics* **102**, 128 (Aug, 2008).
108. J. Baselga, D. Tripathy, J. Mendelsohn, S. Baughman, C. C. Benz, L. Dantis, N. T. Sklarin, A. D. Seidman, C. A. Hudis, J. Moore, P. P. Rosen, T. Twaddell, I. C. Henderson, L. Norton, Phase II study of weekly intravenous recombinant humanized anti-p185HER2 monoclonal antibody in patients with HER2/neu-overexpressing metastatic breast cancer. *Journal of clinical oncology : official journal of the American Society of Clinical Oncology* **14**, 737 (Mar, 1996).
109. M. A. Cobleigh, C. L. Vogel, D. Tripathy, N. J. Robert, S. Scholl, L. Fehrenbacher, J. M. Wolter, V. Paton, S. Shak, G. Lieberman, D. J. Slamon, Multinational study of the efficacy and safety of humanized anti-HER2 monoclonal antibody in women who have HER2-overexpressing metastatic breast cancer that has progressed after chemotherapy for metastatic disease. *Journal of clinical oncology : official journal of the American Society of Clinical Oncology* **17**, 2639 (Sep, 1999).
110. D. J. Slamon, B. Leyland-Jones, S. Shak, H. Fuchs, V. Paton, A. Bajamonde, T. Fleming, W. Eiermann, J. Wolter, M. Pegram, J. Baselga, L. Norton, Use of chemotherapy plus a monoclonal antibody against HER2 for metastatic breast cancer that overexpresses HER2. *The New England journal of medicine* **344**, 783 (Mar 15, 2001).




111. R. M. Neve, U. B. Nielsen, D. B. Kirpotin, M. A. Poul, J. D. Marks, C. C. Benz, Biological effects of anti-ErbB2 single chain antibodies selected for internalizing function. *Biochemical and biophysical research communications* **280**, 274 (Jan 12, 2001).
112. M. Sznol, J. Holmlund, Antigen-specific agents in development. *Seminars in oncology* **24**, 173 (Apr, 1997).
113. P. Carter, M. L. Rodriguez, J. W. Park, G. Zapata, *Preparation and uses of Fab' fragments from E. coli*. J. G. McCaffrey, H. R. Hoogenboom, D. J. Chiswell, Eds., Antibody Engineering: A Practical Approach (IRL Press, Oxford, 1996).
114. R. Schier, J. D. Marks, E. J. Wolf, G. Apell, C. Wong, J. E. McCartney, M. A. Bookman, J. S. Huston, L. L. Houston, L. M. Weiner, et al., In vitro and in vivo characterization of a human anti-c-erbB-2 single-chain Fv isolated from a filamentous phage antibody library. *Immunotechnology : an international journal of immunological engineering* **1**, 73 (May, 1995).
115. A. E. Lenferink, A. D. De Roos, M. J. Van Vugt, M. L. Van de Poll, E. J. Van Zoelen, The linear C-terminal regions of epidermal growth factor (EGF) and transforming growth factor-alpha bind to different epitopes on the human EGF receptor. *The Biochemical journal* **336 ( Pt 1)**, 147 (Nov 15, 1998).
116. N. I. Goldstein, M. Prewett, K. Zuklys, P. Rockwell, J. Mendelsohn, Biological efficacy of a chimeric antibody to the epidermal growth factor receptor in a human tumor xenograft model. *Clinical cancer research : an official journal of the American Association for Cancer Research* **1**, 1311 (Nov, 1995).
117. F. Szoka, Jr., D. Papahadjopoulos, Comparative properties and methods of preparation of lipid vesicles (liposomes). *Annual review of biophysics and bioengineering* **9**, 467 (1980).
118. G. R. Bartlett, Phosphorus assay in column chromatography. *The Journal of biological chemistry* **234**, 466 (Mar, 1959).
119. D. D. Lasic, P. M. Frederik, M. C. Stuart, Y. Barenholz, T. J. McIntosh, Gelation of liposome interior. A novel method for drug encapsulation. *FEBS letters* **312**, 255 (Nov 9, 1992).
120. G. Haran, R. Cohen, L. K. Bar, Y. Barenholz, Transmembrane ammonium sulfate gradients in liposomes produce efficient and stable entrapment of amphipathic weak bases. *Biochimica et biophysica acta* **1151**, 201 (Sep 19, 1993).
121. E. Bohl Kullberg, N. Bergstrand, J. Carlsson, K. Edwards, M. Johnsson, S. Sjoberg, L. Gedda, Development of EGF-conjugated liposomes for targeted delivery of boronated DNA-binding agents. *Bioconjugate chemistry* **13**, 737 (Jul-Aug, 2002).
122. D. A. Marsh, CRC Handbook of Lipid Bilayers. *CRC Press, Boca Raton, FL.*, 163 (1990).
123. K. Subik, J. F. Lee, L. Baxter, T. Strzepek, D. Costello, P. Crowley, L. Xing, M. C. Hung, T. Bonfiglio, D. G. Hicks, P. Tang, The Expression Patterns of ER, PR, HER2, CK5/6, EGFR, Ki-67 and AR by Immunohistochemical Analysis in Breast Cancer Cell Lines. *Breast cancer : basic and clinical research* **4**, 35 (2010).
124. G. D. Lewis, I. Figari, B. Fendly, W. L. Wong, P. Carter, C. Gorman, H. M. Shepard, Differential responses of human tumor cell lines to anti-p185HER2

- monoclonal antibodies. *Cancer immunology, immunotherapy : CII* **37**, 255 (Sep, 1993).
125. C. C. Benz, G. K. Scott, J. C. Sarup, R. M. Johnson, D. Tripathy, E. Coronado, H. M. Shepard, C. K. Osborne, Estrogen-dependent, tamoxifen-resistant tumorigenic growth of MCF-7 cells transfected with HER2/neu. *Breast cancer research and treatment* **24**, 85 (1992).
  126. J. Filmus, M. N. Pollak, R. Cailleau, R. N. Buick, MDA-468, a human breast cancer cell line with a high number of epidermal growth factor (EGF) receptors, has an amplified EGF receptor gene and is growth inhibited by EGF. *Biochemical and biophysical research communications* **128**, 898 (Apr 30, 1985).
  127. J. Filmus, J. M. Trent, M. N. Pollak, R. N. Buick, Epidermal growth factor receptor gene-amplified MDA-468 breast cancer cell line and its nonamplified variants. *Molecular and cellular biology* **7**, 251 (Jan, 1987).
  128. S. Yang, M. A. Raymond-Stintz, W. Ying, J. Zhang, D. S. Lidke, S. L. Steinberg, L. Williams, J. M. Oliver, B. S. Wilson, Mapping ErbB receptors on breast cancer cell membranes during signal transduction. *Journal of cell science* **120**, 2763 (Aug 15, 2007).
  129. D. L. Costantini, K. Bateman, K. McLarty, K. A. Vallis, R. M. Reilly, Trastuzumab-resistant breast cancer cells remain sensitive to the auger electron-emitting radiotherapeutic agent  $^{111}\text{In}$ -NLS-trastuzumab and are radiosensitized by methotrexate. *Journal of nuclear medicine : official publication, Society of Nuclear Medicine* **49**, 1498 (Sep, 2008).
  130. P. Nagy, A. Jenei, A. K. Kirsch, J. Szollosi, S. Damjanovich, T. M. Jovin, Activation-dependent clustering of the erbB2 receptor tyrosine kinase detected by scanning near-field optical microscopy. *Journal of cell science* **112 ( Pt 11)**, 1733 (Jun, 1999).
  131. R. Kaufmann, P. Muller, G. Hildenbrand, M. Hausmann, C. Cremer, Analysis of Her2/neu membrane protein clusters in different types of breast cancer cells using localization microscopy. *Journal of microscopy* **242**, 46 (Apr, 2011).
  132. B. J. Woodcroft, L. Hammond, J. L. Stow, N. A. Hamilton, Automated organelle-based colocalization in whole-cell imaging. *Cytometry. Part A : the journal of the International Society for Analytical Cytology* **75**, 941 (Nov, 2009).
  133. D. A. Lauffenburger, J. J. Linderman, *Receptors Models for Binding, Trafficking, and Signaling*. (Oxford University Press, New York, New York, 1993), pp. 365.
  134. A. S. Perelson, Receptor Clustering on a Cell Surface. I. Theory of Receptor Cross-linking by Ligands Bearing Two Chemically Identical Functional Groups. *Mathematical Biosciences* **48**, 71 (1980).
  135. A. S. Perelson, Receptor clustering on a cell surface. III. Theory of receptor cross-linking by multivalent ligands: description by ligand states. *Mathematical Biosciences* **53**, 1 (1981).
  136. A. S. Perelson, Receptor Clustering on a Cell Surface. II. Theory of Receptor Cross-linking by Ligands Bearing Two Chemically Distinct Functional Groups. *Mathematical Biosciences* **49**, 87 (1980).
  137. C. M. Waters, K. C. Oberg, G. Carpenter, K. A. Overholser, Rate constants for binding, dissociation, and internalization of EGF: effect of receptor occupancy and ligand concentration. *Biochemistry* **29**, 3563 (Apr 10, 1990).

138. C. Wofsy, B. Goldstein, K. Lund, H. S. Wiley, Implications of epidermal growth factor (EGF) induced egf receptor aggregation. *Biophysical journal* **63**, 98 (Jul, 1992).
139. A. Gandolfi, M. A. Giovenco, Reversible binding of multivalent antigen in the control of B lymphocyte activation. *Journal of theoretical biology* **74**, 513 (Oct 21, 1978).
140. C. DeLisi, The biophysics of ligand-receptor interactions. *Quarterly reviews of biophysics* **13**, 201 (May, 1980).
141. B. S. Hendriks, L. K. Opresko, H. S. Wiley, D. Lauffenburger, Quantitative analysis of HER2-mediated effects on HER2 and epidermal growth factor receptor endocytosis: distribution of homo- and heterodimers depends on relative HER2 levels. *The Journal of biological chemistry* **278**, 23343 (Jun 27, 2003).
142. T. C. Werner, J. R. Bunting, R. E. Cathou, The shape of immunoglobulin G molecules in solution. *Proceedings of the National Academy of Sciences of the United States of America* **69**, 795 (Apr, 1972).
143. R. E. Cathou, D. A. Holowka, Evolution of conformational flexibility of immunoglobulin M. *Advances in experimental medicine and biology* **64**, 207 (1975).

### Publishing Agreement

It is the policy of the University to encourage the distribution of all theses, dissertations, and manuscripts. Copies of all UCSF theses, dissertations, and manuscripts will be routed to the library via the Graduate Division. The library will make all theses, dissertations, and manuscripts accessible to the public and will preserve these to the best of their abilities, in perpetuity. I hereby grant permission to the Graduate Division of the University of California, San Francisco to release copies of my thesis, dissertation, or manuscript to the Campus Library to provide access and preservation, in whole or in part, in perpetuity.

  
\_\_\_\_\_  
Author Signature

3/25/2013  
Date